Clear Water Temporal Scour around Oblong Pier with Oblong Collar fixed on Bed

A thesis submitted towards partial fulfilment of the requirements for the degree of

Master of Engineering
in
Water Resources and Hydraulic Engineering

Submitted by

TANIA SULTANA

Examination Roll No: M4WRE24022

Under the guidance of

Dr. SUBHASISH DAS
Associate Professor
School of Water Resources Engineering, Jadavpur University

School of Water Resources Engineering
M.E. (Water Resources & Hydraulic Engineering)
Course affiliated to ***Faculty Council of Engineering & Technology***

Jadavpur University
Kolkata-700032, West Bengal, India
2024

Declaration of Originality and Compliance of Academic Ethics

I hereby declare that this thesis contains literature survey and original research work by the undersigned candidate, as part of my **Master of Engineering** in **Water Resources and Hydraulic Engineering** in the Faculty Council of Interdisciplinary Studies, Law & Management, Jadavpur University during academic session 2023-24.

All information in this document have been obtained and presented in accordance with academic rules and ethical conduct.

I also declare that, as required by these rules and conduct, I have fully cited and referenced all material and results that are not original to this work.

Name	**:**	**TANIA SULTANA**
Exam Roll Number	**:**	**M4WRE24022**
Thesis Title	**:**	**Clear Water Temporal Scour around Oblong Pier with Oblong Collar fixed on Bed**
Signature with Date	**:**	

M.E. (Water Resources & Hydraulic Engg.) course affiliated to
Faculty Council of Engineering & Technology
Jadavpur University
Kolkata, India

Certificate of Recommendation

This is to certify that the thesis entitled "**Clear Water Temporal Scour around Oblong Pier with Oblong Collar fixed on Bed**" is a bonafide work carried out by **Ms. Tania Sultana** under our supervision and guidance for partial fulfilment of the requirement for the Post Graduate Degree of Master of Engineering in Water Resources and Hydraulic Engineering during the academic session 2023-24.

THESIS ADVISOR
Dr. Subhasish Das
Associate Professor
School of Water Resources Engineering
Jadavpur University

DIRECTOR
Prof. (Dr.) Asis Mazumdar
School of Water Resources Engineering
Jadavpur University

DEAN
Prof. (Dr.) Ratan Mondal
Faculty Council of Interdisciplinary Studies, Law & Management
Jadavpur University

M.E. (Water Resources & Hydraulic Engg.) course affiliated to Faculty Council of Engineering & Technology Jadavpur University
Kolkata, India

CERTIFICATE OF APPROVAL **

This foregoing thesis is hereby approved as a credible study of an engineering subject carried out and presented in a manner satisfactorily to warranty its acceptance as a prerequisite to the degree for which it has been submitted. It is understood that by this approval the undersigned do not endorse or approve any statement made or opinion expressed or conclusion drawn therein but approve the thesis only for purpose for which it has been submitted.

Committee of

Final Examination

for the evaluation

of the thesis

** Only in case the thesis is approved.

ACKNOWLEDGEMENTS

I express my sincere gratitude to my supervisor, ***Dr. Subhasish Das****, Associate Professor School of Water Resources Engineering, Jadavpur University, under whose supervision and guidance this work has been carried out. It would have been impossible to carry out this thesis work with confidence without his wholehearted involvement, advice, support and constant encouragement throughout. He has not only helped me in carrying out my thesis but also has given valuable advice to proceed further in my life.*

I also express my sincere gratitude to, ***Prof. (Dr.) Asis Mazumdar****, Director,* ***Prof. (Dr.) Arunabha Majumder****, Emeritus Professor;* ***Prof. (Dr.) Pankaj Kumar Roy****,* ***Dr. Rajib Das*** *and* ***Dr. Gourab Banerjee,*** *Faculty members of School of Water Resources Engineering, Jadavpur University for their valuable suggestions.*

I would also express my sincere thanks to ***Mr. Buddhadev Nandi, Mr. Saikat Mondal and Mr. Plabon Sen*** *Research Scholars of School of Water Resources Engineering, Jadavpur University for their unconditional support and affection during my work. Also, thanks to my classmates* ***Ms. Purbi Ali, Ms. Shubhashree Laha, Mr. Binoy Banik and Ms. Tiyasa Roy*** *for their help.*

Thanks, are also due to all staff of School of Water Resources Engineering and the Regional-cum-Facilitation Centre (RCFC), NMPB, Jadavpur University for their help and support.

Date : 31 May, 2024

Place : Jadavpur University

Ms. Tania Sultana

(Exam Roll No: M4WRE24022)

Abstract

Any countermeasure of scouring around bridge piers is always a challenging issue. Foundations are under constant threat from scouring, which can quietly compromise their integrity over time. While completely preventing scouring is often economically unfeasible, engineers can implement strategies to manage and mitigate its impact. Bridge collapses, leading to fatalities, property damage, and halted transportation, highlight the need for bridge designers to understand the interaction between soil, water movement, and bridge structures. Existing literature indicates that the use of oblong shaped piers is advantageous in multiple contexts. Though analysis of oblong piers with oblong collars around bend channels exists, straight path analyses are unexplored substantially. Hence, the objective of the present work is to analyse scour patterns around oblong piers using oblong collars under straight channels and clear water conditions with uniform cohesionless bed material and steady flow conditions. An experimental analysis is conducted on oblong piers with collars to investigate the variations in scour depth over time and to determine the maximum scour depth. Specifically, our investigation explores non-dimensional temporal scour depth around the oblong collar fixed on the bed within a controlled flume environment. The experimental setup involved varying the collar width to pier width and pier length to pier width ratios with 12 experiments conducted in total. The temporal scour of the sand bed was measured, and equilibrium conditions were identified when the scour rate dropped below 1 mm/hour. Multiple parameters, including scour depth, width, length, area, and volume, were computed based on the experimental data. For oblong piers without oblong collars, the study found that the maximum scour depth occurred at the upstream of pier (0°). This indicates that without oblong collars, scour is more pronounced directly in front of the pier. In contrast, for piers equipped with collars, the maximum scour typically shifted to the downstream of the oblong pier (135°). The scour depths varied with the collar width to pier width ratio (*W*/*D)*. As the *L*/*D* ratio increases, scour depth decreases notably without a collar. The presence of critical *L*/*D* ratios that minimize scour depth for different *W*/*D* ratios. For *W*/*D* ratios ranging from 1.5 to 3.5, these critical *L*/*D* ratios are noted for both *L*/*D* ratios of 2 and 4. These findings suggest that collars significantly alter the flow patterns around oblong piers, reducing the maximum scour depth and changing its location around the oblong pier circumference. This highlights the importance of considering both the width of the collar and the length-to-width ratio of the pier when designing bridge foundations to manage sediment transport effectively. The development of a governing equation for predicting temporal scour depth, validated by observed temporal scour depth. This non-dimensional equation may be utilized to estimate scour depth accurately in real-world scenarios, aiding in the design and maintenance of safer bridge structures. This contributes to the broader field by offering empirical data and predictive capabilities to better manage the risks associated with scouring around oblong bridge pier with oblong collars.

CONTENT

Chapter No.	Topic	Page No.
	Declaration	iii
	Certificate of recommendation	v
	Certificate of approval	vii
	Acknowledgements	ix
	Abstract	xi
	Contents	xii-xiv
	List of figures	xv-xviii
	List of tables	xix
	Nomenclatures	xx-xxi
Chapter-1	**Introduction**	22-29
	1.1 Definition of scours	23
	1.2 Classification of scour	24
	1.2.1 General scour	24
	1.2.2 Localized scour	25-26
	1.3 Flow pattern and mechanism of scouring	26
	1.3.1 Primary or horseshoe vortex and downflow	26-28
	1.3.2 Wake vortex	28-29
Chapter-2	**Literature review**	30-40
Chapter-3	**Methodology**	41-53
	3.1 Objectives	41-42
	3.2 Selection of parameters for experiments	42
	3.2.1 Determination of oblong pier dimension	43
	3.2.2 Determination of oblong collar dimension	43-44
	3.2.3 The parametric range of the present experimental analysis	44-45
	3.2.4 Selection of flow condition	45
	3.3 Experimental setup	48
	3.3.1 Tilting Flume	48-49
	3.3.2 Pump	49
	3.3.3 Sediment bed	50
	3.3.4 Acoustic Doppler Velocimeter	50-51
	3.3.5 Laser Distance Meter	51
	3.3.6 Flow Meter	52
	3.4 General experimental procedure	52-53
Chapter-4	**Dimensionless analysis**	54-60
Chapter-5	**Results and discussion**	61-115

	5.1 Scour depth calculation for $L/D = 4$	63
	5.1.1 Pier without collar	63-65
	5.1.2 Pier with collar $W/D = 3.5$	65-67
	5.1.3 Pier with collar $W/D = 3$	68-70
	5.1.4 Pier with collar $W/D = 2.5$	70-73
	5.1.5 Pier with collar $W/D = 2$	73-75
	5.1.6 Pier with collar $W/D = 1.5$	75-77
	5.2 Scour depth calculation for $L/D = 2$	77
	5.2.1 Pier without collar	77-80
	5.1.2 Pier with collar $W/D = 3.5$	80-82
	5.1.3 Pier with collar $W/D = 3$	82-84
	5.1.4 Pier with collar $W/D = 2.5$	84-87
	5.1.5 Pier with collar $W/D = 2$	87-89
	5.1.6 Pier with collar $W/D = 1.5$	89-92
	5.3 Comparisons of scour depth for different angles of scour position	92-100
	5.4 Comparisons of scour depth variation with W/D for different L/D ratio	100-103
	5.5 Comparisons of scour depth with L/D ratio for different W/D ratios and different angles of scour position	104-107
	5.6 Comparison of volume for different W/D and L/D ratios	107-108
	5.7 Comparison of planar area for different dimensions	108-109
	5.8 Comparison of surface area for different dimensions	109
	5.9 Development of governing equation for temporal scour depth	109-116
	5.10 Correlation coefficient (r)	114
	5.11 Root mean squared error (RMSE)	114
	5.12 Percent bias (PBIAS)	114
	5.13 Nash–Sutcliffe efficiency (NSE)	114-115
Chapter-7	**Conclusions**	117-118
	6.1 Overall remarks	117-118
	6.2 Scope of future work	118
	References	119-125

LIST OF FIGURES

Figure No.	Topic	Page No.
Fig. 1.1.	Types of scours	25
Fig. 1.2.	Scouring in clear water condition and live bed condition redrawn based on Raudkivi (1998)	26
Fig. 1.3.	Schematic diagram of flow pattern around the oblong pier	27
Fig. 1.4.	Scour mechanism around oblong bridge pier fitted without collar plate.	28
Fig. 1.5.	Scour mechanism around oblong bridge pier fitted with collar plate.	28
Fig. 2.1.	Hanskhali Bridge with the oblong shaped piers located in Nadia district, West Bengal, India.	39
Fig. 2.2.	Murti Bridge with the oblong shaped piers located in Jalpaiguri district, West Bengal, India.	40
Fig. 3.1.	Different dimensions of (a) pier and (b) collar for *L*/*D* ratio 2 and (c) pier and (d) collar for *L*/*D* ratio 4	42
Fig. 3.2.	Schematic diagram of (a) pier (b) pier with collar	42
Fig. 3.3.	Tilting flume used during the experimentation.	48
Fig. 3.4.	Schematic diagram of the tilting flume	49
Fig. 3.5.	Pump used to recirculate the flow	49
Fig. 3.6.	Acoustic Doppler Velocimeter. Apparatus of the Acoustic Doppler Velocimeter; 1-Transportation and storage case; 2-Vectrino Velocimeter; 3- External power/signal cable; 4 Tool kit, Nortek; 5-USB to serial converter; 6-Seeding material (bottle of 250 ml); 7-AC/DC voltage transformer, 24 V DC; 8-International kit with AC plugs; 9-USB memory stick with Vectrino software	51
Fig. 3.7.	Laser Distance Meter	51
Fig. 3.8.	Flow Meter	52
Fig. 5.1.	Sand bed before experimental run for without collar, and L/D= 4	63
Fig. 5.2.	Scour bed around the pier after experimental run for without collar, and L/D= 4	64
Fig. 5.3.	Contour map of scour bed without collar for L/D= 4	64
Fig. 5.4.	Temporal variation of scour depth in non-dimensional form for different ϕ without collar, and *L*/*D*= 4	65
Fig. 5.5.	Sand bed before experimental run for *W*/*D*= 3.5, and *L*/*D*= 4	66
Fig. 5.6.	Scour bed around the collar after experimental run for W/D= 3.5, and L/D= 4	66
Fig. 5.7.	Contour map of scour bed for *W*/*D*=3.5, and *L*/*D*= 4	67

Fig. 5. 8.	Temporal variation of scour depth in non-dimensional form for different ϕ W/D= 3.5, and L/D= 4	67
Fig. 5. 9.	Sand bed before experimental run for *W/D*= 3, and *L/D*= 4	68
Fig. 5.10.	Scour bed around the collar after experimental run for *W/D*= 3, and *L/D*= 4	69
Fig. 5.11.	Contour map of scour bed for *W/D*=3, and *L/D*= 4	69
Fig. 5.12.	Temporal variation of scour depth in non-dimensional form for different ϕ *W/D*= 3, and *L/D*= 4	70
Fig. 5.13.	Sand bed before experimental run for W/D= 2.5, and L/D= 4	71
Fig. 5.14.	Scour bed around the collar after experimental run for *W/D*= 2.5, and *L/D*= 4	71
Fig. 5.15.	Contour Map of scour bed for *W/D*=2.5, and *L/D*= 4	72
Fig. 5.16.	Temporal variation of scour depth in non-dimensional form for different ϕ *W/D*= 2.5, and *L/D*= 4	72
Fig. 5.17.	Sand bed before experimental run for W/D= 2, and L/D= 4	73
Fig. 5.18.	Scour bed around the collar after experimental run for *W/D*= 2, and *L/D*= 4	73
Fig. 5.19.	Contour map of scour bed for *W/D*= 2, and *L/D*= 4	74
Fig. 5.20.	Temporal variation of scour depth in non-dimensional form for different ϕ *W/D*= 2, and *L/D*= 4	74
Fig. 5.21.	Sand bed before experimental run for *W/D*= 1.5, and *L/D*= 4	75
Fig. 5.22.	Scour bed around the collar after experimental run for *W/D*= 1.5, *L/D*= 4	76
Fig. 5.23	Contour Map of scour bed for *W/D*= 1.5, and *L/D*= 4	76
Fig. 5.24.	Temporal variation of scour depth in non-dimensional form for different ϕ *W/D*= 1.5, and *L/D*= 4	77
Fig. 5.25.	Sand bed before the experimental run for without collar, and *L/D*=2	78
Fig. 5.26.	Scour bed around the pier after experimental run for without collar, and *L/D*=2	78
Fig. 5.27.	Contour map of scour bed for without collar, and *L/D*=2.	79
Fig. 5.28.	Temporal variation of scour depth in non-dimensional form for different ϕ without collar, and *L/D*=2	79
Fig. 5.29.	and bed before the experimental run for *W/D*= 3.5, and *L/D*=2	80
Fig. 5.30.	Scour bed of sand after experimental run for *W/D*= 3.5, and *L/D*=2	81
Fig. 5.31.	Contour map of scour bed (*W/D*=3.5, *L/D*=2)	81
Fig. 5.32.	Temporal variation of scour depth in non-dimensional form for different ϕ *W/D*= 3.5, and *L/D*=2	82
Fig. 5.33.	Sand bed before the experimental run for *W/D*= 3, and *L/D*=2	83
Fig. 5.34.	Scour bed around the collar after experimental run for *W/D*= 3, and *L/D*=2	83
Fig. 5.35.	Contour map of scour bed for W/D=3, and L/D= 2	84
Fig. 5.36.	Temporal variation of scour depth in non-dimensional form for different ϕ *W/D*= 3, and *L/D*=2	84

Fig. 5.37.	Sand bed before experimental run for *W/D*= 2.5, and *L/D*=2	85
Fig. 5.38	Scour bed around the collar after experimental run for *W/D*= 2.5, and *L/D*=2	85
Fig. 5.39.	Contour map of scour bed for *W/D*=2.5, and *L/D*= 2	86
Fig. 5.40.	Temporal variation of scour depth in non-dimensional form for different ϕ for *W/D*= 2.5, and *L/D*=2	86
Fig. 5.41.	Sand bed before experimental run for *W/D*= 2, and *L/D*=2	87
Fig. 5.42.	Scour bed around the collar after experimental run for *W/D*= 2, and *L/D*=2	88
Fig. 5.43.	Contour map of scour bed for *W/D*=2, and *L/D*=2	88
Fig. 5.44.	Temporal variation of scour depth in non-dimensional form for different ϕ *W/D*= 2, and *L/D*=2	89
Fig. 5.45.	Sand bed before the experimental run for *W/D*= 1.5, and *L/D*=2	90
Fig. 5.46.	Scour bed around the collar after experimental run for *W/D*= 1.5, and *L/D*=2	90
Fig. 5.47.	Contour map of scour bed for *W/D*= 1.5, and *L/D*=2	91
Fig. 5.48	Temporal variation of scour depth in non-dimensional form for different ϕ *W/D*= 1.5, and *L/D*=2	91
Fig. 5.49.	Temporal variation of scour depth in non-dimensional form for different *W/D* ratios when *L/D*=4, and $\phi=0^0$.	92
Fig. 5.50.	Temporal variation of scour depth in non-dimensional form for different W/D ratios when L/D=4, and $\phi=45^0$.	93
Fig. 5.51.	Temporal variation of scour depth in non-dimensional form for different *W/D* ratios when *L/D*=4, and $\phi=90^0$	94
Fig. 5.52.	Temporal variation of scour depth in non-dimensional form for different *W/D* ratios when *L/D*=4, and $\phi=135^0$	95
Fig. 5.53.	Temporal variation of scour depth in non-dimensional form for different *W/D* ratios when *L/D*=4, and $\phi=180^0$	96
Fig. 5.54.	Temporal variation of scour depth in non-dimensional form for different *W/D* ratios when *L/D*=2, and $\phi=0^0$.	97
Fig. 5.55.	Temporal variation of scour depth in non-dimensional form for different *W/D* ratios when *L/D*=2, and $\phi=45^0$	97
Fig. 5.56.	Temporal variation of scour depth in non-dimensional form for different *W/D* ratios when *L/D*=2, and $\phi=90^0$	98
Fig. 5.57.	Temporal variation of scour depth in non-dimensional form for different *W/D* ratios when *L/D*=2, and $\phi=135^0$	99
Fig. 5.58.	Temporal variation of scour depth in non-dimensional form for different *W/D* ratios when *L/D*=2, and $\phi=180^0$	100
Fig. 5.59.	Nondimensional scour depth variation with *W/D* ratio for $\phi=0^0$	101
Fig. 5.60.	Nondimensional scour depth variation with *W/D* ratio for $\phi=45^0$	101
Fig. 5.61.	Nondimensional scour depth variation with *W/D* ratio for $\phi=90^0$	102
Fig. 5.62.	Nondimensional scour depth variation with *W/D* ratio for $\phi=135^0$	103

Fig. 5.63.	Nondimensional scour depth variation with *W/D* ratio for $\phi=180^0$	103
Fig. 5.64.	Nondimensional scour depth variation with *L/D* ratio for $\phi=0^0$	104
Fig. 5.65.	Nondimensional scour depth variation with *L/D* ratio for $\phi=45^0$	105
Fig. 5.66.	Nondimensional scour depth variation with *L/D* ratio for $\phi=90^0$	106
Fig. 5.67.	Nondimensional scour depth variation with *L/D* ratio for $\phi=135^0$	106
Fig. 5.68.	Nondimensional scour depth variation with *L/D* ratio for $\phi=180^0$	107
Fig. 5.69.	Change of scour volume for different *L/D* and *W/D* ratios	108
Fig. 5.70.	Change of scour planar area for different *L/D* and *W/D* ratios	108
Fig. 5.71.	Change of scour surface area for different *L/D* and *W/D* ratios	109
Fig. 5.72.	Comparison of present experimental data with other data in open literature for temporal scour depth	110
Fig. 5.73.	Comparison of present experimental data with other data in open literature for Various *W/D* Ratio	110
Fig. 5.74.	Comparison of present experimental data with other data in open literature for Various L^*/D Ratio	111
Fig. 5.75.	Comparison of Observed and Predicted Values of Temporal Scour Depth for Various *L/D* Ratios	111
Fig. 5.76.	Comparison of present experimental data with other data in open literature for Various U/U_c Ratio	112
Fig. 5.77.	Comparison of present experimental data with other data in open literature for Various *H/D* Ratio	112
Fig. 5.78.	Comparison between experimental and predicted values of temporal scour depth	113
Fig. 5.79.	Comparison between observed and predicted Value for temporal scour depth of Masjedi et al. (2010)	114

LIST OF TABLES

Table No.	Topic	Page No.
Table 2.1.	Functional relationship for non-circular shape pier	39
Table 3.1.	Dimension of pier and collar selected based on previous literatures	43-44
Table 3.2.	The parametric range of present experimental analysis	44
Table 3.3.	Parameters affecting scour depth around the pier with time	45
Table 3.4.	Maximum and minimum values of parameters	47
Table 5.1.	Experiment details	61
Table 5.2.	Experiment apparatus details	62
Table 5.2.	Accuracy analysis of the present study and the reference data.	115

NOMENCLATURES

The following notation is used in the present study-

A_c	–	wetted area, Bh [L^2];
A_p	–	planar surface area of equilibrium scour hole [L^2];
A_s	–	scour surface area [L^2];
A_t	–	net area of collar [L^2];
B	–	width of flume [L];
D	–	oblong pier width [L];
D_{50}	–	median diameter of sand [L];
f	–	function symbol [-];
Fr	–	Froude number of flow, $V/(gh)^{0.5}$ [-];
g	–	gravitational acceleration [LT^{-2}];
h	–	approaching flow depth [L];
H	–	height of collar above bed [L];
L	–	oblong pier length [L];
L^*	–	oblong collar length [L];
k_s	–	pier shape factor [-];
Q	–	discharge [L^3T^{-1}];
Q_c	–	critical discharge [L^3T^{-1}];
t	–	time taken for each experimental evaluation [T];
t_e	–	time for equilibrium depth of scour to develop [T];
U	–	depth-averaged approaching flow velocity [LT^{-1}];
U_C	–	critical velocity of water [LT^{-1}];
u_*	–	shear velocity [LT^{-1}];
u_{*c}	–	critical shear velocity [LT^{-1}];
W	–	collar width [L];
x, y, z	–	coordinate axes [L];

Greek symbols

ρ	–	mass density of fluid [ML^{-3}];
ρ_s	–	mass density of sand [ML^{-3}];
τ_0	–	average bed shear stress [$ML^{-1}T^{-2}$];
v	–	kinematic viscosity [L^2T^{-1}];
Θ_c	–	critical Shield's parameter [-];
ϕ	–	angle of scour position [-];
θ	–	Pier skew angle [-];
α	–	index to the collar shape factor [-];

Subscripts

s	–	instantaneous scour condition;
se	–	equilibrium scour condition;
50	–	50% finer respectively;
i,k	–	direction indices along x- and z-axis respectively;
c	–	critical/threshold condition;
$*$	–	shear;
n	–	non-dimensional;
o	–	average value at bed;
s,f	–	sand and fluid respectively.

Chapter 1

Introduction

The failure of bridge piers due to the onset of scouring around them is a prevalent occurrence in bridges constructed over rivers, streams, and waterways worldwide. The presence of scouring imposes significant repair costs year-round on a global scale. According to Hamill (1999) and Melville and Coleman (2000), the erosive force of flowing water stands as the primary catalyst for scouring around bridge piers. Shirhole and Holt (1991) reported that approximately 1000 bridges in the United States collapsed over a 30-year period, with 60% of these failures attributed to scouring. Huber (1991) noted that in the United States, over the past 75 years, approximately 500 bridges failed, with the majority succumbing to scour-related issues. Similarly, in India, a considerable number of bridges have failed due to scouring (Thakkar, 1992). A study conducted by the Federal Highway Administration (FHWA) found that out of 383 bridge failures resulting from floods, 25% involved damage to piers, while the majority (72%) incurred damage to abutments Chang (1973). This underscores the critical importance of addressing local scour around bridge piers, as emphasized by Brice and Blodgett (1978).

The phenomena of erosion and corrosion are inherent in alluvial materials, though even deeply weathered rock can be susceptible to such incidents. Foundations are under constant threat from scouring, which can quietly compromise their integrity over time. While completely preventing scouring is often economically unfeasible, engineers can implement strategies to manage and mitigate its impact. These strategies draw from both controlled laboratory studies and practical experiences, encompassing both successful interventions and failures. However, despite extensive research efforts, a universally accepted method for analyzing scour around foundations remains elusive, and discrepancies in findings between studies are not uncommon.

Protecting bridge piers from erosion and ensuring adequate foundation depth can incur substantial costs. For instance, at the Varanasi Ganga River bridge on the Amnagar-Mugalsarai Bypass, estimates placed the maximum scour depth at an astonishing 60 meters below the highest flood level Thakkar (1992). To address this challenge, India employs the Lacey-Inglis method for estimating equilibrium scour depth, a method recommended by both the Indian Railways and the Indian Road Congress. The Federal Highway Administration (FHWA) study highlighted the significant impact of pier damage, with 25% of flood-induced bridge failures attributed to it Chang (1973). Furthermore, Brice and Blodgett (1978) underscored the importance of addressing local scour at bridge piers, considering it as critical as abutment scour. The annual direct cost, including repair and replacement expenses, of flood

damage to highways in the USA has been estimated to reach 50 million USD Lagasse et al. (1991).

For decades, various methods have been employed to reduce and regulate the depth of scouring around bridge piers. These methods include techniques such as slotting (Chiew, 1992; Kumar et al., 1999), air injection (Tipireddy and Barkdoll, 2018), sacrificial piles (Melville and Hadfield, 1999), pier angle adjustments (Vaghefi et al., 2016), riprap placement (Lauchlan and Melville, 2001), submerged vanes (Ghorbani and Kells, 2008), raft foundations (Vijayasree et al., 2018), modifying pier shapes (Fael et al., 2016), and reinforcing soil with geotextiles (Imamzadehei et al., 2016), among others. The study on isolated pier scour depth computation formula was conducted by Nandi and Das (2023*b*), Nandi et al. (2024*a*) and Nandi et al. (2024*b*). The study of eccentric multiple piers was conducted by several researchers (Das et al., 2014*a*; Das et al., 2014*b*; Das et al., 2016; Das and Mazumdar, 2018; Das et al., 2019; Nandi and Das, 2023*a*). The flow characteristic near the pier has been studied by Das et al. (2013), Das et al. (2014*c*), Das et al. (2017), and Das et al. (2019).

It should be noted that the use of collars around piers stands as one of the most effective and widely employed methods for reducing scour. Collars serve as a common countermeasure aimed at protecting bridge piers from local scour. When installed, collars prompt the formation of the scour hole downstream of the pier, gradually mitigating its impact. Masjedi et al. (2010), Khosravinia et al. (2018), Kumcu et al. (2014), and Virender et al. (1999) assert that collars effectively decrease local erosion and safeguard bridges against scour-related failures. Altering bridge piers can notably diminish local scour by reducing both streamwise and downward water velocities around the pier. According to Jahangirzadeh et al. (2014), piers equipped with collars can substantially curtail scour development. Over the decades, numerous researchers have advocated for the use of collars, including Heidarpour et al. (2010), Saadati et al. (2017), Grimaldi et al. (2009), Chen et al. (2018), Mashahir and Zarrati (2002), and Zarrati et al. (2004), as a means to mitigate scour hole formation around bridge piers.

1.1 Definition of scours

Scouring in rivers or streams is a natural or man-made phenomenon generated by the flow of water through the passage of a river due to the presence of natural or artificial obstructions, such as hydraulic structures. It occurs at the riverbed due to the corrosion and erosion of sediment. Rivers naturally scour their beds as they change shape, and human-built structures can also trigger or influence scour. Additionally, it is caused by the erosive action of flowing water in rivers or streams, which dissolves and removes material from the streambed and banks. Areas around bridge piers and abutments are particularly susceptible to scour.

In some rivers scour has little effect during a flood, while others face dramatic changes deepening of their beds This difference depends on how confined the floodwater is. When floodwaters are trapped by the surrounding landscape, they cause significant changes in both

the water level and the riverbed elevation. In contrast, floods that can easily spill out onto flat floodplains have minimal impact on both. On the other hand, human activities can also alter the supply of sediment or the transportation of sediments in a river so as to produce extensive modification of the river bed.

For thousands of years, rivers have carved out valleys, showing the power of nature. Human activity barely affected rivers for a long time. But recently, we've built a lot of structures in and around rivers. These structures change how water flows and how much sand and rocks the river carries. Unfortunately, most structures cause erosion nearby and mess up the healthy balance of the river environment. Therefore, it is crucial for designers to understand riverbed scour and its consequences several factors contribute to scour around bridges, i.e., depth of water, velocity of water, pier width, collar width, Froude number, and riverbed materials.

Scour weakens the bridge pier base and can cause it to collapse. Bridge foundations can be washed away by fast-moving water, making bridges unsafe. To ensure bridge safety, engineers must consider the risk of scour while designing the piers of the bridge.

1.2Classification of scour

Rivers naturally experience scour in their beds over time, even without anything built in them. Buildings and other things in the river can also make the scour worse. There are two main types of scours, i.e., general scour and local scour. It is to be mentioned that the general scour affects a large area of the riverbed, and local scour happens around specific structures like bridge piers. The scour can be further categorized based on specific flow conditions. The specifications are presented in detail in Fig. 1.1.

1.2.1 General Scour

Rivers naturally widen and deepen their channels over time and the phenomenon is called general scour. General scour happens when a river can carry more sediment than usual. This can be caused by strong floodwaters or man-made alternations. Some examples of the general scour are presented by Simons and Sentürk (1977) and Jansen (1979). The examples are presented below.

- Erosion downstream of reservoirs resulting from the interception of sediment.
- Water transfers from one river to another, leading to changes in the sediment carrying capacities of both rivers.
- Sand and gravel mining in rivers and flood plains.
- Meander cutoffs.
- Reduction in effective boundary roughness and cross-section due to channel regulation. This type of scour is a response to the flow regime and would occur regardless of whether a structure like a bridge is built.

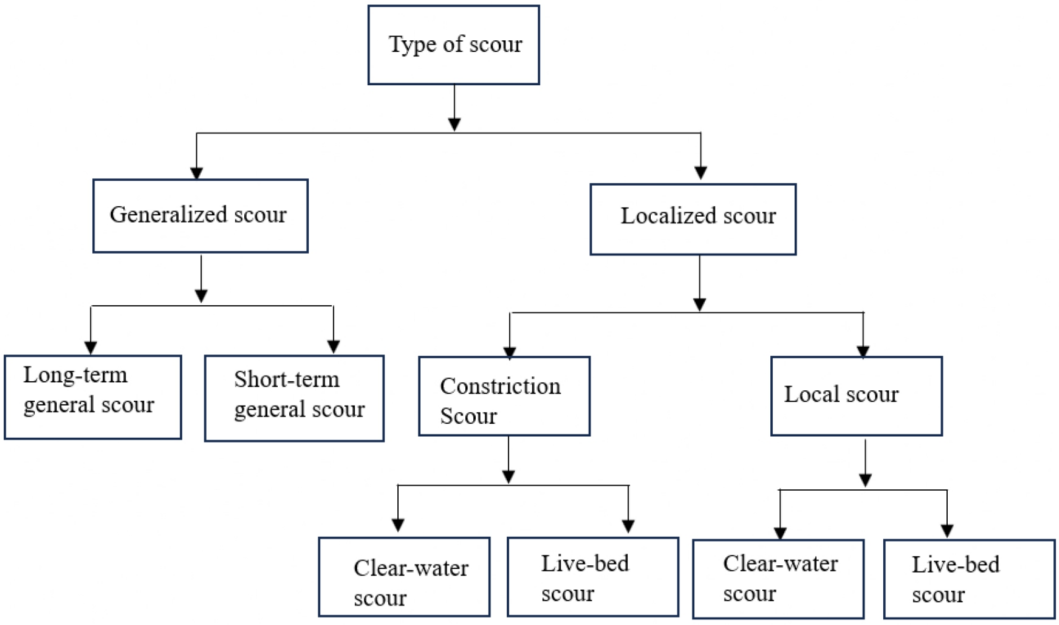


Fig. 1.1. Types of scour.

1.2.2 Localized Scour

a) Local scour is a specific type of erosion that occurs around structures placed in a river, such as bridge piers. It is caused by the direct impact of flowing water striking the structure. The type of structure, whether wide or narrow, can influence the extent of local scour. This local scour exacerbates general erosion and any constriction scour caused by narrowing the river.

b) Bridges can constrict a river channel, increasing water flow velocity. This accelerated flow excavates a deeper scour in the riverbed, known as constriction scour.

c) Clear-water scour occurs when the riverbed upstream of a structure is stable with no loose material. The water flowing over the stable riverbed lacks sufficient force to transport sediment. Thus, the shear stresses on the bed at a certain distance from the bridge pier do not exceed the critical or threshold shear stress for particle movement. As illustrated in Fig. 1.2, in clear-water conditions, scouring initially occurs rapidly. However, the scour depth eventually reaches an equilibrium limit, and the rate of scouring diminishes. The maximum depth of the scour hole is directly proportional to the shear stresses acting on the bed material. In clear-water conditions, this maximum depth is approached asymptotically over time. Consequently, defining an equilibrium time for scour is necessary.

d) Live-bed scour, also referred to as scour with bed material sediment transport, occurs when the flow induces a general movement of the bed material. That is, the shear stresses on the bed are generally greater than the critical ones. Equilibrium scour depths are reached when the amount of material removed from the scour hole by the flow equals the amount of material supplied to the scour hole from upstream.

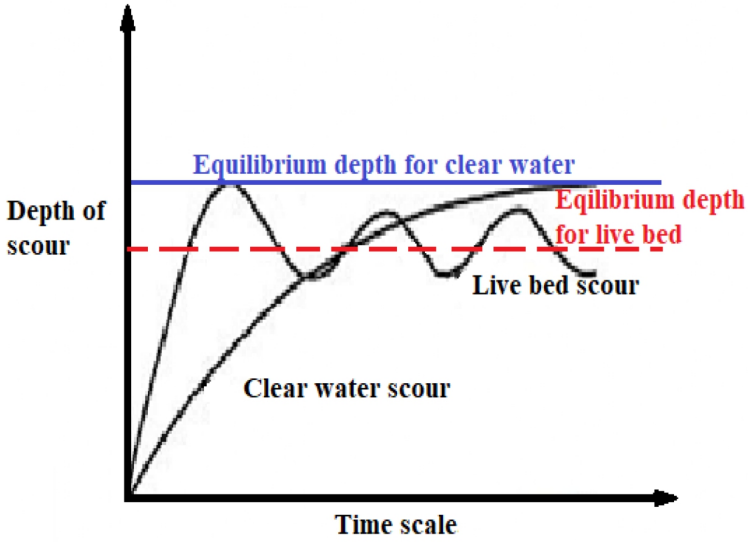


Fig. 1.2. Temporal variation of scour depth in clear water and live bed conditions based on Raudkivi (1998).

The characteristics of scour depth variation over time for live bed conditions are presented in Fig. 1.2 (Raudkivi 1998). The figure indicates that in live-bed conditions, the depth of the scour hole increases rapidly initially, with a higher slope of increment compared to the clear water condition. However, after a critical depth, the depth of scouring shows fluctuating changes with time. A mean average depth for that fluctuating depth is considered and that is called equilibrium depth of scouring for life bed condition. Another observation is that the equilibrium or final depth of local scour is reached quickly in live-bed conditions, whereas it occurs more gradually in clear-water conditions (Melville and Coleman, 2000).

1.3 Flow pattern and mechanism of scouring

The scour mechanism around a bridge pier is an intricate three-dimensional process. It mainly occurs due to the fluid structure interactions and formation of anisotropic turbulence and vortex structure around the bridge pier. The scour around the pier is the erosion of the streambed near the pier foundation due to the inception of a complex vortices system. This system consists of a horseshoe vortex initiated from the down flow at the upstream face of the pier, and wake vortices at the downstream of the pier (Breusers and Raudkivi 1991).

1.3.1 Primary or horseshoe vortex and downflow

When water flows past an oblong pier, it creates a three-dimensional separation, forming a vortex system known as a horseshoe vortex or primary vortex. The horseshoe vortex is presented in Figs. 1.3 and 1.4. This vortex develops in front of the pier and is carried

downstream by the river flow. This vortex looks like a horseshoe when viewed from the top of the pier. The presence of this vortex increases shear stress, leading to higher sediment transport capacity and the formation of a deep scour hole around the pier. This altered flow pattern reduces the shear stress downstream, affecting sediment transport capacity. The extent and depth of scour at bridge elements depend largely on flow characteristics, pier design, and river-bed material. The formation of the horseshoe vortex and associated downward flow creates scour around the circular pier, non-circular pier, abutment, and spur dike etc. These vortices, modified by the upstream pier, affect scouring around the downstream pier. They remove sediment from the upstream pier and deposit some of it into the scour hole around the downstream pier. The horseshoe vortex in front of the pier is identified as the main cause of scour, as noted by Kothyari et al. (1992 a, b), who suggest a layer-by-layer scouring process, as mentioned by Dey (1999). Tseng et al. (2000) further describe a downflow near the upstream face of the pier, which merges with the separated flow to form the stretched horseshoe vortex around the pier.

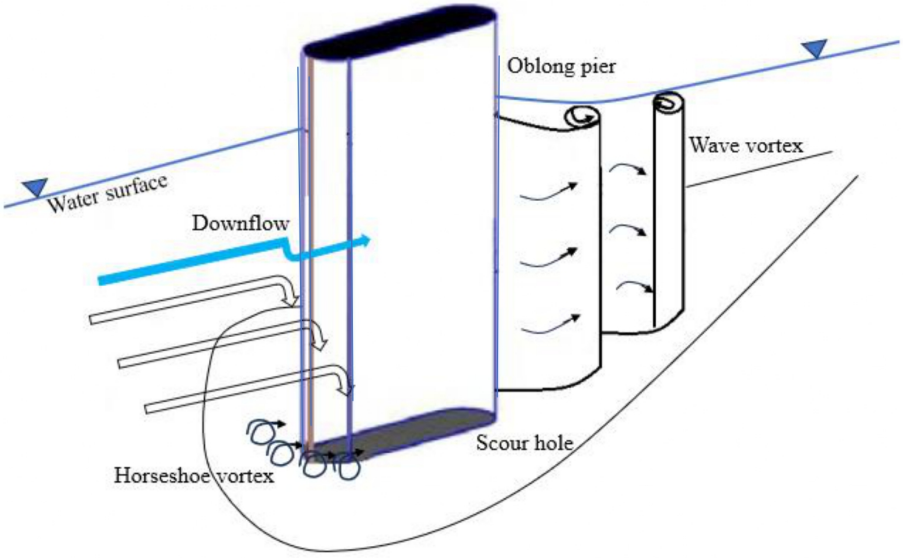


Fig. 1.3. Schematic diagram of flow pattern around the oblong pier.

The flow characteristics around a pier attached to collar plates are shown in Fig. 1.5. The figure indicates that the collar acts as a barrier to the horseshoe vortex, preventing direct impact and downflow from reaching the sediment bed (Fig. 1.5).

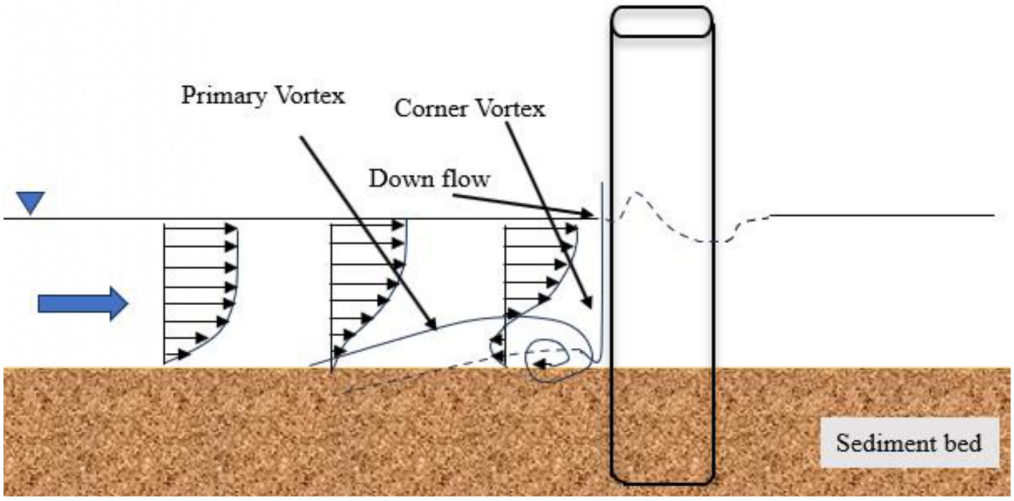


Fig. 1.4. Scour mechanism around oblong bridge pier fitted without collar plate.

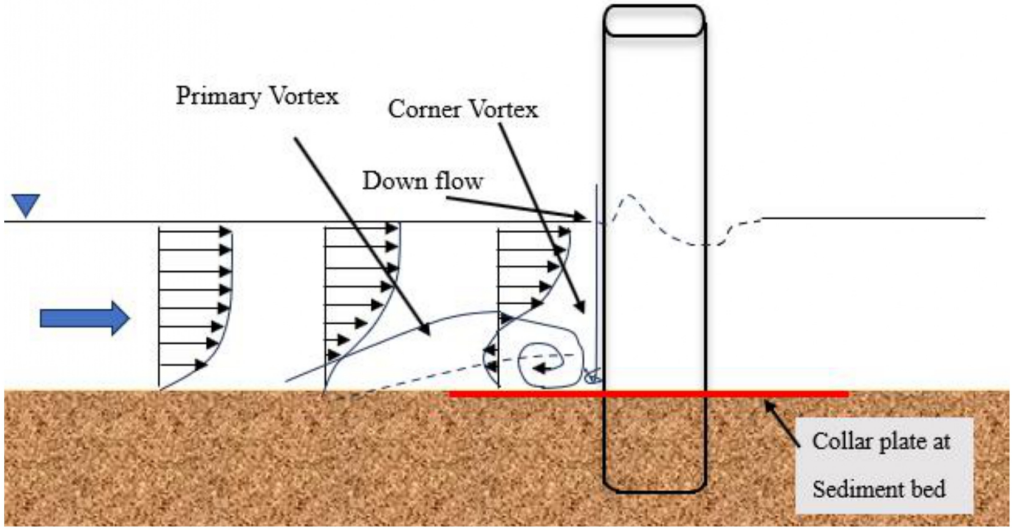


Fig. 1.5. Scour mechanism around oblong bridge pier fitted with collar plate.

1.3.2 Wake vortex

A wake vortex emerges on the downstream side of the piers due to flow separation at the pier's sides. The occurrence of wake vortex is presented in Fig. 1.3. Raudkivi (1986) described these vortices as cast-off vortices and these have vertical axes. A vortex forms on one side detaches and moves downstream. Soon after, another vortex forms on the opposite side and eventually sheds as well. The wake vortices gradually dissolve as they move downstream. While wake vortex scour at the downstream of the pier poses minimal or no destructive potential, horseshoe vortex scour occurring at the pier face poses a threat to undermine the pier. At the majority of bridges, wake vortex scour is minimal, and confluence scour is absent.

Therefore, there is a need for a comprehensive plan of action to address the impacts of scour, and to consider innovative, effective, and cost-efficient countermeasures for designing new bridges and rehabilitating or replacing existing ones affected by scour. Given that collars offer a promising solution for reducing scour around piers, the present thesis work analyzes an effective type of pier geometry with a collar. It is worth noting that circular piers are commonly used in both literature and practical applications. However, this study specifically focuses on experimentally analyzing different pier shapes with collars, excluding the circular ones. The next chapter will provide a detailed literature review centered on this objective.

Chapter 2

Literature review

In this chapter, a comprehensive literature review is conducted on existing experimental and numerical studies concerning noncircular piers with collars. The open literature illustrates that numerous researchers have conducted both experimental and numerical investigations to comprehend scour patterns at bridge piers and abutments. Many studies have been undertaken to predict scour, resulting in the development of numerous equations by various researchers. The findings of these researchers are discussed in the subsequent sections of the chapter.

Bhattacharya et al. (2003) studied the reduction of local scour around non-cylindrical bridge piers with collars at high angles of attack. The main objective of this study was to investigate the effect of a collar on the reduction of maximum local scour depth around a non-cylindrical bridge pier. The authors considered various angles of attack and different elevations of collar along the pier, conditions for minimum scour were found by experimentations. They attempted to modify the equation of Dey (1997) to more accurately determine the maximum depth of scour around a non-cylindrical pier by introducing two new functions to the equation of Dey (1997) for a cylindrical bridge pier. The authors concluded that with the increase in collar height, the scour depth decreased. The authors also concluded that the variation of scour reduction with angle of attack was non-linear but there was no fixed pattern of variation.

Mashahir et al. (2004) studied experimentally, the time development of scouring around a circular and a rectangular pier protected by a collar. The authors used a collar that was 3 times wider than the pier diameter for a circular pier and the pier width for a rectangular pier. They used the collars at the streambed level. The authors investigated the effect of collars on the time development of scouring considerably. They investigated that for clear water conditions, the scouring around an unprotected pier developed very fast initially. However, the rate of scouring was reduced due to deeper scour holes later. They also found out that in the circular pier, unlike the unprotected pier the rate of scouring at the upstream face of the pier, was considerably low for the initial 30 hours and it increased again. However, for the rectangular pier, there was no sign of scouring for the upstream of the pier up to 52 hours of flow. In this case, there was a very slow development of scouring at two sides of the collar. Finally, the authors concluded that the use of a rectangular collar was more effective on a rectangular pier compared to a circular pier. The authors also concluded that the collar more effectively slowed down the development of scour than a wider foundation with a similar width and elevation.

Zarrati et al. (2004) carried out different experimental studies to investigate the methods to control scouring around bridge piers. They used different structures for scour reduction i.e., riprap, collars, slots through the pier, and a group of small piles in front of the rectangular pier, etc. The experiments were carried out for the sediment motion with piers aligned and skewed at the angles, 5° and 10°, respectively, to the flow, and with collars of different widths and at various elevations. They observed that the wider collars at lower levels were more effective. The authors also noticed that the effectiveness of collars was reduced by the increasing angle of the skewness of the pier. They noticed a maximum reduction of scouring of 74%, 56%, and 35% for a collar with a similar width of the pier at streambed level, and the pier was aligned, skewed at 5° and 10°, respectively to the flow.

Zarrati et al. (2004) in another work, studied experimentally the use of independent and continuous pier and collars in combination with riprap for scour reduction around bridge pier groups. They studied the efficiency of collars through various experiments. They compared the data, they generated from their experiments with the data available in the open literature on single piers with collars and bridge pier groups without collars. The authors observed that for the case of two piers in line, the combination of continuous collars and riprap effectively reduced the scour by about 50% for the front pier and 60% for the rear piers. They also observed, that for two piers in line, the independent collars indicated better efficiency compared to continuous collars around both piers. In their observation, it was also presented that the efficiency of collars on a rectangular pier aligned with the flow was more compared to two piers in line. Finally, they concluded that their experiments indicated less effectiveness for collars in the reduction of scouring around two transverse piers.

Mashahir et al. (2008) studied the process of reduction of local scouring at bridge piers as a time-dependent process experimentally. They carried out their study by using collars around a pier to reduce the rate of scouring considerably. Collars were attached to a pier which looked like horizontal plates. Collars worked as a barrier to the downflow and prevented its direct impingement into the streambed. They used a rectangular pier of 5 cm wide, 15 cm height, and collars with 3 different lengths i.e. 25cm, 35cm, and 45 cm, and constant width (3 times of the pier width). In their experiment, the pier model had a circular nose and tail and was made from clear Perspex. Collars were placed at the streambed level and all tests were conducted at the threshold of bed material motion where maximum depth of scour hole was expected. The authors carried out long-time tests to study the development of the scour hole around the pier. They investigated that the length of the collar was an important factor that affected the rate of scouring. They observed that in the collar with 25 cm and 35 cm length, the flow undermined the collar and penetrated below its upstream edge after 8 and 24 hours respectively. However, later the development of scouring was boosted due to the horseshoe vortex. They also observed that for the collar with 45 cm length, flow could not penetrate below the upstream edge of the collar after 185 hours. They observed that though the scouring at the upstream region of the pier was absent, at the sides of the collar, the maximum depth of the scouring (4.35 cm) was present indicating a 60% reduction in scouring.

Garg et al. (2008) studied the combination of various scour protection devices around an oblong-shaped bridge pier. The efficiency of scour protection devices was studied through experiments individually and in combination. They tested several protections for checking their performance individually and possible combinations of all these devices around the oblong pier. The components included a collar plate, a sleeve, and a collared sleeve encircling the pier. Additionally, there were vanes positioned on the upstream side of the bridge pier, along with a passive delta-wing-like device situated at the upstream junction of the pier. Initially, the optimal dimensions and locations of individual protective devices encircling the pier were tested. Subsequently, the devices were examined in combination to assess their collective performance. The findings revealed that the combination of collars and vanes around an oblong pier yielded the most substantial reduction in scour, amounting to approximately 86.36%. They concluded that the combination of two devices was better than the performance of individual devices. The overall factor of safety for a composite device was much higher than that of any of the individual devices.

Negm et al. (2009) studied the optimal shape of the collar to minimize the local scour around the bridge piers. They used a collar which was a protective tool to minimize the maximum local scour around the bridge pier. The authors used three different shapes of collars such as triangular, circular, trapezoidal, and rectangular as protective plates around the bridge pier. They tested every different collar under similar subcritical flow conditions with tail Froude numbers ranging from about 0.2 to 0.55. The experiment was conducted using a recirculating flume of 4m in length, 20cm in depth, and 60cm in width. They measured the water surface and analyzed the scour profiles in detail. The authors developed a statistical equation and proposed to predict the maximum relative scour depth around the bridge pier. They concluded that the use of the optimal shape (rectangular collar) greatly reduces the maximum relative scour depth around the bridge pier to the extent of 90% when the collar width is 5 times the pier width compared to the no collar case.

Mashahir et al. (2010) studied experimentally the application of riprap alone and a combination of riprap and collar to prevent the scour around rectangular bridge piers. The authors investigated piers aligned with the skewed angle at 5°, 10°, and 20° to the flow. In their experiment, they used piers with three different aspect ratios equal to 1:3, 1:5, and 1:7, respectively. They used a constant width of a collar which was equal to three times wider than the piers width around the piers and placed the collar at the streambed level. All experiments were conducted at the threshold of motion of the bed material. They extended the previous method of calculation on stable riprap size around circular piers to the rectangular piers with three different aspect ratios (1:3, 1:5, and 1:7) and three skew angles (5°, 10° and 20°) with and without collar protection. They concluded that the aspect ratio did not affect the stable riprap size when piers were aligned with the flow and increasing skew angle and aspect ratio of the piers, the stable size and extent of the riprap layer also increased. They also concluded that the application of the collar decreased the stable riprap size and quantity of riprap stones. However, the effect of the collar also decreased with increasing pier skew angle and aspect ratio.

Masjedi et al. (2010*a*) studied the oblong collars for reducing the effects of local scour at a bridge pier for the time aspect of the scour development. The study was conducted using a 180° laboratory flume bend. The author conducted one oblong pier with positions of 60° under constant flow conditions. They studied experimentally the time development of the local scour around the oblong pier fitted with and without collar plates. They used four different sizes of collars (1.5, 2, 2.5, and 3 of pier width at stranded level) fitted on the temporal development of scour depth around the oblong pier. They observed that a collar width that was 3 times of pier width represents the maximum reduction (78%) of scour depth. The author compared their study on the time development of the scour hole around the model pier with and without a collar installed with similar studies on bridge piers. The results of the model study indicated that the maximum depth of scour is highly dependent on the experimental duration.

In another work, Masjedi et al. (2010*b*) investigated the time aspect of the local scour development around an oblong pier with an oblong collar in a flume with a 180° bend. They studied the bridge failure case due to the scour hole around the pier that was generated by the river floods. The authors conducted the experiment by using one oblong pier in positions of 60° under constant flow conditions. The experimental study was carried out using a physical hydraulic model that was operated under clear-water conditions in cohesionless bed material. They investigated the time development of the local scour around the oblong pier both the with and without collar plates, respectively. The effect of size and elevation of a collar on the time development of scour was investigated. They observed that the maximum depth of scour was extremely dependent on the experimental duration. The investigation revealed that when an oblong collar with a width of 3 of pier width was positioned at an elevation of 0.1B below the bed, the minimum depth (92% reduction) of scour occurred. The authors concluded that with the expansion of the collar plate dimensions, there was a concurrent decrease in the extent of scour. The depth of scouring was measured through experimental observation, leading to the development of an empirical relation with a 95% regression coefficient.

Heidarnejad et al. (2011) studied the evaluation of the effect of a collar for scouring around an oblong pier in a 180° bend. In their experiment, they used a 6 cm diameter and 18 cm length pier and collar with 1.5, 2, 2.5, and 3 times of pier diameter at bed level in a position of 60° in bend with the constant discharge (32 l/s) and 12 cm water depth under clear water conditions. They concluded that as the maximum depth of the collar plate increases, the scour decreases and a minimum depth of scour is dependent on the collar with 3 times of pier width.

Zokaei et al. (2013) studied the scouring around circular and rectangular piers protected by collars using low-density sediment due to shortening experiment duration. They tested rectangular piers both aligned with the flow and skewed at angles of 5º, 10º, and 20º. They observed that in comparison of low-density sediment with natural sediment, although the relative equilibrium depths were roughly similar, the time to achieve equilibrium conditions decreased to less than 10 hours with low-density sediment. They revealed that for circular and aligned rectangular piers with increasing flow intensity, the collar could reduce maximum scour hole depth by about 20% to 60%, respectively.

Ismael et al. (2014) carried out an experimental study using downstream-facing airfoil shaped piers to reduce scour depth. This study examined three piers (upstream-facing airfoil, downstream-facing airfoil, and circular) under live-bed conditions with a flow intensity of 58 l/s over a duration of 5 hours. In their study, it was observed that the downflow diverged away from the front of the downstream-facing airfoil-shaped pier, resulting in a small vortex that did not impact the pier. The decrease in scour hole volume amounted to approximately 87% compared to a circular pier, with the maximum scour depth reduced by 59% compared to an upstream-facing airfoil and 68% compared to a circular pier.

Salman Beg and Mubeen Beg (2017) carried out an experimental investigation on the variation of scour depth to identify the efficacy of the application of collars to a bevel-nosed rectangular pier to reduce the scour depth. They tested the bevel-nosed rectangular pier (aligned with the flow direction) at low angles of attack with the direction of constant flow condition. They carried out their experiment by using a pier without a collar, with one collar and two collars under steady-state clear water. They found that 76.7% and 81.54% reduction in scour depth was present with the application of one collar at 0° and 15° angles of attack. On the other hand, 43.8% and 45.2% reduction in scour depth were present with the application of two collars at 0° and 15° angles of attack.

Farooq et al. (2017) studied experimentally the influence of pier modification techniques for reducing scour around bridge piers. They observed the temporal development of scour depth around pier modification (plain circular pier, plain octagonal pier, octagonal pier with collar, octagonal threaded pier, octagonal pier with openings) under constant flow conditions. The authors used two different shapes of the pier, i.e., octagonal and circular. The provision of a collar around the octagonal pier reduced more scour depth to that of the other two configurations. They observed that providing a collar around the octagonal-shaped pier resulted in the maximum reduction of scour depth. The scour depth around both circular and octagonal piers was observed and was found to be 9.1% less around the former pier. For the pier with collar, the depth of scour was found 6.8% and 12.3% less than that for the pier with cable and the pier with opening respectively.

Ghaderi and Abbasi (2019) carried out a numerical analysis to identify the local scouring around airfoil-shaped bridge piers with and without collars by using the FLOW-3D model. The authors observed that enlarging the width of the pier's base led to a decrease in the maximum scour depth, effectively mitigating the scouring depth behind the piers. The authors observed that the hole dimensions at the airfoil-shaped pier with length to diameter ratio of 5 were less than other models. The authors concluded that minimal scouring occurs at the rear due to the absence of wake vortices. As the length of the pier increases, the rate of maximum scour depth reduction also increases. Notably, the pier with a length-to-diameter ratio of 5 exhibited the most significant reduction, amounting to 18.69%.

Farooq and Ghumman (2019) studied the effect of pier shape and alternation on scouring around the bridge pier experimentally. This study aims to alleviate flow stagnation and vortex formation in front of the bridge pier. This is achieved through the implementation of a collar, a hooked collar, a cable, and strategically placed openings, both individually and

in combination, around a well-suited pier design. They carried out the study by six different pier shapes to find out the influence of pier shape on local scouring for a length to width ratio smaller than or equal to 3. The authors observed that a plain octagonal shape pier was more effective in reducing scour compared to other pier shapes. In their study, it was noted that the effectiveness of pier modifications was assessed through experimentation with various combinations of collar, hooked collar, cable, and openings on an octagonal bridge pier. This was compared against an unmodified octagonal pier. The researchers concluded that the optimal configuration involved a hooked collar along with a cable and openings surrounding the octagonal pier. This combination resulted in a significant reduction of approximately 53% in scour depth compared to an octagonal pier without a collar.

Moghanloo et al. (2019) studied the effect of increase collar thickness on the flow pattern using the Victorino 3D velocimeter around the oblong bridge pier placed at 90° in a 180° sharp bend with a balanced bed. Data acquisition was performed. In their tests, the collar was consistently positioned at 0.4 times the pier diameter above the initial bed surface. They observed that increasing the collar thickness by a factor of 4 caused the barrier surface to be positioned in the flow path, diverting the flow towards the bed as it collided with the collar's edge. This diversion led to a 30% increase in the maximum depth of the scour hole upstream of the pier. Additionally, the thicker collar increased the tendency of streamlines upstream of the pier to move towards the inner bank, resulting in a 20% increase in maximum sedimentation near the inner bank. They concluded that at 80° of the bend, the highest turbulent kinetic energy (0.000062 m^2/s^2.kg) is observed which decreases scour by 60% when the collar thickness increases.

Abed and Majeed (2020) studied the behavior and effect of the scouring pattern and the spacing between bridge piers by numerical simulation. They carried out their study for a specified hydraulic condition such as velocity of flow, flow depth, and the sediment effective diameter. The authors also studied the cross-section shape of piers and their effect on the scouring depth around bridge piers, using commercial CFD software, ANSYS-Fluent. The authors noticed a reversed proportion between scour depth and the spacing between piers. In their analysis, the pier spacing increased with the decreasing scour depths, for the spacing ratios 2, 3.5, 4.6, 5.5. The maximum scour depths were 32, 34, 37, and 50 mm respectively. They concluded that the minimum scouring depth happened with a triangle-noise pier, then with an oblong shape pier, and a circular section of the pier had maximum scour.

Farooq et al. (2020) carried out an experimental study on the optimal parameters of an octagonal hooked collar to reduce scour around a single bridge pier under a steady uniform state, and with clear water. The author observed that increasing the hooked collar width which was 2.5 times the width of the pier, reduced the maximum scour depth significantly. The researchers observed that the most effective combination involved a hooked collar with width 2.5 times that of the pier and a sidewall height equivalent to 0.45 times the pier width. They concluded the best combination minimized around 73.3% of scour hole depth, compared to an octagonal pier without any modification. With the help of experimental results, they

proposed a new equation to predict the scour depth around a bridge pier fitted with the hooked collar.

Farooq et al. (2021) carried out the performance evaluation of scour protection around a bridge pier by experimental analysis. The authors used several approaches to counterbalance the base of piers from scour and they observed that the collar with protection was more effective for reducing the scour. The authors experimented with the rectangular cross-sectional pier with a rectangular hooked collar at streambed level under clear water conditions. In their experiment, they used different dimensions of hooked collar wall height to hooked collar width (0.05 to 0.30). They observed for all the side wall heights that due to the change of the wall height from 0.3 times of pier width to a higher value, the scour started to increase. On the other hand, by reducing the width of the hooked collar up to 1.5 times of pier width, the authors observed the equilibrium scour depth was significantly decreasing. They concluded that the case of 1.5 times of pier width along with a side wall height of 0.3 times of pier width was the most effective dimension for a hooked collar which may be utilized for rectangular unprotected piers.

Dehghan et al. (2021) studied the effect of collar width ratio on the flow pattern around an oblong pier in a 180° channel (rectangular) bend experimentally. The channel was 1 m in width and 0.7 m in height with upstream and downstream paths 6.5 m and 5 m long, respectively. Experiments were conducted under clear water approach flow conditions. The authors observed that the inclusion of collars around an oblong pier induces vortices opposing the longitudinal flow, leading to the distortion and disruption of streamlines downstream of the pier while diminishing downflow strength at the pier nose. They also observed that doubling the collar width resulted in 0.93 and 0.68 times the vorticity and power of the secondary flow, respectively, at the pier upstream.

Keshavarz et al. (2021) studied the flow patterns around models for rectangular and oblong piers with a collar located at the 90° angle in the middle of the 180° sharp bend. They observed the 3D flow velocity data using a Victorino 3D velocimeter. They discussed the contour plots of mean velocity components, the variations of mean angular velocity, shear stress, secondary flow intensity, kinetic energy, and streamlined flow. They showed through their results that the scour area was much higher with the installation of the rectangular pier than with the use of the oblong pier. Moreover, they concluded that the installation of the oblong pier decreased the maximum secondary flow intensity and angular velocity by 35% and 45%, respectively in comparison to the rectangular pier. Additionally, it was discovered that there was no significant difference in the maximum turbulence kinetic energy around the two piers' reduced shear stress.

Safaei et al. (2021) studied experimentally the efficiency of the flexible collar on a bridge pier for reducing scour depth. Extensive research has been conducted by the authors to reduce and control destructive phenomena. They carried out their experiment with the help of the direct method. The experiment was conducted under clear water conditions with an adjustable chain collar, which was three times bigger than the pier's width. In their experiment, three different diameters of the chain collar were used such as 5 mm, 10 mm, and 15 mm, and

three dimensionless flow parameters (*U/Uc*= 0.73, 0.85, and 0.96) were selected to investigate the effect of flow conditions. They concluded that the scour depth was related to changes in the diameter of the collar chain, as the final scour depth decreased by increasing the diameter of the chain from 5 mm to 15 mm. The authors proposed the best condition of the chain collar which was 15 mm diameter.

Moghanloo et al. (2022) studied experimentally to evaluate the effect of the level and thickness of the collar on scouring around the pier in a 180° sharp bend and a relative curvature radius equal to 2. They conducted all experiments with the same discharge equal to 70 l/s. They showed that placing the collar at the initial bed surface and collar (0.4 times of pier width) placed at below the initial bed level with a thickness of 0.12 and collar with 0.06 times of the pier width, achieved the most effective reduction in scouring when the pier was positioned at a 90° bend. They concluded that reduction of the maximum scour hole depth by 70% compared to not using the collar. At 60° and 120° positions, the thickness parameter didn't significantly affect scouring, and the optimal collar level was the same as for the pier at a 90° bend.

Bento et al. (2023) studied both numerically and experimentally the scour pattern around an oblong pier. The author studied Computational Fluid Dynamics (CFD) with the Sediment Simulation in Intakes with Multiblock option (SSIIM) tool to numerically examine the scour depth around an oblong bridge pier and the temporal and distribution of bed shear stress in time. They used Laboratory data and scour characterization results around a 0.11 m wide oblong bridge pier to calibrate and validate the numerical model. The averaged form of the Navier–Stokes equations was employed to simulate turbulent flow fields for extended time scales. They concluded that the calibrated numerical models can accurately replicate measured scour depths in laboratory settings, with an average relative error of less than 3%, particularly around oblong bridge piers.

Dehghan et al. (2023) studied the effects of the width of the collar on the scouring effect around the rectangular piers in a 180° bend experimentally. The authors investigated the mechanism of scouring surrounding the combination of pier and collar. They also investigated experimentally the effect of various collar width to pier width ratios on the reduction of scouring parameters surrounding the rectangular piers in various 180° sharp bend positions. The authors carried out their experiment under the clear water and threshold of sediment motion in the upstream straight path. They observed that collar width to pier width ratios equal to 3 to 4 perform the best at reducing the maximum depth of scouring in front of the nose of piers. They also observed that the increasing width of the collar reduces the maximum depth of scouring. The authors also noticed that lengthening the pier diminishes the collar's ability to effectively delay the scour process at the pier nose and also reduces the extent of maximum scour reduction. In their findings, it was determined that the most significant reduction in scour depth took place around the pier and its collar, specifically in the 90° section. This reduction was observed when the collar width to pier width ratio of 4, was installed around the piers having length-to-width ratios of 2 and 3, resulting in reductions of approximately 75% and 70%, respectively.

Farooq et al. (2023) investigated the effects of hooked-collar on the scour development around a vertical pier with a lenticular cross-section experimentally. They considered the flow around the pier as uniform, steady, and under the clear-water condition. The effects of hooked collar dimensions and the elevation from the bed were measured for the axial scour profiles without and with a lenticular hooked collar. A wide range of hooked-collar geometries such as the ratio of collar width to the pier width (from 1.5 to 3.5), the ratio of hooked-collar wall height to the pier width (from 0.15 to 0.6), and the ratio of collar elevation to the pier width (0.5, 0, and 0.5) were tested. They observed that the equilibrium scour depth decreased with the ratio of the hooked collar to the pier width when the collar width was twice the pier width. They also observed that the scour depth steadily reduced when the hook collar to pier width ratio approached 0.3. The authors achieved maximum efficiency of scour reduction when the hooked collar was placed on the bed surface. Finally, the authors developed models for the prediction of maximum scour depth near the lenticular bridge pier with a modified collar. The findings revealed a non-linear increase in the volume of the scour hole around a lenticular pier in correlation with the maximum scour depth, and this behavior remained unaffected by the geometry of the hooked collar.

Solati et al. (2023) studied the scour pattern around nine different shapes of the pier in 180° sharp bend under unsteady currents. They conducted three different locations of pier along a 180° bend, across four flood durations. Additionally, four ratios of rising limb to flood duration were considered for the 100-minute flood durations. In total, 196 tests were conducted, encompassing seven tests carried out within the bend without piers. They showed that the deepest scour hole in front of piers of various shapes depended on flood duration, with the ratio of ascending to descending branch having minimal impact on the final maximum scour hole depth around the pier. The author also concluded that the scour hole volume was influenced by the pier's nose and cross-sectional shape, with the rectangular pier exhibiting a greater scour hole volume compared to other pier shapes.

After a detailed literature review, the developed non-dimensional governing equations of the variation of the scour parameters with spatial and temporal coordinates by different researchers for different shapes of the pier are listed in Table 2.1.

Based on the literature reviewed above, it is evident that numerous studies have been conducted on scour around the bridge pier. These studies have shown significant results in reducing scour around oblong piers with oblong collars. However, while many investigations have focused on oblong piers with collars situated on bend channels, there remains a gap in research concerning oblong piers with oblong collars positioned on straight channels. Additionally, the detailed geometric influence of collar dimension on scour phenomena, particularly concerning temporal variations around oblong piers with oblong collars for straight channels, has not been thoroughly explored.

Photographs of oblong piers in various locations across West Bengal, as shown in Figs. 2.1 and 2.2.

Table 2.1. Functional relationship for non-circular shape pier.

Literature	Pier shape	Function
Negm et al. (2009)	Rectangular	$\frac{d_s}{h} = \exp\left(5.48\mathrm{Fr} - 0.16W - 1.32k_s - 2.5\right)$
Dehghan et al. (2023)	Rectangular	$\frac{d_s}{h} = 0.0538\frac{L}{D} - 0.2305\frac{W}{D} + 1.0468$
Masjedi et al. (2010)	Oblong	$\frac{d_s}{D} = f\left(\frac{W}{D}, \frac{H}{D}, \frac{t}{t_m}\right)$
Bhattacharya et al. (2003)	Oblong	$\frac{d_s}{D} = 1.03N\left(\frac{h}{D}\right)^{0.35} \mathrm{Fr}^{0.58} f_1\left(\frac{L}{D}\right) f_2(\alpha)$
Safaei et al. (2021)	Square	$\frac{d_s}{D} = f_3\left(\frac{ds}{ds_{\max}}, \frac{W}{D}, \frac{U}{U_c}, \frac{t}{t_e}\right)$
Heidarnejad et al. (2011)	Oblong	$\frac{d_s}{D} = f_4\left(\frac{W}{D}, \frac{H}{D}, \frac{t}{t_e}\right)$
Farooq et al. (2020)	Octagonal	$\frac{d_s}{D} = \frac{W}{D} \times \frac{A_c}{A_t} \times \frac{L_{hc}}{D}$
Farooq et al. (2022)	Lenticular	$\eta = \frac{d_{sp} - ds}{ds} = f_5\left(\frac{H}{D}, \frac{A_c}{A_t}\right)$
Ghaderi et al. (2019)	Airfoil	$f_6\left(\frac{D_{50}}{D}, \frac{Ut}{D}, \frac{L}{D}\right) = 0$



Fig. 2.1. Hanskhali bridge with oblong shaped piers located in Nadia district, West Bengal, India.



Fig. 2.2. Murti Bridge with oblong shaped piers located in Jalpaiguri district, West Bengal, India.

Therefore, the present study aims to address these gaps by conducting experimental research on oblong piers with oblong collars along straight paths. The experimental work focused on identifying the effect of variation of collar dimension on scour reduction along the oblong pier with an oblong collar. Our final objective is to develop a nondimensional governing equation for scour reduction by oblong piers with oblong collars along straight paths. The experimental methodology and setup are elaborated upon in the subsequent chapter.

Chapter 3

Methodology

In the present chapter, the methodology of the experimental procedure of the present study is presented. The selection of the experimental flow condition, dimension of the pier and collar, and parameters that affect scour depth around the pier and experimental setup are elaborated in detail here.

3.1 Objectives

The research presented in this thesis emanates from experimental investigations carried out at the Fluvial Hydraulics Laboratory, located within the School of Water Resources Engineering at Jadavpur University. Our study aims to analyses the scour patterns around oblong piers using oblong collars under clear water conditions. Specifically, our investigation explores scenarios characterized by uniform cohesionless bed material, consistent flow conditions and clear water flow. Through precise experimentation and analysis conducted within this controlled setting, our objective is to enhance comprehension of bed morphology under such conditions.

To assess the scour profile around oblong piers with and without collars, twelve experiments were conducted. These experiments were divided into two sets. The first set involved a pier with dimensions of 14 cm in length and 7 cm in width, with collar dimensions ranging from 1.5 to 3.5 times greater than the pier's dimensions. Conversely, the second set of experiments utilized a pier measuring 28 cm in length and 7 cm in width, with collar dimensions also varying from 1.5 to 3.5 times greater than the pier's dimensions. The various pier and collar dimensions are illustrated in Fig. 3.1.

It is important to note that the selection of these dimensions and their associated ratios for the pier and collar was not arbitrary. A comprehensive analysis of existing literature was conducted to identify pertinent parameters, which will be discussed in the subsequent sections.

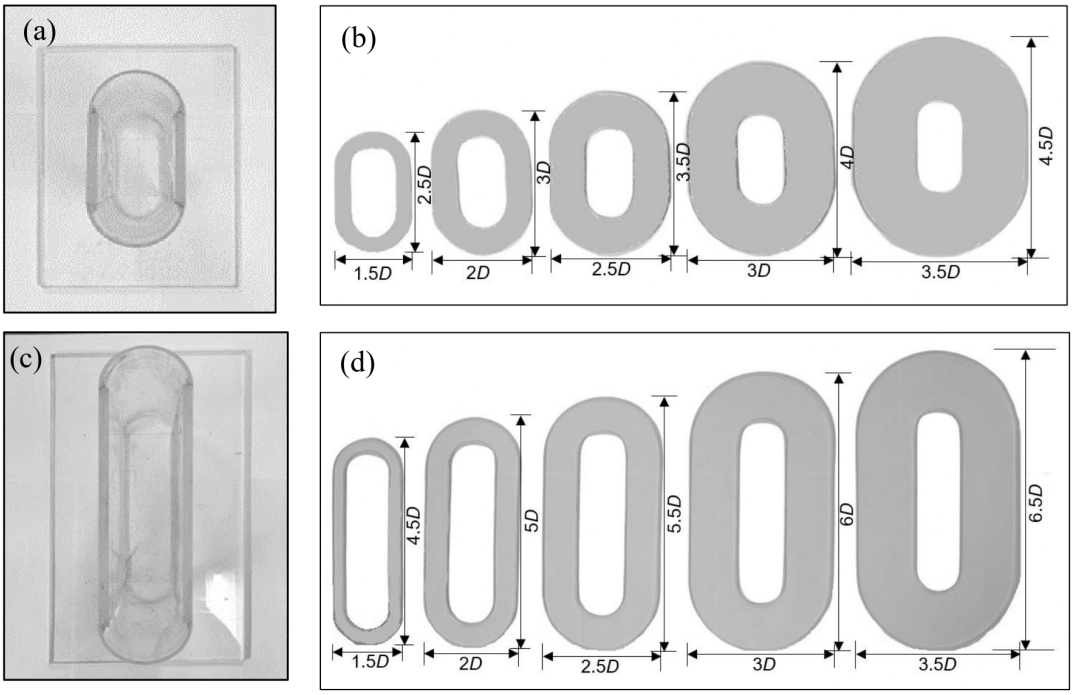


Fig. 3.1. Different dimensions of (a) pier and (b) collar for *L*/*D* ratio 2 and (c) pier and (d) collar for *L*/*D* ratio 4.

3.2 Selection of parameters for experiments

The selection of the parameters of the experimental apparatus plays a pivotal role in the design and execution of scientific investigations. The precision and accuracy of experimental outcomes depend heavily on the careful consideration and optimization of various parameters associated with the apparatus used. This introductory phase involves a meticulous evaluation of key factors such as equipment specifications, operating conditions, and measurement techniques, all of which collectively contribute to the reliability and validity of experimental results. Figure 3.2 represents the dimensions of the pier and collar.

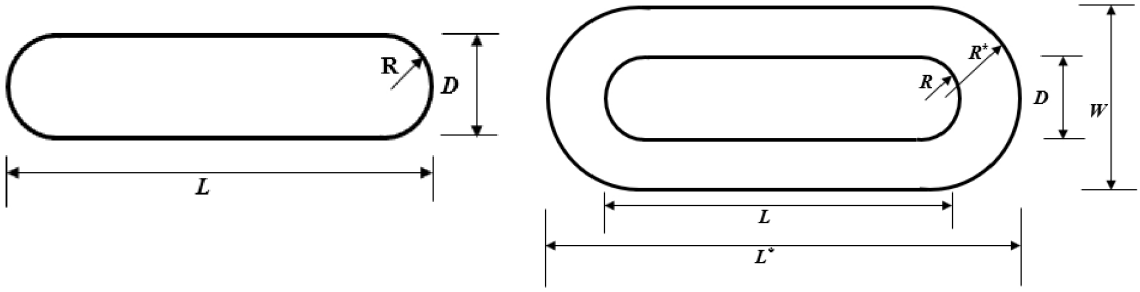


Fig. 3.2. Schematic diagrams of (a) pier and (b) pier with collar.

3.2.1 Determination of oblong pier dimension

In the present analysis, the length of the pier (L) was chosen as 14 cm to maintain a length-to-width ratio of 2, consistent with the experimental findings of Bhattacharya et al. (2003) and Dehghan et al. (2021). It's important to note that the width of the pier is fixed at 7 cm in the laboratory. Hence, the selection of a length of 14 cm aligns with the experimental range utilized by Garg et al. (2008), Bhattacharya et al. (2003), Dehghan et al. (2021) and Masjedi et al. (2010).

On the other hand, a different length of 28 cm was utilized to maintain a length-to-width ratio of 4, consistent with the experimental analysis by Dehghan et al. (2021), Moghanloo et al. (2019), Moghanloo et al. (2020) and Zarrati et al. (2004). Also, according to Melville and Sutherland (1988), the ratio of pier length to width should be greater than 3.

Throughout the experiment, care was taken to ensure that the width of the experimental flume exceeded seven times the pier width (D) to mitigate the wall friction factor. The minimum ratio of flume width to pier width, as suggested by Raudkivi and Ettema (1983), is 6.25, which could be employed without any measurable effect from the side walls on the local scour at the pier.

3.2.2 Determination of oblong collar dimension

The width of the collar (W) is chosen 10.5 cm, 14 cm, 17.5 cm, 21 cm and 24.5 cm to maintain the collar width to pier width ratio 1.5, 2, 2.5,3 and 3.5 with the experimental analysis by Bhattacharya et al. (2003), Mashahir et al. (2004), Zarrati et al. (2004), Garg et al. (2008), Negm et al. (2009), Masjedi et al. (2010) and Dehghan et al. (2021).

The position of the collar plate is chosen at bed level to reduce scour as much as possible. It is consistent with the experimental ranges used by Bhattacharya et al. (2003), Mashahir et al. (2004), Zarrati et al. (2004), Garg et al. (2008), Negm et al. (2009), Masjedi et al. (2010), Moghanloo et al. (2019, 2020) and Dehghan (2021).

The dimensions of the pier and collar are chosen based on thorough literature reviews. The details are presented in Table 3.1. It is to be mention that collar length (L^*) is express as a function of pier width (D), as presented in the table below.

Table 3.1. Dimension of pier and collar selected based on previous literatures.

Literature	Pier width (D) (cm)	Pier length (L) (cm)	Collar width (W)	Collar length (L^*)
Bhattacharya et al. (2003)	4	8, 12, 16	3D	5D, 7.5D, 10D
Mashahir et al. (2004)	5	25	3D	5D

Zarrati et al. (2004)	5	25	2*D*, 3*D*	7*D*, 8*D*
Mashahir et al. (2008)	5	15	3*D*	5*D*, 7*D*, 9*D*
Negm et al. (2009)	3	40	1.5*D*, 3*D*, 3.5*D*, 5*D*	-
Mashahir et al. (2010)	5	15	3*D*	5*D*
Masjedi et al. (2010)	6	18	1.5*D*, 2*D*, 2.5*D*, 3*D*	5*D*, 4.5*D*, 3*D*, 3.5*D*
Zokaei et al. (2013)	5	25	3*D*	8*D*
Moghanloo et al. (2019)	5	20	4*D*	8*D*
Moghanloo et al. (2020)	5	20	7*D*	16*D*
Dehghan et al. (2021)	5	20	2*D*, 4*D*	-
Dehghan et al. (2023)	5	10, 15, 20	1.5*D*, 2*D*, 2.5*D*, 3*D*, 4*D*, 5*D*	-
Present study	7	14, 28	1.5*D*, 2*D*, 2.5*D*, 3*D*, 3.5*D*	4.5*D*, 5*D*, 5.5*D*, 6*D*, 6.5*D*

3.2.3 The parametric range of the present experimental analysis

The parametric range of the present experimental analysis is presented in Table 3.2.

Table 3.2. The parametric range of present experimental analysis.

Exp. Number	Details	*L/D*	*W/D*	*D* cm	*L* cm	*W* cm	*L** cm	*Q* l/s	*h* cm	*R* cm	σ_g	D_{50} mm	U/U_c	Fr
1	Oblong pier	4	0	7	14	0	0	25.5	11.5	3.5	1.68	0.724	0.825	0.26
2	Oblong pier with collar	4	1.5	7	14	10.5	31.5	25.5	11.5	3.5	1.68	0.724	0.825	0.26
3		4	2.0	7	14	14.0	35	25.5	11.5	3.5	1.68	0.724	0.825	0.26
4		4	2.5	7	14	17.5	38.5	25.5	11.5	3.5	1.68	0.724	0.825	0.26
5		4	3.0	7	14	21.0	42	25.5	11.5	3.5	1.68	0.724	0.825	0.26
6		4	3.5	7	14	24.5	45.5	25.5	11.5	3.5	1.68	0.724	0.825	0.26
7	Oblong pier	2	0	7	28	0	0	25.5	11.5	3.5	1.68	0.724	0.825	0.26
8	Oblong pier with collar	2	1.5	7	28	10.5	17.5	25.5	11.5	3.5	1.68	0.724	0.825	0.26
9		2	2.0	7	28	14.0	21	25.5	11.5	3.5	1.68	0.724	0.825	0.23
10		2	2.5	7	28	17.5	24.5	25.5	11.5	3.5	1.68	0.724	0.825	0.23
11		2	3.0	7	28	21	28	25.5	11.5	3.5	1.68	0.724	0.825	0.23
12		2	3.5	7	28	24.5	31.5	25.5	11.5	3.5	1.68	0.724	0.825	0.23

It is to be mentioned that the range of the parameters of the following experimental apertures is chosen based on the thorough literature reviews of the existing experimental, analysis on the oblong pier.

3.2.4 Selection of flow condition

The discharge rate selected was 25.5 l/s. This choice was influenced by prior research conducted in our laboratory, where a significant number of experiments utilized the same discharge rate. Consequently, we selected this specific discharge rate to facilitate future comparisons between our study and others in the field.

The flow depth within the flume was regulated using a tailgate mechanism. Across all experimental runs, the incoming flow depth (h) was consistently set at 11.5 cm. Additionally, the bed slope S_0 maintained at a ratio of 1:2400 remained unchanged throughout all the experiments.

Table 3.3. Parameters affecting scour depth around the pier with time.

Literature	**Pier Shape**	Q	B	h	D_{50}	D	W	H	K_s	θ	ρ_s	σ_g	U/U_c	**Fr**	d_s	t
Mohammad et al. (2008)	Rectangular	Q	B	h	D_{50}	D	W	H	×	θ	×	×	U/U_c	×	d_s	t
Masjedi et al. (2010)	Oblong	Q	B	×	D_{50}	D	W	×	×	θ	×	×	U/U_c	Fr	d_s	t
Albani et al. (2006)	Oblong	Q	B	×	D_{50}	D	W	×	×	θ	×	σ_g	U/U_c	Fr	d_s	t
Ettema et al. (2004)	Oblong	Q	B	×	D_{50}	D	W	×	×	θ	×	σ_g	U/U_c	Fr	d_s	t
Masjedi et al. (2010)	Oblong	Q	B	×	D_{50}	D	W	×	×	θ	×	σ_g	U/U_c	Fr	d_s	t
Melville and Raudkivi (1996)	Oblong	Q	B	×	D_{50}	D	W	×	×	θ	×	σ_g	U/U_c	Fr	d_s	t
Masjedi et al. (2010)	Oblong	Q	B	×	D_{50}	D	W	×	×	θ	×	σ_g	U/U_c	Fr	d_s	t
Negm et al. (2009)	Rectangular	×	B	×	x	D	W	×	×	×	×	σ_g	U/U_c	Fr	×	×
Mashahir et al. (2004)	Oblong	×	B	×	D_{50}	D	W	H	×	×	×	σ_g	U/U_c	Fr	d_s	t
Farooq et al. (2017)	Octagonal	Q	B	h	D_{50}	D	W	H	×	×	ρ_s	σ_g	U/U_c	Fr	d_s	t
Farooq et al. (2020)	Octagonal	Q	B	h	D_{50}	D	W	×	×	×	ρ_s	σ_g	U/U_c	Fr	d_s	t
Safaei et al. (2021)	Square	Q	B	h	D_{50}	D	×	×	K_s	×	ρ_s	σ_g	U/U_c	Fr	d_s	t
Farooq et al. (2019)	Octagonal	Q	B	h	D_{50}	D	×	×	×	×	ρ_s	×	U/U_c	Fr	d_s	t
Ghaderi et al. (2019)	Airfoil	×	B	h	D_{50}	D	×	×	×	×	ρ_s	×	U/U_c	Fr	d_s	t
Ismarl et al. (2014)	Airfoil	Q	B	h	D_{50}	D	W	×	×	×	ρ_s	σ_g	×	×	d_s	t
Present study	Oblong	Q	B	h	D_{50}	D	W	H	K_s	θ	ρ_s	σ_g	U/U_c	Fr	d_s	t

The critical bed shear stress (τ_{0c}) was determined by using the expression for the critical Shields parameter, $\Theta\left(=\tau_{0c}/\Delta\rho_f gd\right)$ which was developed by van Rijn (1984). From van Rijn's (1984) empirical equations of the Shields curve the value of the critical Shields parameter was calculated where the particle parameter, $D_*\left(=d\left(\Delta g/\nu^2\right)^{0.333}\right)$ = 20.06. Then the equation of critical bed shear stress becomes as $\tau_{0c} = 0.0319\,\Delta\rho_f gd$ (equivalent to 0.4084 N/m^2).

The critical condition of the bed was examined before the experiment run using steps 2 to 6. The depth-averaged approaching flow velocity (U) was estimated using Manning's equation ($U = \frac{1}{n} R^{\frac{2}{3}} S^{\frac{1}{2}}$). Here, the coefficient of roughness (n) was determined by using Strickler's formula ($n = \frac{1}{24} d_{50}^{\frac{1}{6}}$). From the sieve analysis experiment, the median diameter of sand (D_{50}) was determined as 0.825 cm.

Then critical shear velocity (U_{*c}) was calculated using $U_{*c} = \sqrt{\frac{\tau_0}{\rho_f}}$ = 0.01997. Therefore, U_c can be calculated from $\frac{U_c}{U_{*c}} = 5.75\log\left(\frac{h}{2d_{50}}\right) + 6$ where U_{*c}, h, d_{50} are already known. U_c calculate is 0.34 m/s.

It is to be mention that the range of use in the present analysis falls within the parametric range utilized by earlier researchers, as shown in Table 3.4. Since the present analysis uses a lot of data from previous studies, gathering the measured parameters from the original sources was quite difficult. Some research articles do not provide access to the measured data that other researchers used. It is to be mention that in the present analysis, the all the parameter affecting the scour depth with time is considered and it is presented in Table 3.3.

Table 3.4. Maximum and minimum values of parameters.

Literature	Pier Shape	Range	Q	B	h	D_{50}	D	W	K_s	ρ_s	σ_g	U/U_c	Fr	d_s	t
			l/s	cm	cm	mm	cm	cm		kg/m^3				cm	hr
Masjedi et al. (2010a)	Oblong	min	35	60	45	2	6	9	0.85	2700	1.7	0.89	0.41	0.60	0.03
		max	35	60	45	2	6	18	0.85	2700	1.7	0.89	0.41	3.09	5.03
Albani (2006)	Oblong	min	35	60	45	2	6	12	0.85	2700	1.7	0.89	0.41	1.50	0.08
		max	35	60	45	2	6	12	0.85	2700	1.7	0.89	0.41	6.50	5.01
Ettema. (2004)	Oblong	min	35	60	45	2	6	12	0.85	2700	1.7	0.89	0.41	1.90	0.12
		max	35	60	45	2	6	12	0.85	2700	1.7	0.89	0.41	5.98	4.98
Masjedi et al. (2010b)	Oblong	min	35	60	45	2	6	12	0.85	2700	1.7	0.89	0.41	2.10	0.83
		max	35	60	45	2	6	12	0.85	2700	1.7	0.89	0.41	6.00	7.00
Melville and Raudkivi (1996)	Oblong	min	35	60	45	2	6	15	0.85	2700	1.7	0.89	0.41	2.00	0.02
		max	35	60	45	2	6	15	0.85	2700	1.7	0.89	0.41	6.01	5.02
Mashahir (2004)	Oblong	min	35	75	45	0.95	5	15	1.22	2700	1.2	0.92	0.30	1.31	0.63
		max	35	75	45	0.95	5	15	1.22	2700	1.2	0.92	0.30	6.79	51.7
Farooq (2017)	Octagonal	min	67	100	18	0.42	7	22	0.93	2790	1.4	0.89	0.26	0.50	0.78
		max	67	100	18	0.42	7	22	0.93	2790	1.4	0.89	0.26	4.80	7.99
Farooq (2020)	Octagonal	min	48	100	15	0.88	6	9	0.93	2560	1.4	0.89	0.26	0.50	0.14
		max	48	100	15	0.88	6	21	0.93	2560	1.4	0.89	0.26	5.11	24.1
Ismael (2014)	Airfoil	min	58	80	12.5	1.45	4	20	0.80	2650	3.1	0.89	0.51	1.77	0.49
		max	58	80	12.5	1.45	24	120	0.80	2650	3.1	0.89	0.20	8.31	5.01
Present study	Oblong	min	25.5	81	11.5	0.73	7	10.5	0.85	2700	1.7	0.82	0.26	0.04	0.08
		max	25.5	81	11.5	0.73	7	24.5	0.85	2700	1.7	0.82	0.26	3.72	9.00

3.3 Experimental setup

The experimental arrangement, data acquisition system and variables measured in the model study are described. Various experiments were conducted to investigate the development of scour depth around oblong piers with collars. Detailed descriptions of the experimental setup and conditions are provided. All experiments were performed at the Fluvial Hydraulics Laboratory (refer to Fig. 3.3.) located at the School of Water Resources Engineering, Jadavpur University, Kolkata.



Fig. 3.3. Tilting flume used during the experimentation.

3.3.1 Tilting flume

The experiments take place in a recirculating flume measuring 11 m in length, 0.81 m in width, and 0.60 m in depth (as depicted in Figs. 3.3. and 3.4.). The working section of the flume is uniformly filled with sand to a thickness of 0.20 m. The sand bed spans a length of 7 m and a width of 0.81 m, positioned 2.9 m upstream from the flume inlet. For most of its length, the working section comprises a steel bottom and Plexiglas side walls on two sides to facilitate visual observations. A centrifugal pump at the upstream end of the flume serves the recirculating flow system

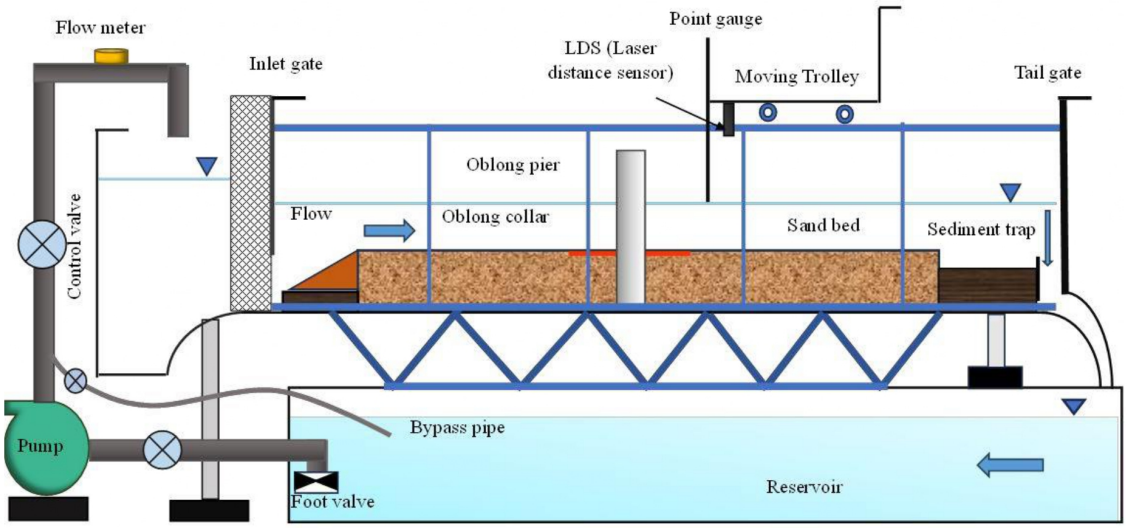


Fig. 3.4. Schematic diagram of the tilting flume.

3.3.2 Pump

The hydraulic machines which convert mechanical energy into hydraulic energy are known as pumps. Hydraulic energy is in the form of pressure energy. In our setup, a centrifugal pump, rated at 10 horsepower and variable speed, serves the recirculating flow system positioned at the upstream end of the flume (refer to Fig. 3.5.). Water is conveyed through a 200 mm diameter pipeline directly into the flume. The pump operates at 1430 revolutions per minute (rpm), with a power output of 7.5 kilowatts (kW), and can achieve a maximum discharge rate of 30 l/s. Additionally, there are two pumps available for alternate use. Discharge measurement is facilitated by water passing through a flow meter.



Fig. 3.5. Pump used to recirculate the flow.

3.3.3 Sediment bed

A set of experiments is conducted using the sand bed material, as depicted in Fig. 3.4. In the laboratory, we conducted a mechanical sieve analysis and measured the specific gravity of sand particles. The particle sizes were determined as follows: D_{50} is 0.724 mm, D_{16} is 0.44 mm, D_{84} is 1.458 mm and D_{90} is 1.65 mm. Additionally, the geometric standard deviation of sediment size (σ_g) is calculated to be 1.68. The density of the sand is measured to be 2.58.

After positioning the piers correctly and ensuring proper alignment, a uniform sand bed was prepared. For a successful experiment, it's crucial to have a well-prepared, smooth and uniform sand surface, as it significantly contributes to achieving accurate and reliable experimental results. A flat sand bed measuring 3 m in length and 0.81 m in width was meticulously arranged, and its flatness was verified using a spirit level. The preparation of the sand bed was done for each new arrangement of piers.

3.3.4 Acoustic doppler velocimeter

The Vectrino is a high-resolution acoustic velocimeter used to measure turbulence and 3D water velocity in a wide variety of applications from the laboratory to the ocean. The basic measurement technology is coherent Doppler processing, which is characterized by accurate data and no appreciable zero offset. We measure the temporal evolution of scour depth using an Acoustic Doppler Velocimeter, as shown in Fig. 3.6. Model number of the Vectrino Velocimeter: VECTRINO PROFILER FIXED PROBE 10 MHz, 4198-1-131. Probe ID: VON 9619, Hardware ID: VNO 1617 Uw Housing.



Fig. 3.6. Acoustic Doppler Velocimeter. Apparatus of the Acoustic Doppler Velocimeter; 1- Transportation and storage case; 2- Vectrino Velocimeter; 3- External power/signal cable; 4 Tool kit, Nortek; 5-USB to serial converter; 6-Seeding material (bottle of 250 ml); 7-AC/DC voltage transformer, 24 V DC; 8-International kit with AC plugs; 9-USB memory stick with Vectrino software.

3.3.5 Laser distance meter

Laser distance meters are utilized to precisely measure the distance between objects without physical contact, employing laser technology for this purpose. The grid point was measured using a Laser Distance Meter, specifically the DISTOTM D110 model, as shown in Fig. 3.7. It is important to note that these measurements were taken after the sand bed had been thoroughly dried. This ensured the accuracy and reliability of the grid point data.



Fig. 3.7. Laser Distance Meter.

3.3.6 Flow meter

A Flow Meter is a device designed to monitor, measure, or record the flow rate, pressure, or discharge of liquids or gases. It serves a crucial role in various applications across industries, ensuring precise management and control of fluid dynamics. In our experiment, we used a flow meter to measure the discharge rate, as depicted in Fig. 3.8. Specifically, we employed the DASMESH model flow meter for these measurements, ensuring the acquisition of precise and dependable data for our analysis.



Fig. 3.8. Flow Meter.

3.4 General experimental procedure

The present study focuses on examining the scour profile around an oblong pier with an oblong collar under clear water conditions. Detailed descriptions of the experimental setup and study conditions are provided. All experiments were conducted at the Fluvial Hydraulic Laboratory of the School of Water Resources Engineering at Jadavpur University, Kolkata, India. The experiments were conducted with a constant water depth of 11.5 cm and a discharge rate of 25.5 l/s. The Froude number (Fr) ranged from 0.17 to 0.29.

The oblong pier was first placed at the center of the flume. Prior to each experiment, meticulous attention was given to levelling the sand bed uniformly along the entire length of the flume and perpendicular to the pier with the collar. Subsequently, the bed level was measured using a point gauge at random locations to ensure the flume's levelness. The preparation of the sand bed played a crucial role in the experiment, as any unevenness or flaws in the channel bed could potentially compromise the integrity of the experiment.

To initiate the experiment, the flume is gradually filled with water to the desired depth. Extra caution is exercised during this process, particularly for experiments where sediment movement is restricted. Any irregularities in the bed surface could lead to the formation of ripples, dunes, or general sand movement if the shear stress approaches the critical threshold on the smooth bed.

Once the water level is reached, the pump is activated, and the flow rate is adjusted using control valves and a bypass valve. Simultaneously, the tailgate is adjusted to maintain the desired depth consistently throughout the experiments. Throughout the testing period, the location and extent of maximum scour depth are continuously recorded.

The frequency of scour depth measurements varied during the test, with more frequent readings taken during the initial hour and less frequent readings as the test progressed. The

maximum scouring rate typically occurs between 1 to 3 hours into the experiment, decreasing in frequency thereafter.

All experiments run for a duration of 6 to 7 hours. Upon completion, the pump is stopped to allow the flume to gradually drain without disturbing the scour topography. The scour area is then measured using a laser distance sensor (LDS), and contour lines of different collar and pier dimensions are analyzed using Surfer software.

The above section outlines the methodology adopted in the present study. While various researchers in the literature have used different methodologies, we identified several parameters that affect temporal scour depth. Consequently, a dimensionless framework incorporating all these parameters is presented in the next chapter.

Chapter 4

Dimensionless Analysis

In this chapter, a comprehensive dimensionless analysis of the experimental parameters from the current study is conducted. This analysis aims to provide a deeper understanding of the underlying relationships and behaviors observed in the experimental data by eliminating units and focusing on the relative magnitudes and interactions of the parameters involved.

Development of scour depth d_s changed with temporal time t can be a function of

$$d_s = f_7(B, h, H, D_{50}, D, W, L, L^*, K_s, \theta, \rho, \rho_s, \sigma_g, \mathrm{Fr}, U, U_c, t) \tag{4.1}$$

where, d_s is the depth of scour with time t and the dimension of d_s is $[L]$ or $\left[M^0L^1T^0\right]$

ρ is fluid density for flow which has a dimension of $\left[ML^{-3}\right]$ or $\left[M^1L^{-3}T^0\right]$

h is the depth of flow and the dimension of h is $[L]$ or $\left[M^0L^1T^0\right]$

U is the mean velocity of flow and the dimension is $\left[LT^{-1}\right]$ or $\left[M^0L^1T^{-1}\right]$

D_{50} is the mean size of sand particles which has an also dimension of length $[L]$ or $\left[M^0L^1T^0\right]$

ρ_s is sediment density and the dimension of ρ_s is $\left[ML^{-3}\right]$ or $\left[M^1L^{-3}T^0\right]$

U_c is critical flow velocity having a dimension the same as the mean velocity of flow $\left[LT^{-1}\right]$ or $\left[M^0L^1T^{-1}\right]$

L is the pier length which has a dimension of $[L]$ or $\left[M^0L^1T^0\right]$

D is the pier width which has a dimension of $[L]$ or $\left[M^0L^1T^0\right]$

L^* is the collar length which has a dimension of $[L]$ or $\left[M^0L^1T^0\right]$

W is the collar width which has a dimension of $[L]$ or $\left[M^0L^1T^0\right]$

H is the height of the collar above the bed which has a dimension of $[L]$ or $\left[M^0L^1T^0\right]$

θ is the pier skewed angle which has a dimensionless of $\left[M^0L^0T^0\right]$

K_s is the pier shape factor which has a dimensionless of $\left[M^0L^0T^0\right]$

Fr is the Froude Number which has a dimensionless of $\left[M^0L^0T^0\right]$

σ_g is Standard Deviation which has a dimensionless of $\left[M^0L^0T^0\right]$

B is the width of the channel which has a dimension of $\left[L\right]$ or $\left[M^0L^1T^0\right]$

t is the temporal time which has a dimension of $\left[T\right]$ or $\left[M^0L^0T^1\right]$

Now, the Buckingham Pi theorem is used to determine the dimensionless parameters. The theorem states that if there are m number of variables and n fundamental dimensions, then there will be (*m* - *n*) π terms.

The total number of variable (*m*)= 18

And the number of fundamental dimensions is *M* (mass), *L* (length), and *T* (time).

Therefore, *n* = 3.

Hence the number of π terms = *m* – *n* =18 – 3 = 15

$$f_8(\pi_1,\pi_2,\pi_3....\pi_{15}) = 0 \tag{4.2}$$

After considering the repeating variables of Eq. (1) as per Buckingham Pi theorem, a total of 15 numbers of Pi (π) terms are identified and they are presented as follows.

$$\pi_1 = W^{a1}U^{b1}\rho^{c1}ds \tag{4.3}$$

$$\pi_2 = W^{a2}U^{b2}\rho^{c2}B \tag{4.4}$$

$$\pi_3 = W^{a3}U^{b3}\rho^{c3}h \tag{4.5}$$

$$\pi_4 = W^{a4}U^{b4}\rho^{c4}H \tag{4.6}$$

$$\pi_5 = W^{a5}U^{b5}\rho^{c5}D_{50} \tag{4.7}$$

$$\pi_6 = W^{a6}U^{b6}\rho^{c6}D \tag{4.8}$$

$$\pi_7 = W^{a7}U^{b7}\rho^{c7}U_c \tag{4.9}$$

$$\pi_8 = W^{a8}U^{b8}\rho^{c8}L \tag{4.10}$$

$$\pi_9 = W^{a9}U^{b9}\rho^{c9}L^* \tag{4.11}$$

$$\pi_{10} = W^{a10}U^{b10}\rho^{c10}K_s \tag{4.12}$$

$$\pi_{11} = W^{a11}U^{b11}\rho^{c11}\theta \tag{4.13}$$

$$\pi_{12} = W^{a12}U^{b12}\rho^{c12}Fr \tag{4.14}$$

$$\pi_{13} = W^{a13}U^{b13}\rho^{c13}\sigma_g \tag{4.15}$$

$$\pi_{14} = W^{a14}U^{b14}\rho^{c14}\rho_s \tag{4.16}$$

$$\pi_{15} = W^{a15}U^{b15}\rho^{c15}t \tag{4.17}$$

1. Now for the first π terms we can write-

$$\pi_1 = W^{a1}U^{b1}\rho^{c1}ds \tag{4.18}$$

Now expressing individual parameters in basic dimension in Eq. (4.18), it yields,

$$M^0L^0T^0 = \left(M^0L^1T^0\right)^{a1}\left(M^0L^1T^{-1}\right)^{b1}\left(M^1L^{-3}T^0\right)^{c1}\left(M^0L^1T^0\right) \tag{4.19}$$

Eq. (4.19), further yields

$$M^0L^0T^0 = \left(M^0L^{a1}T^0\right)\left(M^0L^{b1}T^{-b1}\right)\left(M^{c1}L^{-3c1}T^0\right)\left(M^0L^1T^0\right) \tag{4.20}$$

Equating the power of M, L and T on either side we get the value of *a1, b1* and *c1* and by putting this value in the above π term we get the 1st non-dimensional term from Eq. (4.20) as expressed below.

$$\pi_1 = \frac{d_s}{W} \tag{4.21}$$

2. Similarly we can write 2nd π term as-

$$\pi_1 = W^{a1}U^{b1}\rho^{c1}B \tag{4.22}$$

Now expressing individual parameters in basic dimension in Eq. (4.22), yields,

$$M^0L^0T^0 = \left(M^0L^1T^0\right)^{a2}\left(M^0L^1T^{-1}\right)^{b2}\left(M^1L^{-3}T^0\right)^{c2}\left(M^0L^1T^0\right) \tag{4.23}$$

Eq. (4.23), further yields

$$M^0L^0T^0 = \left(M^0L^{a2}T^0\right)\left(M^0L^{b2}T^{-b2}\right)\left(M^{c2}L^{-3c2}T^0\right)\left(M^0L^1T^0\right) \tag{4.24}$$

Equating the power of M L and T on either side we get the value of a2, b2 and c2 and by putting this value in the above π term we get the 2nd non-dimensional term as

$$\pi_2 = \frac{B}{W} \tag{4.25}$$

3. Similarly we can write 3nd π term as-

$$\pi_3 = W^{a3}U^{b3}\rho^{c3}h \tag{26}$$

Now expressing individual parameters in basic dimension in Eq. (4.26), yields,

$$M^0L^0T^0 = \left(M^0L^1T^0\right)^{a3}\left(M^0L^1T^{-1}\right)^{b3}\left(M^1L^{-3}T^0\right)^{c3}\left(M^0L^1T^0\right) \tag{4.27}$$

Eq. (4.27), further yields

$$M^0L^0T^0 = \left(M^0L^{a3}T^0\right)\left(M^0L^{b3}T^{-b3}\right)\left(M^{c3}L^{-3c3}T^0\right)\left(M^0L^1T^0\right) \tag{4.28}$$

Equating the power of M L and T on either side we get the value of a3, b3 and c3 and by putting this value in the above π term we get the 3rd non-dimensional term as

$$\pi_3 = \frac{h}{W} \tag{4.29}$$

4. Similarly we can write the 4th π term as-

$$\pi_4 = W^{a4}U^{b4}\rho^{c4}H \tag{4.30}$$

Now expressing individual parameters in basic dimension in Eq. (4.30), yields,

$$M^0L^0T^0 = \left(M^0L^1T^0\right)^{a4}\left(M^0L^1T^{-1}\right)^{b4}\left(M^1L^{-3}T^0\right)^{c4}\left(M^0L^1T^0\right) \tag{4.31}$$

Eq. (4.31), further yields

$$M^0L^0T^0 = \left(M^0L^{a4}T^0\right)\left(M^0L^{b4}T^{-b4}\right)\left(M^{c4}L^{-3c4}T^0\right)\left(M^0L^1T^0\right) \tag{4.32}$$

Equating the power of M L and T on either side we get the value of a4, b4 and c4 and by putting this value in the above π term we get the 4th non-dimensional term as

$$\pi_4 = \frac{H}{W} \tag{4.33}$$

5. Similarly we can write the 5th π term as-

$$\pi_5 = W^{a5} U^{b5} \rho^{c5} D_{50} \tag{4.34}$$

Now Expressing individual parameters in basic dimension in Eq. (4.34), yields,

$$M^0 L^0 T^0 = \left(M^0 L^1 T^0\right)^{a5} \left(M^0 L^1 T^{-1}\right)^{b5} \left(M^1 L^{-3} T^0\right)^{c5} \left(M^0 L^1 T^0\right) \tag{4.35}$$

Eq. (4.35), further yields

$$M^0 L^0 T^0 = \left(M^0 L^{a5} T^0\right)\left(M^0 L^{b5} T^{-b5}\right)\left(M^{c5} L^{-3c5} T^0\right)\left(M^0 L^1 T^0\right) \tag{4.36}$$

Equating the power of M L and T on either side we get the value of a5, b5 and c5 and by putting this value in the above π term we get the 5th non-dimensional term as

$$\pi_5 = \frac{D_{50}}{W} \tag{4.37}$$

6. Similarly we can write the 6th π term as-

$$\pi_6 = W^{a6} U^{b6} \rho^{c6} D \tag{4.38}$$

Now expressing individual parameters in basic dimension in Eq. (4.38), yields,

$$M^0 L^0 T^0 = \left(M^0 L^1 T^0\right)^{a6} \left(M^0 L^1 T^{-1}\right)^{b6} \left(M^1 L^{-3} T^0\right)^{c6} \left(M^0 L^1 T^0\right) \tag{4.39}$$

Eq. (4.39), further yields

$$M^0 L^0 T^0 = \left(M^0 L^{a6} T^0\right)\left(M^0 L^{b6} T^{-b6}\right)\left(M^{c6} L^{-3c6} T^0\right)\left(M^0 L^1 T^0\right) \tag{4.40}$$

Equating the power of M L and T on either side we get the value of a6, b6 and c6 and by putting this value in the above π term we get the 6th non-dimensional term as

$$\pi_6 = \frac{D}{W} \tag{4.41}$$

7. Similarly we can write the 7th π term as-

$$\pi_7 = W^{a7} U^{b7} \rho^{c7} U_c \tag{4.42}$$

Now expressing individual parameters in basic dimension in Eq. (4.48), it yields,

$$M^0 L^0 T^0 = \left(M^0 L^1 T^0\right)^{a7} \left(M^0 L^1 T^{-1}\right)^{b7} \left(M^1 L^{-3} T^0\right)^{c7} \left(M^0 L^1 T^{-1}\right) \tag{4.43}$$

Eq. (4.43), further yields

$$M^0 L^0 T^0 = \left(M^0 L^{a7} T^0\right)\left(M^0 L^{b7} T^{-b7}\right)\left(M^{c7} L^{-3c7} T^0\right)\left(M^0 L^1 T^{-1}\right) \tag{4.44}$$

Equating the power of M L and T on either side we get the value of a7, b7 and c7 and by putting this value in the above π term we get the 7th non-dimensional term as

$$\pi_7 = \frac{U_C}{U} \tag{4.45}$$

8. Similarly we can write the 8th π term as-

$$\pi_8 = W^{a8} U^{b8} \rho^{c8} L \tag{4.46}$$

Now expressing individual parameters in basic dimension in Eq. (4.46), it yields,

$$M^0 L^0 T^0 = \left(M^0 L^1 T^0\right)^{a8} \left(M^0 L^1 T^{-1}\right)^{b8} \left(M^1 L^{-3} T^0\right)^{c8} \left(M^0 L^1 T^0\right) \tag{4.47}$$

Eq. (4.47), further yields

$$M^0 L^0 T^0 = \left(M^0 L^{a8} T^0\right)\left(M^0 L^{b8} T^{-b8}\right)\left(M^{c8} L^{-3c8} T^0\right)\left(M^0 L^1 T^0\right) \tag{4.48}$$

Equating the power of M L and T on either side we get the value of a8, b8 and c8 and by putting this value in the above π term we get the 8th non-dimensional term as

$$\pi_8 = \frac{L}{W} \tag{4.49}$$

9. Similarly we can write the 9th π term as-

$$\pi_9 = W^{a9} U^{b9} \rho^{c9} L^* \tag{4.50}$$

Now Expressing individual parameters in basic dimension in Eq. (4.50), it yields,

$$M^0 L^0 T^0 = \left(M^0 L^1 T^0\right)^{a9} \left(M^0 L^1 T^{-1}\right)^{b9} \left(M^1 L^{-3} T^0\right)^{c9} \left(M^0 L^1 T^0\right) \tag{4.51}$$

Eq. (4.51), further yields

$$M^0 L^0 T^0 = \left(M^0 L^{a9} T^0\right)\left(M^0 L^{b9} T^{-b9}\right)\left(M^{c9} L^{-3c9} T^0\right)\left(M^0 L^1 T^0\right) \tag{4.52}$$

Equating the power of M L and T on either side we get the value of a9, b9 and c9 and by putting this value in the above π term we get the 9th non-dimensional term as

$$\pi_9 = \frac{L^*}{W} \tag{4.53}$$

10. Similarly we can write the 10th π term as-

$$\pi_{10} = W^{a10} U^{b10} \rho^{c10} K_s \tag{4.54}$$

Now Expressing individual parameters in basic dimension in Eq. (4.54), it yields,

$$M^0 L^0 T^0 = \left(M^0 L^1 T^0\right)^{a10} \left(M^0 L^1 T^{-1}\right)^{b10} \left(M^1 L^{-3} T^0\right)^{c10} \left(M^0 L^0 T^0\right) \tag{54.5}$$

Eq. (4.55), further yields

$$M^0 L^0 T^0 = \left(M^0 L^{a10} T^0\right)\left(M^0 L^{b10} T^{-b10}\right)\left(M^{c10} L^{-3c10} T^0\right)\left(M^0 L^0 T^0\right) \tag{4.56}$$

Equating the power of M L and T on either side we get the value of a10, b10 and c10 and by putting this value in the above π term we get the 10th non-dimensional term as

$$\pi_{10} = K_s \tag{4.57}$$

11. Similarly we can write the 11th π term as-

$$\pi_{11} = W^{a11} U^{b11} \rho^{c11} \theta \tag{4.58}$$

Now Expressing individual parameters in basic dimension in Eq. (4.58), it yields,

$$M^0 L^0 T^0 = \left(M^0 L^1 T^0\right)^{a11} \left(M^0 L^1 T^{-1}\right)^{b11} \left(M^1 L^{-3} T^0\right)^{c11} \left(M^0 L^0 T^0\right) \tag{4.59}$$

Eq. (4.59), further yields

$$M^0L^0T^0 = \left(M^0L^{a11}T^0\right)\left(M^0L^{b11}T^{-b11}\right)\left(M^{c11}L^{-3c11}T^0\right)\left(M^0L^0T^0\right) \tag{4.60}$$

Equating the power of M L and T on either side we get the value of a11, b11 and c11 and by putting this value in the above π term we get the 11th non-dimensional term as

$$\pi_{11} = \theta \tag{4.61}$$

12. Similarly we can write the 12th π term as-

$$\pi_{12} = W^{a12}U^{b12}\rho^{c12}\text{Fr} \tag{4.62}$$

Now expressing individual parameters in basic dimension in Eq. (4.62), yields,

$$M^0L^0T^0 = \left(M^0L^1T^0\right)^{a12}\left(M^0L^1T^{-1}\right)^{b12}\left(M^1L^{-3}T^0\right)^{c12}\left(M^0L^0T^0\right) \tag{4.63}$$

Eq. (4.63), further yields

$$M^0L^0T^0 = \left(M^0L^{a12}T^0\right)\left(M^0L^{b12}T^{-b12}\right)\left(M^{c12}L^{-3c12}T^0\right)\left(M^0L^0T^0\right) \tag{4.64}$$

Equating the power of M L and T on either side we get the value of a12, b12 and c12 and by putting this value in the above π term we get the 12th non-dimensional term as

$$\pi_{12} = \text{Fr} \tag{4.65}$$

13. Similarly we can write the 13th π term as-

$$\pi_{13} = W^{a13}U^{b13}\rho^{c13}\sigma_g \tag{4.66}$$

Now Expressing individual parameters in basic dimension in Eq. (4.66), it yields,

$$M^0L^0T^0 = \left(M^0L^1T^0\right)^{a13}\left(M^0L^1T^{-1}\right)^{b13}\left(M^1L^{-3}T^0\right)^{c13}\left(M^0L^0T^0\right) \tag{4.67}$$

Eq. (4.67), further yields

$$M^0L^0T^0 = \left(M^0L^{a13}T^0\right)\left(M^0L^{b13}T^{-b13}\right)\left(M^{c13}L^{-3c13}T^0\right)\left(M^0L^0T^0\right) \tag{4.68}$$

Equating the power of M L and T on either side we get the value of a13, b13 and c13 and by putting this value in above π term we get the 13th non-dimensional term as

$$\pi_{13} = \sigma_g \tag{4.69}$$

14. Similarly we can write the 14th π term as-

$$\pi_{14} = W^{a14}U^{b14}\rho^{c14}\rho_s \tag{4.70}$$

Now expressing individual parameters in basic dimension in Eq. (4.70), it yields,

$$M^0L^0T^0 = \left(M^0L^1T^0\right)^{a14}\left(M^0L^1T^{-1}\right)^{b14}\left(M^1L^{-3}T^0\right)^{c14}\left(M^1L^{-3}T^0\right) \tag{4.71}$$

Eq. (4.71), further yields

$$M^0L^0T^0 = \left(M^0L^{a14}T^0\right)\left(M^0L^{b14}T^{-b14}\right)\left(M^{c14}L^{-3c14}T^0\right)\left(M^1L^{-3}T^0\right) \tag{4.72}$$

Equating the power of M L and T on either side we get the value of a14, b14 and c14 and by putting this value in the above π term we get the 14th non-dimensional term as

$$\pi_{14} = \frac{\rho_s}{\rho} \tag{4.73}$$

15. Similarly we can write the 15th π term as-

$$\pi_{15} = W^{a15}U^{b15}\rho^{c15}t \tag{4.74}$$

Now expressing individual parameters in basic dimension in Eq. (4.74), yields,

$$M^0L^0T^0 = \left(M^0L^1T^0\right)^{a15}\left(M^0L^1T^{-1}\right)^{b15}\left(M^1L^{-3}T^0\right)^{c15}\left(M^0L^0T^1\right) \tag{4.75}$$

Eq. (4.76), further yields

$$M^0L^0T^0 = \left(M^0L^{a15}T^0\right)\left(M^0L^{b15}T^{-b15}\right)\left(M^{c15}L^{-3c15}T^0\right)\left(M^0L^0T^1\right) \tag{4.76}$$

Equating the power of M, L and T on either side we get the value of $a15$, $b15$ and $c15$ and by putting this value in the above π term we get the 15th non-dimensional term as

$$\pi_{15} = \frac{Ut}{W} \tag{4.77}$$

Now the non-dimensional group will be in the following form-

$$f_9\left(\frac{d_s}{W}, \frac{B}{W}, \frac{h}{W}, \frac{H}{W}, \frac{D_{50}}{W}, \frac{D}{W}, \frac{U_C}{U}, \frac{L}{W}, \frac{L^*}{W}, K_s, \theta, \mathrm{Fr}, \sigma_g, \frac{\rho_s}{\rho}, \frac{Ut}{W}\right) = 0 \tag{4.78}$$

By re-arranging the above dimensionless group, we can write the above equation as follows

$$\frac{d_s}{D} = f_{10}\left(\frac{W}{D}, \frac{B}{D}, \frac{h}{D}, \frac{D_{50}}{D}, \frac{U_C}{U}, \frac{L^*}{D}, K_s, \theta, \mathrm{Fr}, \sigma_g, \frac{H}{D}, \frac{\rho_s}{\rho}\frac{L}{D}, \frac{Ut}{D}\right) \tag{4.79}$$

Removing independent pi terms from the above equation

$$\frac{d_s}{D} = f_{11}\left(\frac{W}{D}, \frac{L^*}{D}, \frac{L}{D}, \frac{Ut}{D}\right) \tag{4.80}$$

We have identified fifteen pi terms, among which four are dependent on d_s/D. The remaining Pi terms do not vary with the non-dimensional scour depth. The relationships between d_s/D and W/D, L^*/D, L/D, and Ut/D are presented in graphs in the subsequent chapter, where the development of the non-dimensional temporal scour depth is also discussed.

Chapter 5

Results and discussion

The present chapter discusses the findings of the present experiential works on scour reduction around an oblong pier equipped with an oblong collar. The chapter also deals with the scour depth reduction by the use of a collar compared to the pier without any collar. Different geometrical variations of the collar are used to identify suitable collar demotions. It is to be mentioned that two different sizes of pier are used for the present analysis. The present experimental work is carried out under the constant flow condition of flowing water and constant depth of flow. The experiments are conducted under clear water conditions. Different constant parameters that are used for the present experiments are presented in Table 3.2. It is to be mentioned that ten different combinations of pier length to pier width ratio (L/D) and collar width to pier width ratio (W/D) are used for ten different experiments. Apart from that two cases are conducted without fitting the collar to the pier. Hence 12 different experiments are carried out and the corresponding W/D and L/D values are presented in Table 5.1.

Table 5.1. Experiment details.

Exp. number	*L*/*D*	*W*/*D*
1	4	Without collar
2		1.5
3		2.0
4		2.5
5		3.0
6		3.5
7	2	Without collar
8		1.5
9		2.0
10		2.5
11		3.0
12		3.5

The details of the experimental apparatus are presented in Table 5.2.

Table 5.2. Experiment apparatus details.

Sl. Number	Experiential apparatus	Details
1	CANON camera	Canon EOS 77D DSLR Camera with 18-55mm Lens
2	ADV meter	
3	Laser Distance Meter	
4	Flow Meter	
5	Pump	
6	Sand	0.724 mm
7	Water	Normal clear water

Images of sand bed before the flow of water and after the flow of water with the visible presence of scour are captured with CANON made camera. To water depth of the flow was maintained at a constant label by regulating the gate valve of the flume manually. The discharge of the flow is measured by a flow meter that is mounted on the pump exit. The temporal scour of the sand bed is measured during the experiment by acoustic Doppler velocimetry (ADV). After that when the equilibrium time is reached, the water is released and the scour depth of the dry- sand bed is measured by a Laser Distance Meter (LDM). It is to be mentioned that, when the scour rate reaches below 1 mm/hour, the equilibrium condition is considered. Finally, the data of experiential operation are fitted to the Golden software Surfer software edition and the scour contour is generated for further analysis. Also, the data are fitted to Origin graph plot software, 2022 edition to generate the temporal variation of the scour on the sand bed for further parametric comparisons. Different cases of experiments and the corresponding comparisons are presented in succeeding sections accordingly.

5.1 Scour depth calculation for *L/D* = 4

A total of six sets of experiments are conducted to investigate the scour depth in dry-sand at different positions around the pier (both the case of with and without collar) considering the pier length to pier width dation equal to 4. It is to be mentioned that a total of five collar width to pier width ratios varying from 1.5 to 3.5 are used for the study. The findings of the different cases are explained in sections 6.1.1 and 6.1.6, respectively. It is to be mentioned that for all the cases a velocity of water 27.3 cm/s is used around the flume.

5.1.1 Pier without collar

Initially, an experiment is conducted considering a simple oblong pier without any collar. having length to width ratio of 4. Figure 5.1 represents the dry-sand bed of this case before the commencement of the flow. The flow direction in presented by a blue arrow mark in the figure. A flow of water inside the flume is continued for 9 hours to achieve the equilibrium depth. Later, releasing the water from the flume, the dry sand bed as shown in Fig. 5.2 indicates the visible presence of scour at the upstream (0^0) and both sides of the pier (45^o). However, at 45^o position, there is little deposition of sand. There is little scour at the position of 135^o. There is visible deposition of sand at the downstream of the pier (180^o).



Fig. 5.1. Sand bed before experimental run for without collar, and *L/D*= 4.



Fig. 5.2. Scour bed around the pier after experimental run for without collar, and *L/D*= 4.

The dry-sand scour data are collected and fitted to surfer software. The contour is generated and it is presented in Fig. 5.3. In the contour, the pier is presented with deep grey color. The positive and negative values of contour lines represent the deposition and scour, respectively. The contour predictions are almost equivalent to the actual captured image of the experiment shown in Fig. 5.2. Figure 5.3 indicates the presence of maximum scour near the position of angle 0°. The maximum scour depth is 3.344 cm.

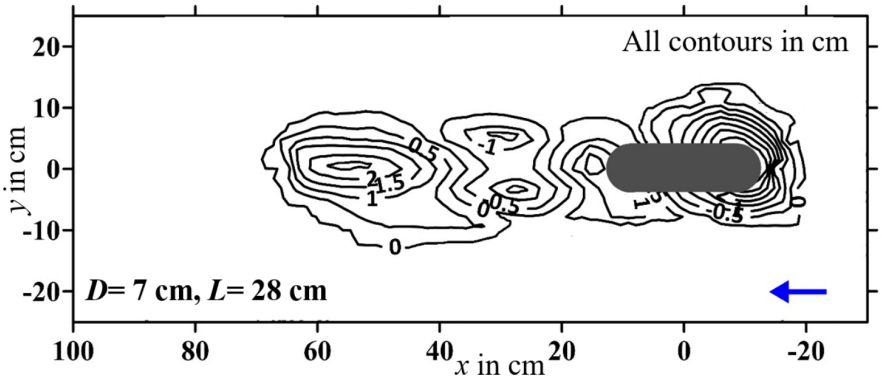


Fig. 5.3. Contour map of scour bed without collar for *L/D*= 4.

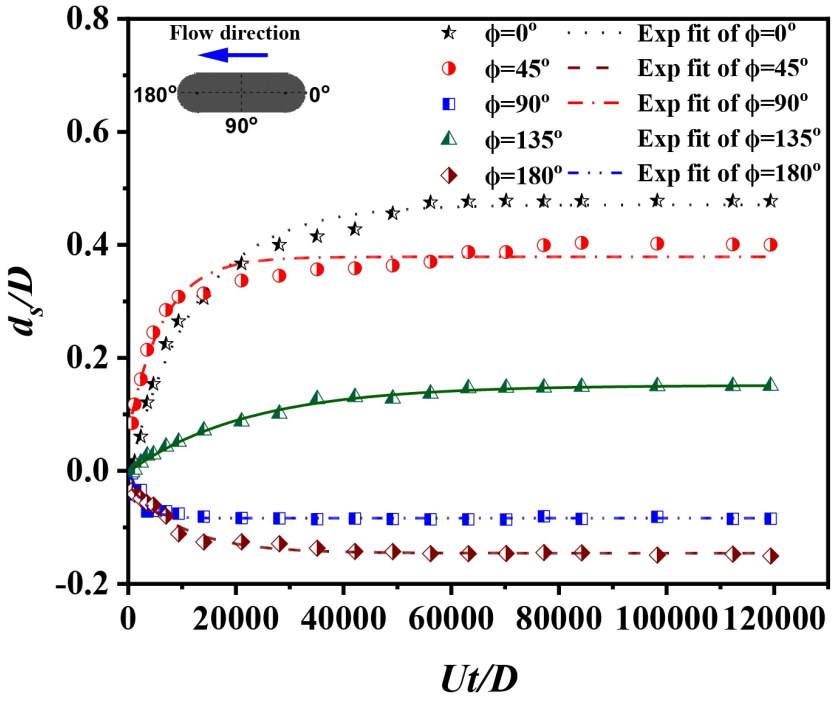


Fig. 5.4. Temporal variation of scour depth in non-dimensional form for different ϕ without collar, and *L/D*= 4.

The temporal variation of the scour depth is studied and presented in Fig. 5.4 for different positions around the collar. The figure indicates that the non-dimensional scour depth increases rapidly with non-dimensional time for 0° and 45° cases initially. Later the increment rate is sloth and after around 4 hours, the scour rate almost remains unchanged and equilibrium is reached. However, there is a lower rate of scour for the 135° case initially compared to the previous cases. Figure 5.4 also indicates the deposition of sand for the cases of 90° and 180° respectively. The rate of deposition is higher for the case of 180° compared to the case of 90°. For all the cases, both for the scour and deposition, the experimental data are fitted to the exponential data fit and for all the cases, the R^2 value remains between 0.98 to 0.99.

5.1.2 Pier with collar *W/D*= 3.5

The experiment is conducted considering the oblong pier with the collar having the collar width to pier width ratio of 3.5. Figure 5.5 represents the dry-sand bed of this case before the commencement of the flow. The flow direction in presented by a blue arrow mark in the figure. A flow of water inside the flume is continued for 5 hours to achieve the equilibrium depth. Later, releasing the water from the flume, the dry sand bed as shown in Fig. 5.6 indicates the visible presence of scour at the downstream (135^0). However, at 180° position,

there is little scour of sand. There is very little scour rate at the positions of 0^{o}, 45^{0} and 90^{o}. There is visible deposition of sand at the downstream of the collar.



Fig. 5.5. Sand bed before experimental run for *W/D*= 3.5, and *L/D*= 4.



Fig. 5.6. Scour bed around the collar after experimental run for *W/D*= 3.5, and *L/D*= 4.

The dry-sand scour data are collected and fitted to surfer software. The contour is generated and it is presented in Fig. 5.7. In the contour, the pier is presented by deep grey color and the collar is presented by ruby red color. The positive and negative values of contour lines represent the deposition and scour, respectively. The contour predictions are almost equivalent to the actual captured image of the experiment shown in Fig. 5.7. Figure 5.7 indicates the presence of maximum scour near the position of angle 135^{o}. The maximum scour depth is 2.13 cm.

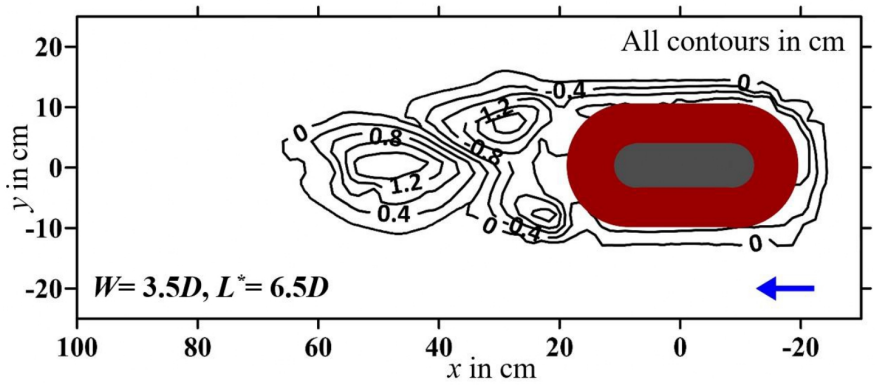


Fig. 5.7. Contour map of scour bed for W/D=3.5, and L/D= 4.

The temporal variation of the scour depth is studied and presented in Fig. 5.8 for different positions around the collar. The figure indicates that the non-dimensional scour depth increases rapidly with non-dimensional time for 180° and 135° cases initially. Later the increment rate is sloth and after around 2 hours, the scour rate almost remains unchanged and equilibrium is reached. However, there is a lower rate of scour for the 0°, 45° and 90° cases initially compared to the previous cases. For all the cases, the experimental data are fitted to the exponential data fit and for all the cases, the R^2 value remains within 0.97 to 0.98.

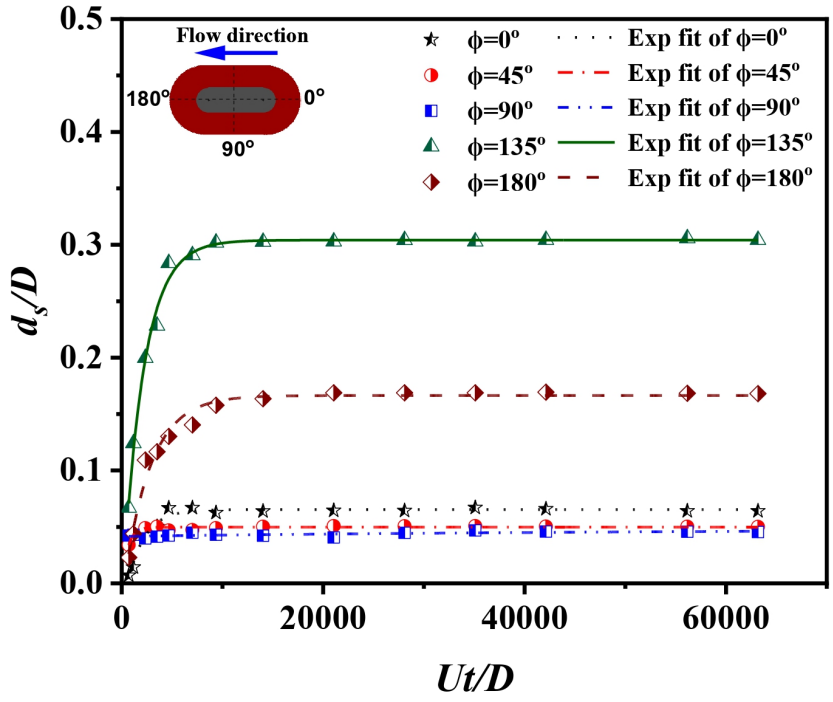


Fig. 5.8. Temporal variation of scour depth in non-dimensional form for different ϕ W/D= 3.5, and L/D= 4.

5.1.3 Pier with collar *W/D*= 3

The experiment is conducted considering the oblong pier with the collar. It has a collar width to pier width ratio of 3. Figure 5.9 represents the dry-sand bed of this case before the commencement of the flow. The flow direction in presented by a blue arrow mark in the figure. A flow of water inside the flume is continued for 6 hours to achieve the equilibrium depth. Later, releasing the water from the flume, the dry sand bed as shown in Fig. 5.10 indicates the visible presence of scour at the downstream (135^0). However, at 180^o position, there is little scour of sand. There is very little scour rate at the position of 90^o, 45^0 and 0^0. There is visible deposition of sand at the downstream of the collar.

The dry-sand scour data are collected and fitted to surfer software. The contour is generated and it is presented in Fig. 5.11. In the contour, the pier is presented by deep grey color and the collar is presented by ruby red color. The positive and negative values of contour lines represent the deposition and scour, respectively. The contour predictions are almost equivalent to the actual captured image of the experiment shown in Fig. 5.11. Figure 5.11 indicates the presence of maximum scour near the position of angle 135^o. The maximum scour depth is 2.1 cm.



Fig. 5.9. Sand bed before experimental run for *W*/*D*= 3, and *L*/*D*= 4.



Fig. 5.10. Scour bed around the collar after experimental run for W/D= 3, and L/D= 4.

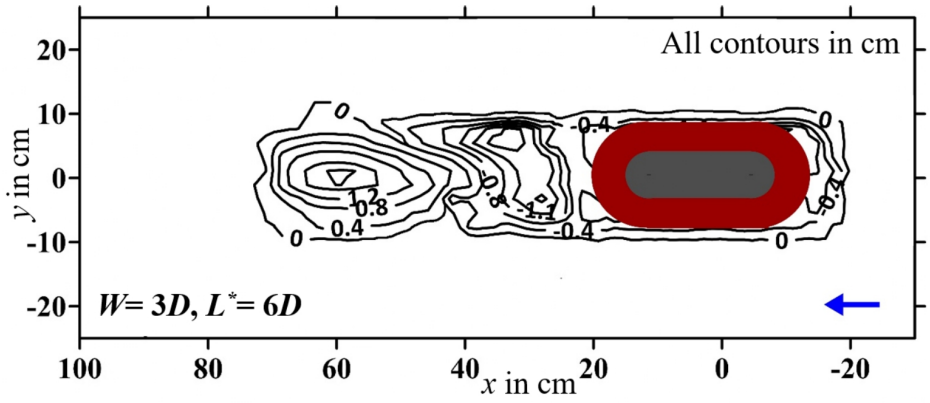


Fig. 5.11. Contour map of scour bed for W/D=3, and L/D= 4.

The temporal variation of the scour depth is studied and presented in Fig. 5.12 for different positions around the collar. The figure indicates that the non-dimensional scour depth increases rapidly with nondimensional time for 180^o and 135^o cases initially. Later the increment rate is sloth and after around 2 hours, the scour rate almost remains unchanged and equilibrium is reached. However, there is a lower rate of scour for the 0^o, 45^0 and 90^0 cases initially compared to the previous cases. For all the cases, both for the scour and deposition, the experimental data are fitted to the exponential data fit and for all the cases, the R^2 value remains between 0.97 to 0.98.

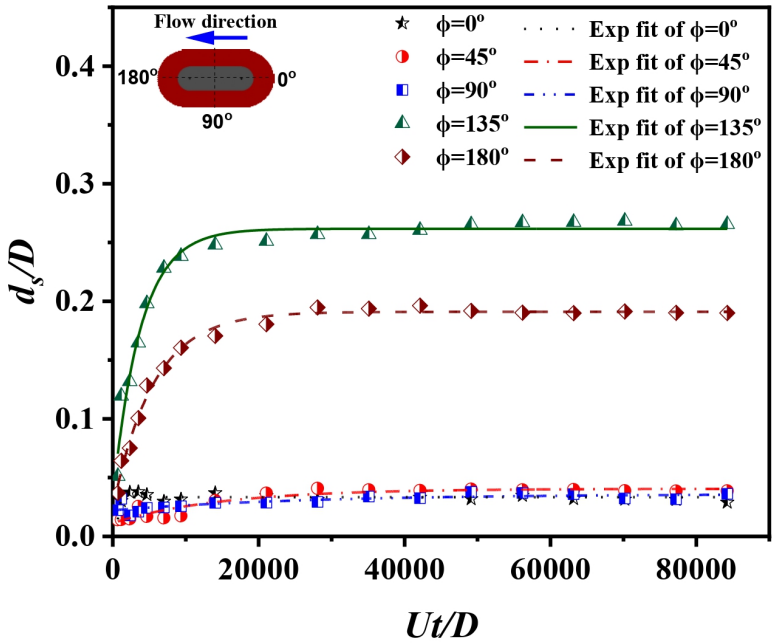


Fig. 5.12. Temporal variation of scour depth in non-dimensional form for different ϕ *W*/*D*= 3, and *L*/*D*= 4.

5.1.4 Pier with collar *W*/*D*= 2.5

The experiment is conducted considering the oblong pier with the collar. It has a collar width to pier width ratio of 2.5. Fig. 5.13 represents the dry-sand bed of this case before the commencement of the flow. The flow direction in presented by the blue arrow mark in the figure. A flow of water inside the flume is continued for 6.5 hours to achieve the equilibrium depth. Later, releasing the water from the flume, the dry sand bed as shown in Fig. 5.14 indicates the visible presence of scour at the downstream (135^0). However, at 180° position, there is little scour of sand. There is very little deposition at the position of 90° and 45^0. There is visible deposition of sand at the downstream of the collar.

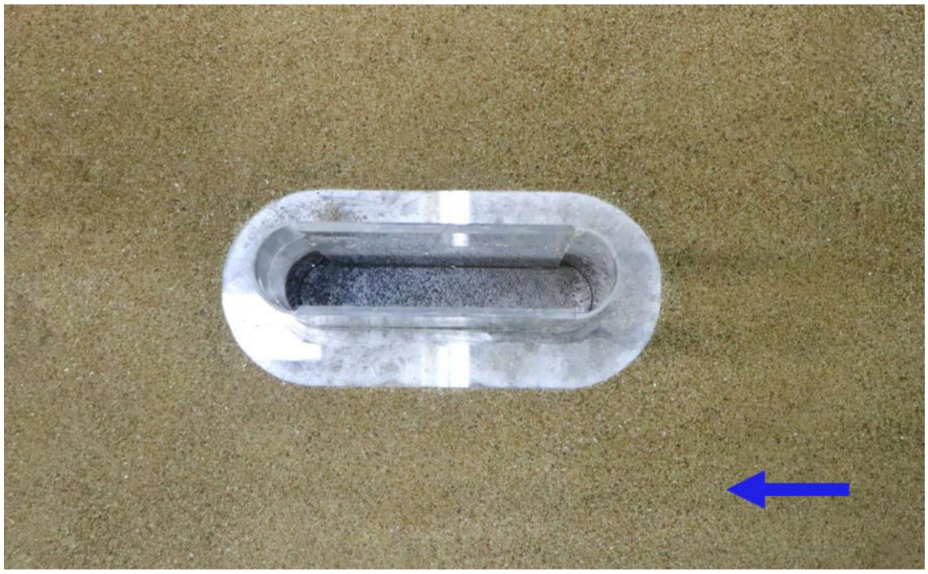


Fig. 5.13. Sand bed before experimental run for W/D= 2.5, and L/D= 4.



Fig. 5.14. Scour bed around the collar after experimental run for W/D= 2.5, and L/D= 4.

The dry-sand scour data are collected and fitted to surfer software. The contour is generated and it is presented in Fig. 5.15. In the contour, the pier is presented by deep grey color and the collar is presented by ruby red color. The positive and negative values of contour lines represent the deposition and scour, respectively. The contour predictions are almost equivalent to the actual captured image of the experiment shown in Fig. 5.15. Figure 5.15 indicates the presence of maximum scour near the position of angle 135^{o}. The maximum scour depth is 2.19 cm.

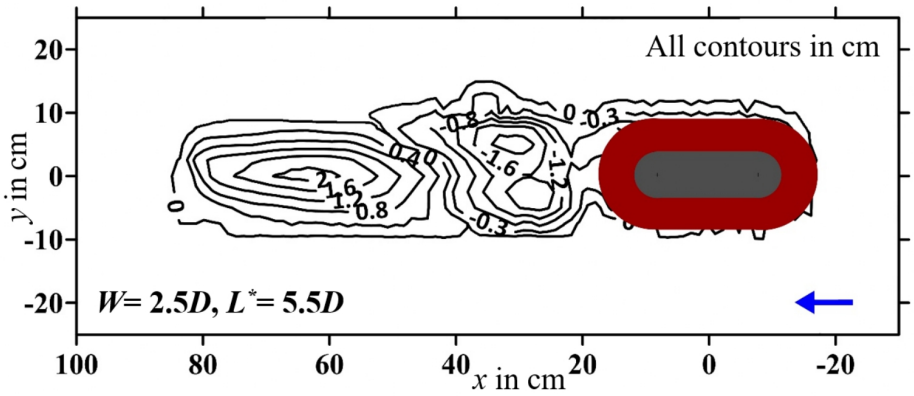


Fig. 5.15. Contour Map of scour bed for *W/D*=2.5, and *L/D*= 4.

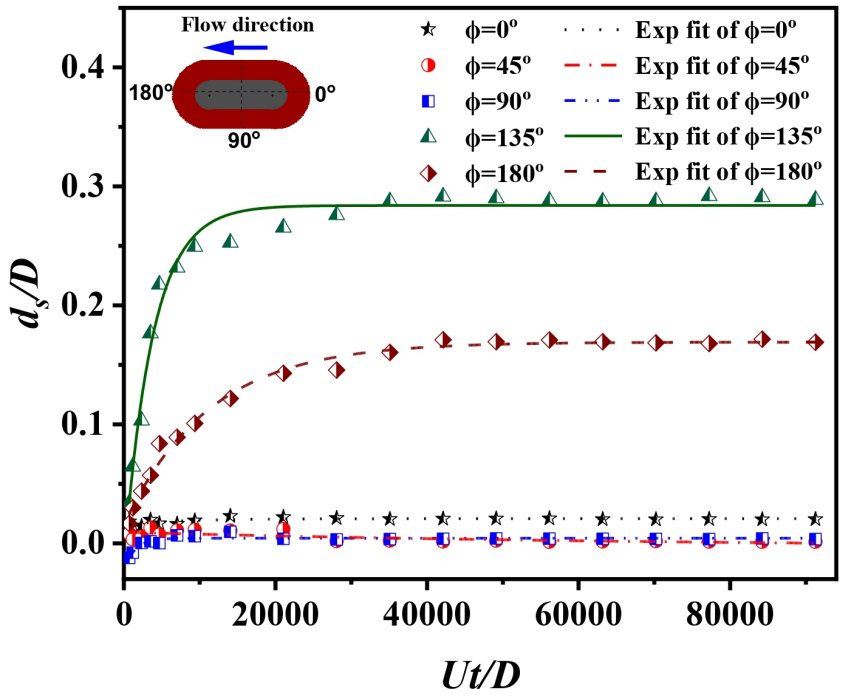


Fig. 5.16. Temporal variation of scour depth in non-dimensional form for different ϕ *W/D*= 2.5, and *L/D*= 4.

The temporal variation of the scour depth is studied and presented in Fig. 5.16 for different positions around the collar. The figure indicates that the non-dimensional scour depth increases rapidly with non-dimensional time for 180° and 135° cases initially. Later the increment rate is sloth and after around 2 hours, the scour rate almost remains unchanged and equilibrium is reached. However, there is a lower rate of scour for the 0°, 45° and 90° cases initially compared to the previous cases. For all the cases, both for the scour and deposition,

the experimental data are fitted to the exponential data fit and for all the cases, the R^2 value remains between 0.97 to 0.98.

5.1.5 Pier with collar *W/D*= 2

The experiment is conducted considering the oblong pier with the collar. It has a collar width to pier width ratio of 2. Figure 5.17 represents the dry-sand bed of this case before the commencement of the flow. The flow direction in presented by a blue arrow mark in the figure. A flow of water inside the flume is continued for 8 hours to achieve the equilibrium depth. Later, releasing the water from the flume, the dry sand bed as shown in Fig. 5.19 indicates the visible presence of scour at the upstream (0^0), side of the collar (45^0) and downstream (135^0). However, 180^0 position, there is little scour of sand. There is very little deposition at the position of 90^o. There is visible deposition of sand at the downstream of the collar.



Fig. 5.17. Sand bed before experimental run for *W*/*D*= 2, and *L*/*D*= 4.



Fig. 5.18. Scour bed around the collar after experimental run for *W/D*= 2, and *L/D*= 4.

The dry-sand scour data are collected and fitted to surfer software. The contour is generated and it is presented in Figure 5.19. In the contour, the pier is presented by deep grey color and the collar is presented by ruby red color. The positive and negative values of contour lines represent the deposition and scour, respectively. The contour predictions are almost equivalent to the actual captured image of the experiment shown in Fig. 5.18. Figure 5.19 indicates the presence of maximum scour near the position of angle 135°. The maximum scour depth is 2.3 cm.

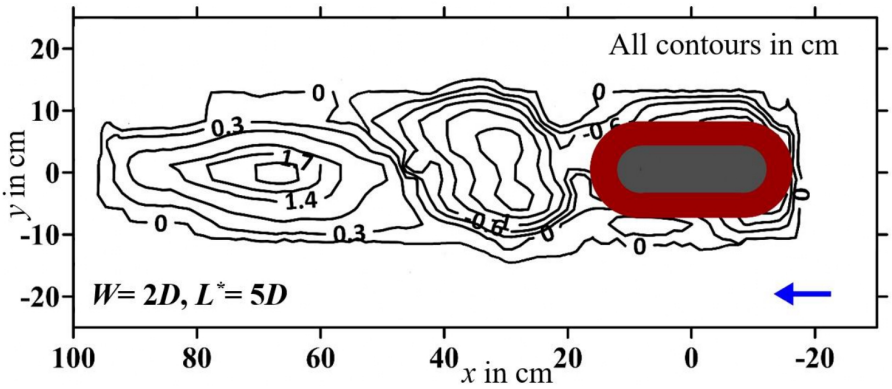


Fig. 5.18. Contour map of scour bed for *W*/*D*= 2, and *L*/*D*= 4.

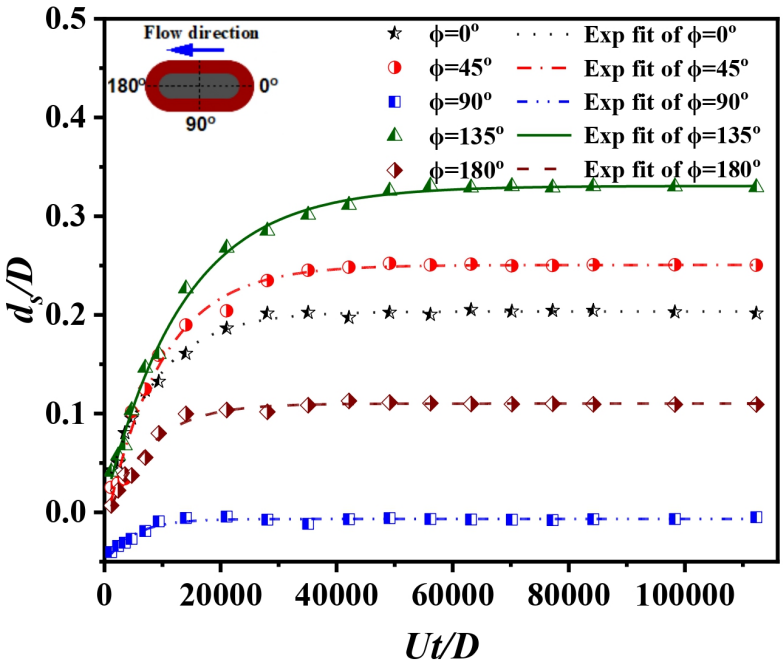


Fig. 5.19. Temporal variation of scour depth in non-dimensional form for different ϕ *W*/*D*= 2, and *L*/*D*= 4.

The temporal variation of the scour depth is studied and presented in Fig. 5.20 for different positions around the collar. The figure indicates that the non-dimensional scour depth increases rapidly with non-dimensional time for 0^o and 45^o cases initially. After some time, scour depth increases at the position of 135^0. Later the increment rate is sloth and after around 3 hours, the scour rate almost remains unchanged and equilibrium is reached. However, there is a lower rate of scour for the 180^o case initially compared to the previous cases. Fig. 5.20 also indicates the deposition of sand for the cases of 90^o. The rate of deposition is slow for the case of 90^o. For all the cases, both for the scour and deposition, the experimental data are fitted to the exponential data fit and for all the cases, the R^2 value remains between 0.98 to 0.99.

5.1.6 Pier with collar *W*/*D*= 1.5

The experiment is conducted considering an oblong pier with a collar. It has a collar width to pier width ratio of 1.5. Figure 5.21 represents the dry-sand bed of this case before the commencement of the flow. The flow direction in presented by a blue arrow mark in the figure. A flow of water inside the flume is continued for 7.5 hours to achieve the equilibrium scour depth. Later, releasing the water from the flume, the dry sand bed as shown in Fig. 5.22 indicates the visible presence of scour at the upstream (0^0) and side of the collar (45^0). However, at 135^o position, there is little scour of sand. There is very little deposition at the position of 90^o and 180^0. There is visible deposition of sand at the downstream of the collar.



Fig. 5.21. Sand bed before experimental run for *W*/*D*= 1.5, and *L*/*D*= 4.



Fig. 5.22. Scour bed around the collar after experimental run for W/D= 1.5, L/D= 4.

The dry-sand scour data are collected and fitted to surfer software. The contour is generated and it is presented in Fig. 5.23. In the contour, the pier is presented by deep grey color and the collar is presented by ruby red color. The positive and negative values of contour lines represent the deposition and scour, respectively. The contour predictions are almost equivalent to the actual captured image of the experiment shown in Fig. 5.23. Figure 5.23 indicates the presence of maximum scour near the position of angle 0°. The maximum scour depth is 2.8 cm.

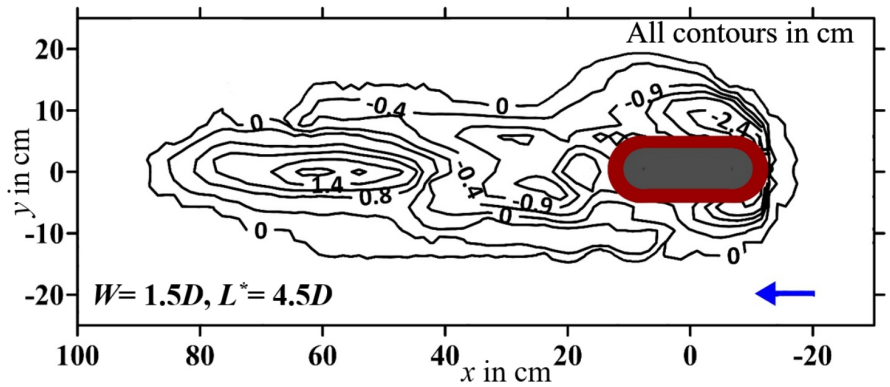


Fig. 5.23. Contour Map of scour bed for W/D= 1.5, and L/D= 4.

The temporal variation of the scour depth is studied and presented in Fig. 5.24 for different positions around the collar. The figure indicates that the non-dimensional scour depth increases rapidly with non-dimensional time for 0° and 45° cases initially. Later the increment rate is sloth and after around 3 hours, the scour rate almost remains unchanged and equilibrium is reached. However, there is a lower rate of scour for the 180°, 135° and 90°

cases initially compared to the previous cases. For all the cases, the experimental data are fitted to the exponential data fit and for all the cases, the R^2 value remains within 0.98 to 0.99.

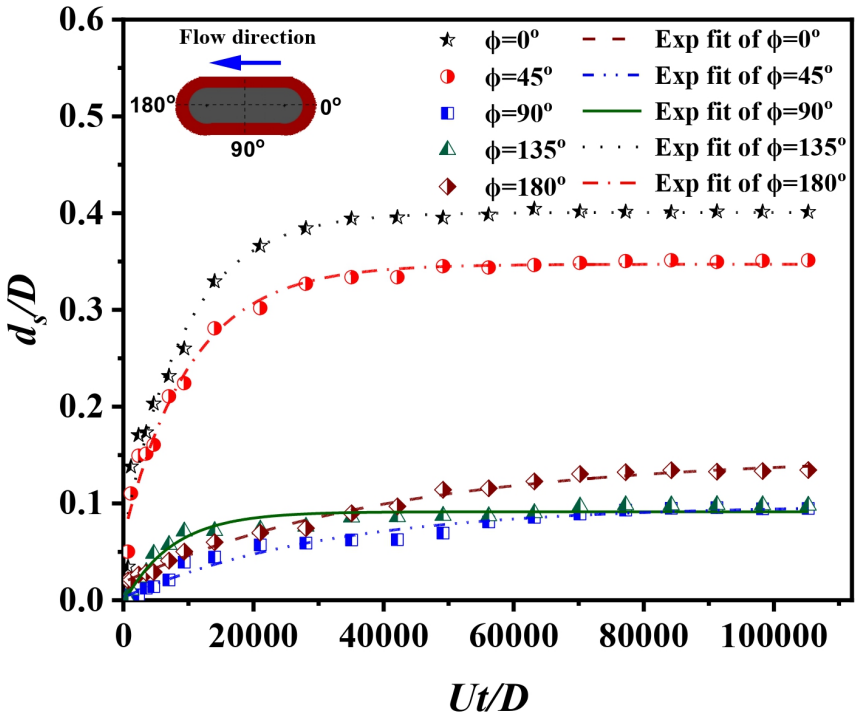


Fig. 5.24. Temporal variation of scour depth in non-dimensional form for different ϕ *W*/*D*= 1.5, and *L*/*D*= 4.

5.2 Scour depth calculation for *L*/*D* = 2

A total of six other experiments are conducted to investigate the scour depth in dry-sand at different positions around the pier and collar (both the case of with and without collar) considering the pier length to pier width dation equal to 2. It is to be mentioned that a total of five collar width to pier width ratios varying from 1.5 to 3.5 are used for the study. The findings of the different cases are explained in sections 6.2.1 and 6.2.6 respectively. It is to be mentioned that for all the cases a velocity of water 27.3 cm/s is used around the flume.

5.2.1 Pier without collar

Initially, an experiment is conducted considering a simple oblong pier without any collar. having length to width ratio of 2. Fig. 5.25 represents the dry-sand bed of this case before the commencement of the flow. The flow direction in presented by a blue arrow mark in the figure. A flow of water inside the flume is continued for 9 hours to achieve the equilibrium depth. Later, releasing the water from the flume, the dry sand bed as shown in Fig. 5.26

indicates the visible presence of scour at the upstream (0^0) and on both sides of the pier (45^o). However, at 180^o position, there is a little deposition of sand. There is little scour at the position of 90^o. There is a visible deposition of sand at the downstream of the pier (135^o).



Fig. 5.25. Sand bed before the experimental run for without collar, and *L/D*=2.



Fig. 5.26. Scour bed around the pier after experimental run for without collar, and *L/D*=2.

The dry-sand scour data are collected and fitted to surfer software. The contour is generated and it is presented in Fig. 5.27. In the contour, the pier is presented with deep grey color. The positive and negative values of contour lines represent the deposition and scour, respectively. The contour predictions are almost equivalent to the actual captured image of

the experiment shown in Fig. 5.26. Figure 5.27 indicates the presence of maximum scour near the position of angle 0°. The maximum scour depth is 3.72 cm.

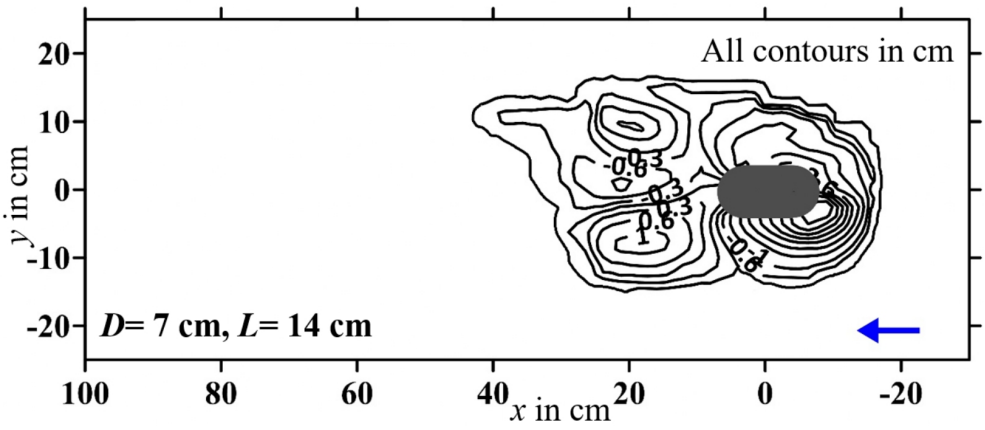


Fig. 5.27. Contour map of scour bed for without collar, and *L/D*=2.

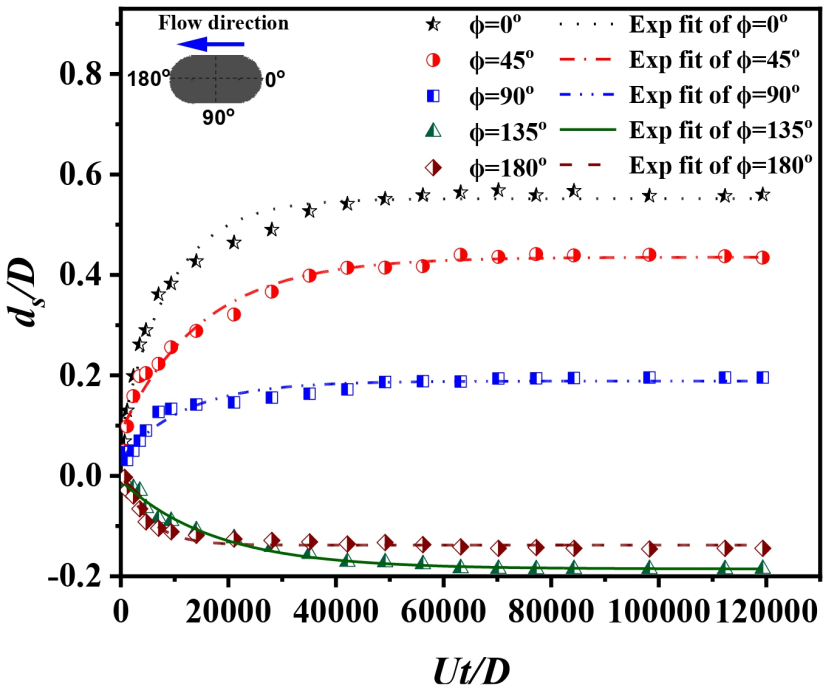


Fig. 5.28. Temporal variation of scour depth in non-dimensional form for different ϕ without collar, and *L/D*=2.

The temporal variation of the scour depth is studied and presented in Fig. 5.28 for different positions around the pier. The figure indicates that the nondimensional scour depth increases rapidly with nondimensional time for 0° and 45° cases initially. Later the increment rate is sloth and after around 4 hours, the scour rate almost remains unchanged and

equilibrium is reached. However, there is a lower rate of scour for the 90° case initially compared to the previous cases. Figure 5.28 also indicates the deposition of sand for the cases of 135° and 180° respectively. The rate of deposition is higher for the case of 180° compared to the case of 135°. For all the cases, both for the scour and deposition, the experimental data are fitted to the exponential data fit and for all the cases, the R^2 value remains between 0.98 to 0.99.

5.2.2 Pier with collar *W/D*= 3.5

The experiment is conducted considering an oblong pier with a collar. It has a collar width to pier width ratio of 3.5. Figure 5.28 represents the dry-sand bed of this case before the commencement of the flow. The flow direction in presented by a blue arrow mark in the figure. A flow of water inside the flume is continued for 6 hours to achieve the equilibrium depth. Later, releasing the water from the flume, the dry sand bed as shown in Fig. 5.29 indicates the visible presence of scour at the downstream (135^0). However, at 180° position, there is little scour of sand. There is very little scour rate at the positions of 0°, 45^0 and 90°. There is visible deposition of sand at the downstream of the collar.



Fig. 5.29. Sand bed before the experimental run for *W/D*= 3.5, and *L/D*=2.

The dry-sand scour data are collected and fitted to surfer software. The contour is generated and it is presented in Fig. 5.31. In the contour, the pier is presented by deep grey color and the collar is presented by ruby red color. The positive and negative values of contour lines represent the deposition and scour, respectively. The contour predictions are almost equivalent to the actual captured image of the experiment shown in Fig. 5.30. Figure 5.31 indicates the presence of maximum scour near the position of angle 135°. The maximum scour depth is 1.574 cm.



Fig. 5.30. Scour bed of sand after experimental run for *W/D*= 3.5, and *L/D*=2.

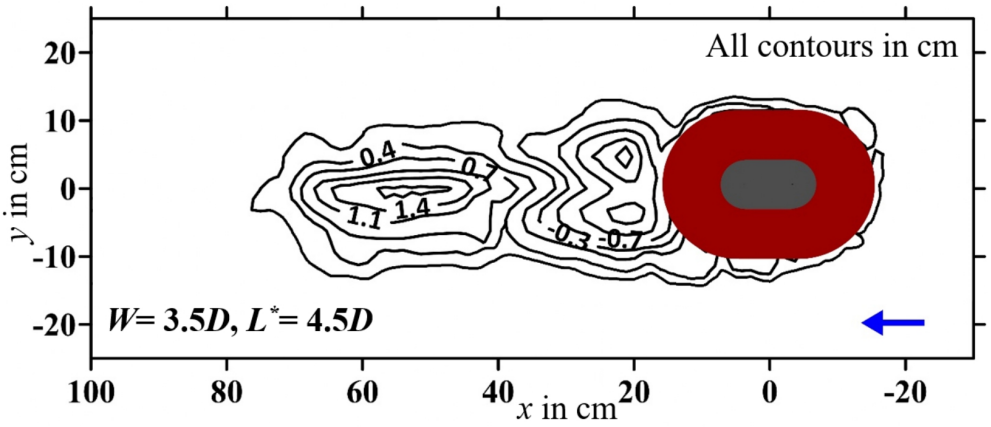


Fig. 5.31. Contour map of scour bed (*W/D*=3.5, *L/D*=2).

The temporal variation of the scour depth is studied and presented in Fig. 5.32 for different positions around collar. The figure indicates that the non-dimensional scour depth increases rapidly with non-dimensional time for 180^o and 135^o cases initially. Later the increment rate is sloth and after around 2 hours, the scour rate almost remains unchanged and equilibrium is reached. However, there is a lower rate of scour for the 0^o, 45^0 and 90^0 cases initially compared to the previous cases. For all the cases, the experimental data are fitted to the exponential data fit and for all the cases, the R^2 value remains within 0.98 to 0.99.

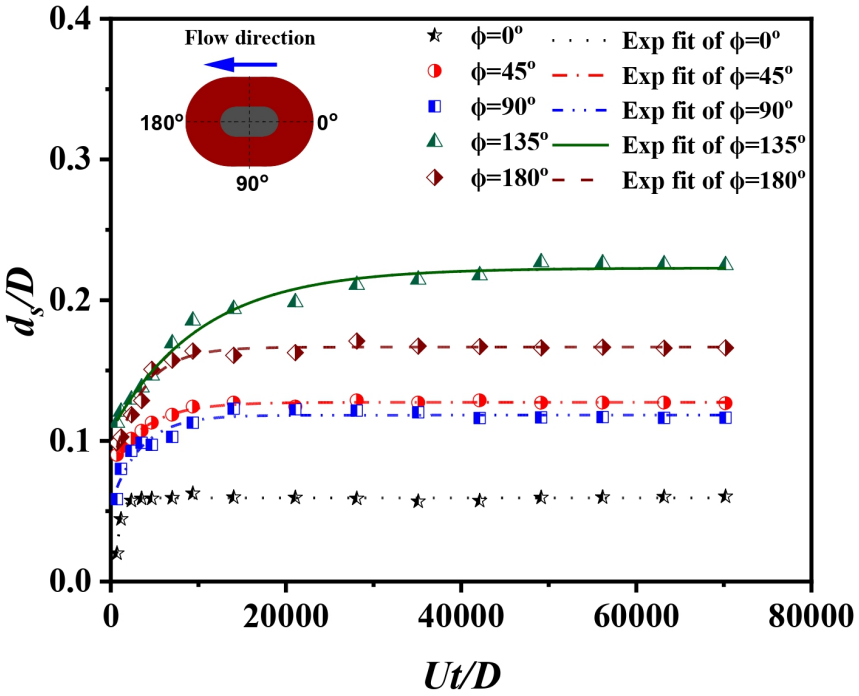


Fig. 5.32. Temporal variation of scour depth in non-dimensional form for different ϕ *W/D*= 3.5, and *L/D*=2.

5.2.3 Pier with collar *W/D*= 3

The experiment is conducted considering an oblong pier with a collar. It has a collar width to pier width ratio of 3. Fig. 5.33 represents the dry-sand bed of this case before the commencement of the flow. The flow direction in presented by a blue arrow mark in the figure. A flow of water inside the flume is continued for 6 hours to achieve the equilibrium depth. Later, releasing the water from the flume, the dry sand bed as shown in Fig. 5.34 indicates the visible presence of scour at the downstream (135^0). However, at 180^o position, there is little scour of sand. There is very little scour rate at the position of 90^o, 45^0 and 0^0. There is visible deposition of sand at the downstream of the collar.

The dry-sand scour data are collected and fitted to surfer software. The contour is generated and it is presented in Fig. 5.35. In the contour, the pier is presented by deep grey color and the collar is presented by ruby red color. The positive and negative values of contour lines represent the deposition and scour, respectively. The contour predictions are almost equivalent to the actual captured image of the experiment shown in Fig. 5.34. Figure 5.35 indicates the presence of maximum scour near the position of angle 135^o. The maximum scour depth is 1.94 cm.



Fig. 5.33. Sand bed before the experimental run for *W/D*= 3, and *L/D*=2.



Fig. 5.34. Scour bed around the collar after experimental run for *W/D*= 3, and *L/D*=2.

The temporal variation of the scour depth is studied and presented in Fig. 5.36 for different positions around collar. The figure indicates that the nondimensional scour depth increases rapidly with nondimensional time for 180^o and 135^o cases initially. Later the increment rate is sloth and after around 3 hours, the scour rate almost remains unchanged and equilibrium is reached. However, there is a lower rate of scour for the 0^o, 45^0 and 90^0 cases initially compared to the previous cases. For all the cases, both for the scour and deposition, the experimental data are fitted to the exponential data fit and for all the cases, the R^2 value remains between 0.98 to 0.99.

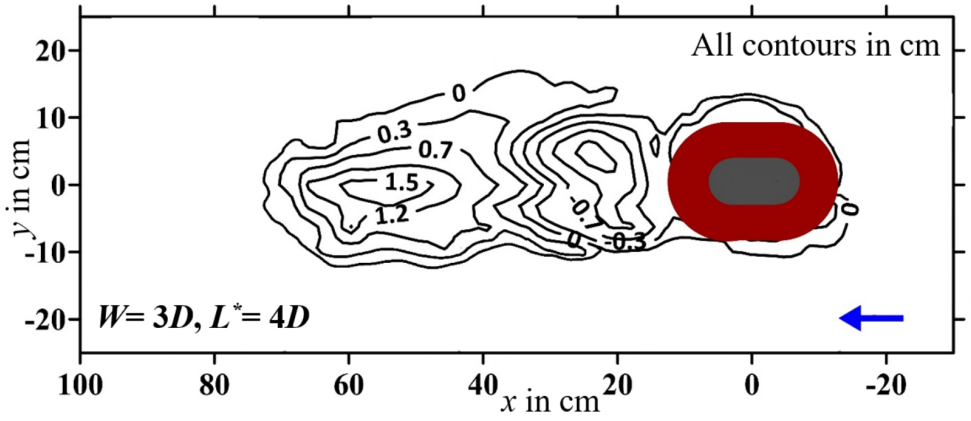


Fig. 5.35. Contour map of scour bed for *W/D*=3, and *L/D*= 2.

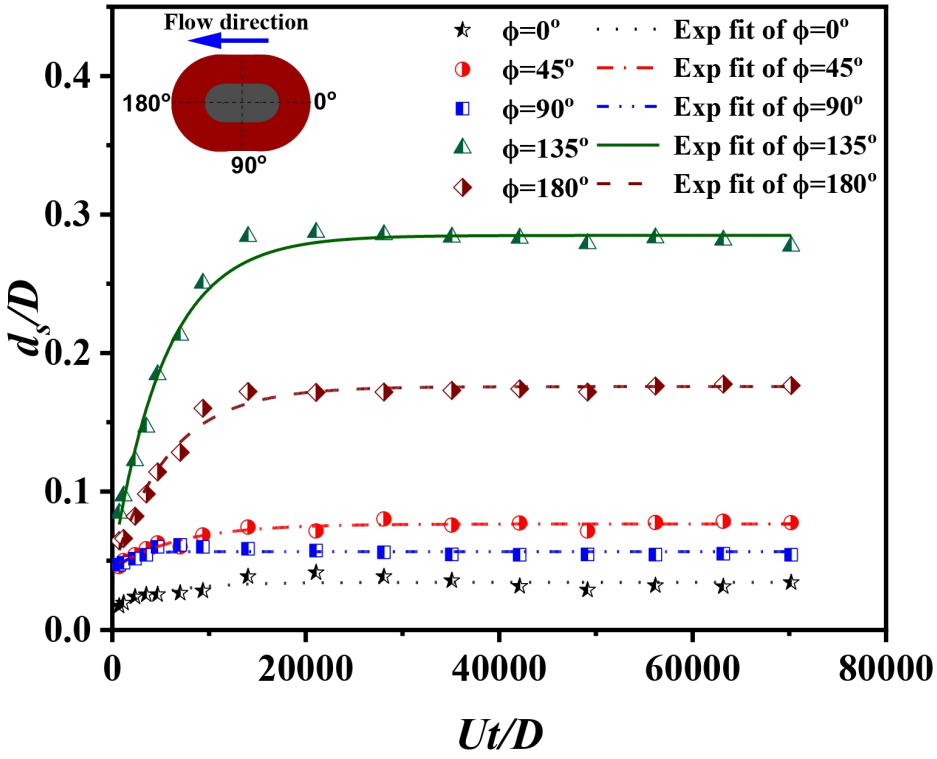


Fig. 5.36. Temporal variation of scour depth in non-dimensional form for different ϕ *W/D*= 3, and *L/D*=2.

5.2.4 Pier with collar *W/D*= 2.5

The experiment is conducted considering an oblong pier with a collar. It has a collar width to pier width ratio of 2.5. Figure 5.37 represents the dry-sand bed of this case before the commencement of the flow. The flow direction in presented by a blue arrow mark in the

figure. A flow of water inside the flume is continued for 6 hours to achieve the equilibrium depth. Later, releasing the water from the flume, the dry sand bed as shown in Fig. 5.38 indicates the visible presence of scour at the downstream (135^0). However, at 180^o, 90^o and 45^0 position, there is little scour of sand. There is a visible deposition of sand at the downstream side of the collar.

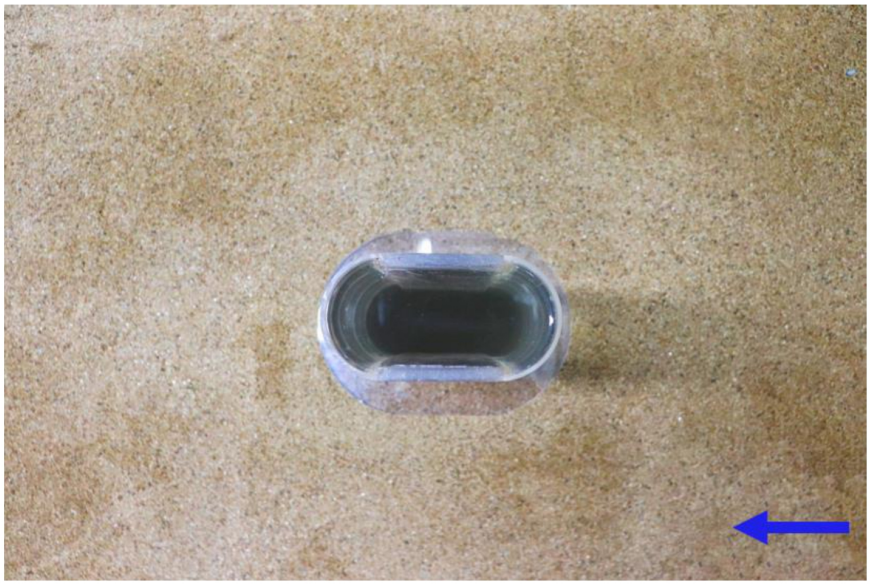


Fig. 5.37. Sand bed before experimental run for *W/D*= 2.5, and *L/D*=2.

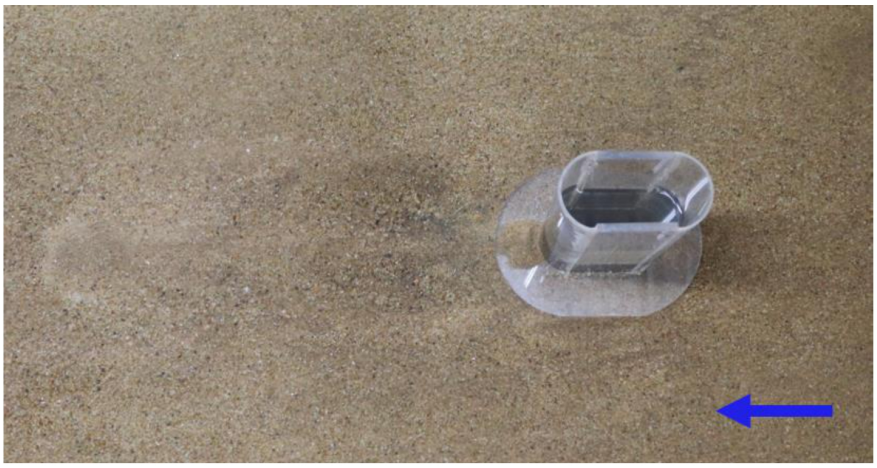


Fig. 5.38. Scour bed around the collar after experimental run for *W/D*= 2.5, and *L/D*=2.

The dry-sand scour data are collected and fitted to surfer software. The contour is generated and it is presented in Figure 5.39. In the contour, the pier is presented by deep grey color and the collar is presented by ruby red color. The positive and negative values of contour lines represent the deposition and scour, respectively. The contour predictions are almost

equivalent to the actual captured image of the experiment shown in Fig. 5.38. Figure 5.39 indicates the presence of maximum scour near the position of angle 135°. The maximum scour depth is 1.73 cm.

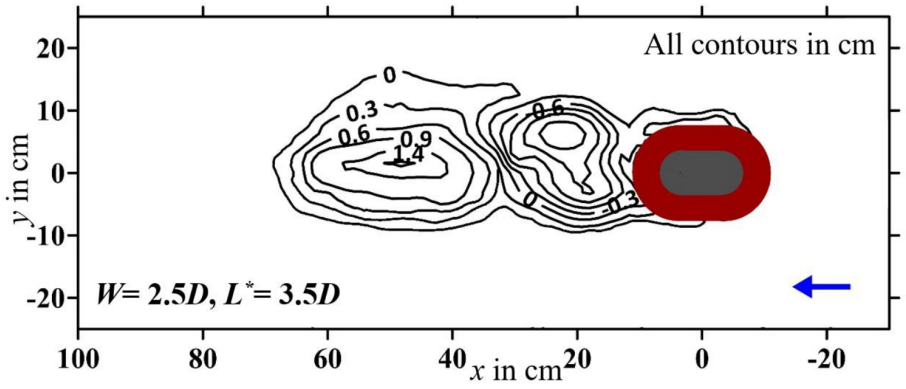


Fig. 5.39. Contour map of scour bed for *W/D*=2.5, and *L/D*= 2.

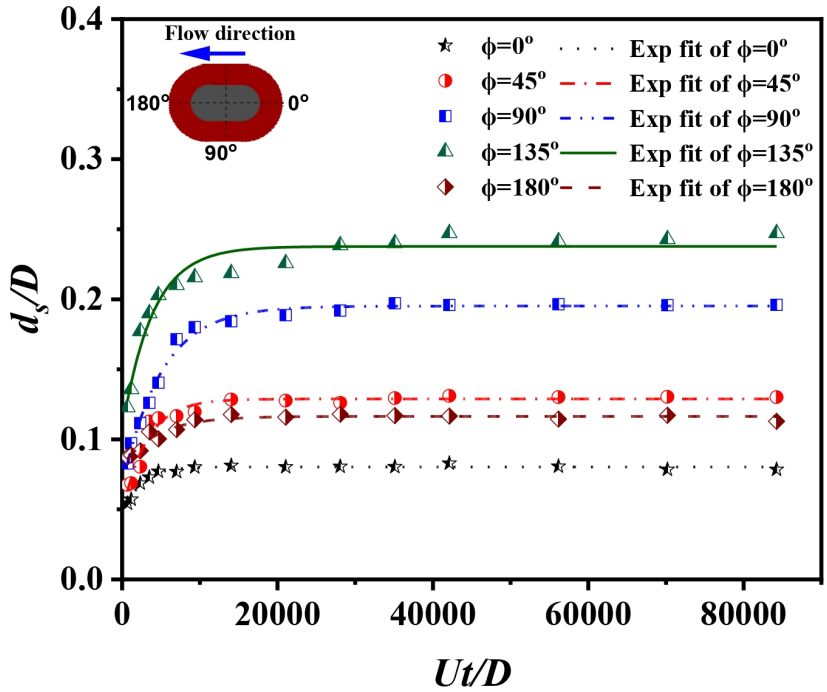


Fig. 5.40. Temporal variation of scour depth in non-dimensional form for different ϕ for *W/D*= 2.5, and *L/D*=2.

The temporal variation of the scour depth is studied and presented in Figure 5.40 for different positions around collar. The figure indicates that the nondimensional scour depth increases rapidly with nondimensional time for 180° and 135° cases initially. Later the increment rate is sloth and after around 3 hours, the scour rate almost remains unchanged and

equilibrium is reached. However, there is a lower rate of scour for the 0^o, 45^0 and 90^0 cases initially compared to the previous cases. For all the cases, the experimental data are fitted to the exponential data fit and for all the cases, the R^2 value remains within 0.98 to 0.99.

5.2.5 Pier with collar *W/D*= 2

The experiment is conducted considering an oblong pier with a collar. It has a collar width to pier width ratio of 2. Fig. 5.41 represents the dry-sand bed of this case before the commencement of the flow. The flow direction in presented by a blue arrow mark in the figure. A flow of water inside the flume is continued for 6 hours to achieve the equilibrium depth. Later, releasing the water from the flume, the dry sand bed as shown in Fig. 5.42 indicates the visible presence of scour at the side of the collar (45^0 and 90^0). However, at 0^0 and 135^0 positions, there is little scour of sand. There is very little deposition at the position of 180^0. There is visible deposition of sand at the downstream of the collar.



Fig. 5.41. Sand bed before experimental run for *W*/*D*= 2, and *L*/*D*=2.



Fig. 5.42. Scour bed around the collar after experimental run for *W/D*= 2, and *L/D*=2.

The dry-sand scour data are collected and fitted to surfer software. The contour is generated and it is presented in Fig. 5.43. In the contour, the pier is presented by deep grey color and the collar is presented by ruby red color. The positive and negative values of contour lines represent the deposition and scour, respectively. The contour predictions are almost equivalent to the actual captured image of the experiment shown in Fig. 5.42. Figure 5.43 indicates the presence of maximum scour near the position of angle 45°. The maximum scour depth is 2.013 cm.

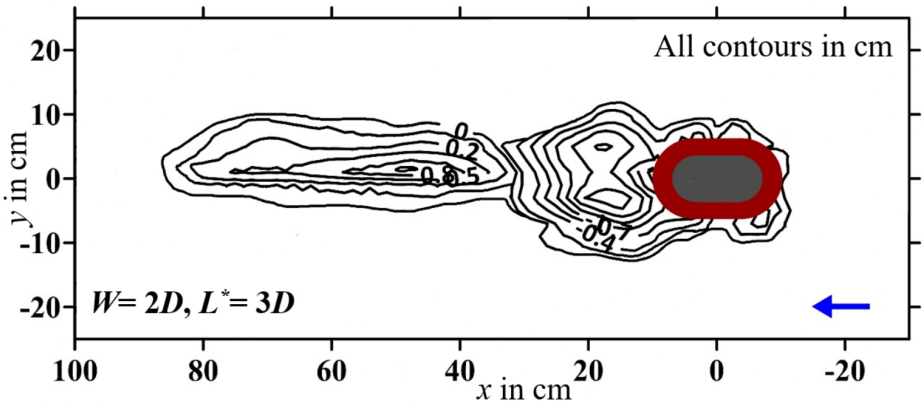


Fig. 5.43. Contour map of scour bed for *W/D*=2, and *L/D*=2.

The temporal variation of the scour depth is studied and presented in Fig. 5.44 for different positions around the collar. The figure indicates that the nondimensional scour depth increases rapidly with nondimensional time for 45° and 90° cases initially. Later the increment rate is sloth and after around 3 hours, the scour rate almost remains unchanged and equilibrium is reached. However, there is a lower rate of scour for the 0° and 135° cases initially compared to the previous cases. Figure 5.44 also indicates the deposition of sand for

the cases of 180°. The rate of deposition is slow for the case of 180°. For all the cases, both for the scour and deposition, the experimental data are fitted to the exponential data fit and for all the cases, the R^2 value remains between 0.98 to 0.99.

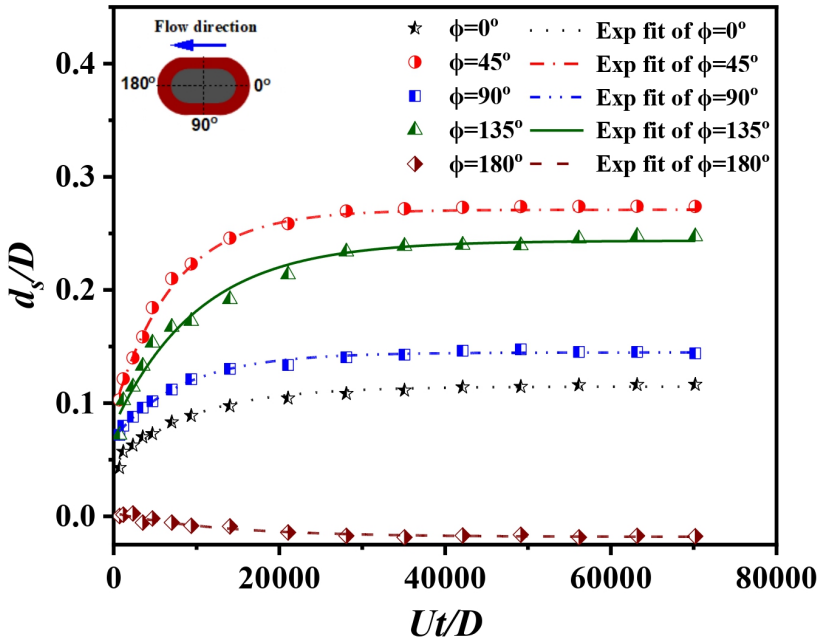


Fig. 5.44. Temporal variation of scour depth in non-dimensional form for different ϕ *W/D*= 2, and *L/D*=2.

5.2.6 Pier with collar *W/D*= 1.5

The experiment is conducted considering an oblong pier with a collar. It has a collar width to pier width ratio of 1.5. Figure 5.45 represents the dry-sand bed of this case before the commencement of the flow. The flow direction is presented by a blue arrow mark in the figure. A flow of water inside the flume is continued for 6 hours to achieve the equilibrium scour depth. Later, releasing the water from the flume, the dry sand bed as shown in Fig. 5.46 indicates the visible presence of scour at the upstream (0^0) and side of the collar (45^0). However, at the 90° position, there is little scour of sand. There is very little deposition at the position of 135° and 180^0. There is visible deposition of sand at the downstream of the collar.



Fig. 5.45. Sand bed before the experimental run for *W/D*= 1.5, and *L/D*=2.



Fig. 5.46. Scour bed around the collar after experimental run for *W/D*= 1.5, and *L/D*=2.

The dry-sand scour data are collected and fitted to surfer software. The contour is generated and it is presented in Fig. 5.47. In the contour, the pier is presented by deep grey color and collar is presented by ruby red color. The positive and negative values of contour lines represent the deposition and scour, respectively. The contour predictions are almost equivalent to the actual captured image of the experiment shown in Fig. 5.46. Figure 5.47 indicates the presence of maximum scour near the position of angle 0^{o}. The maximum scour depth is 2.46 cm.

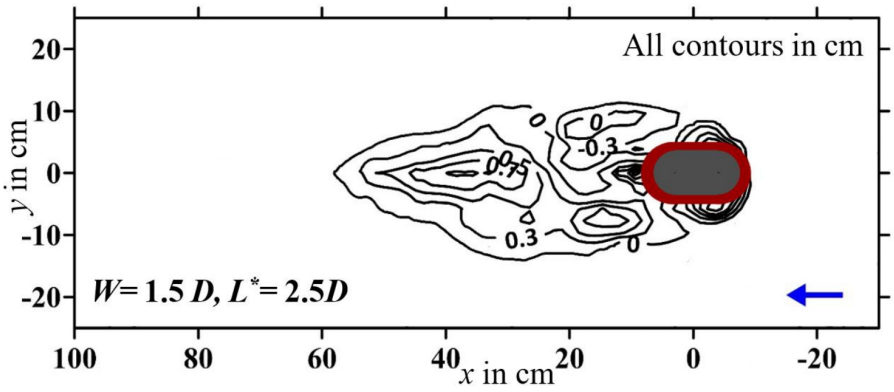


Fig. 5.47. Contour map of scour bed for *W/D*= 1.5, and *L/D*=2.

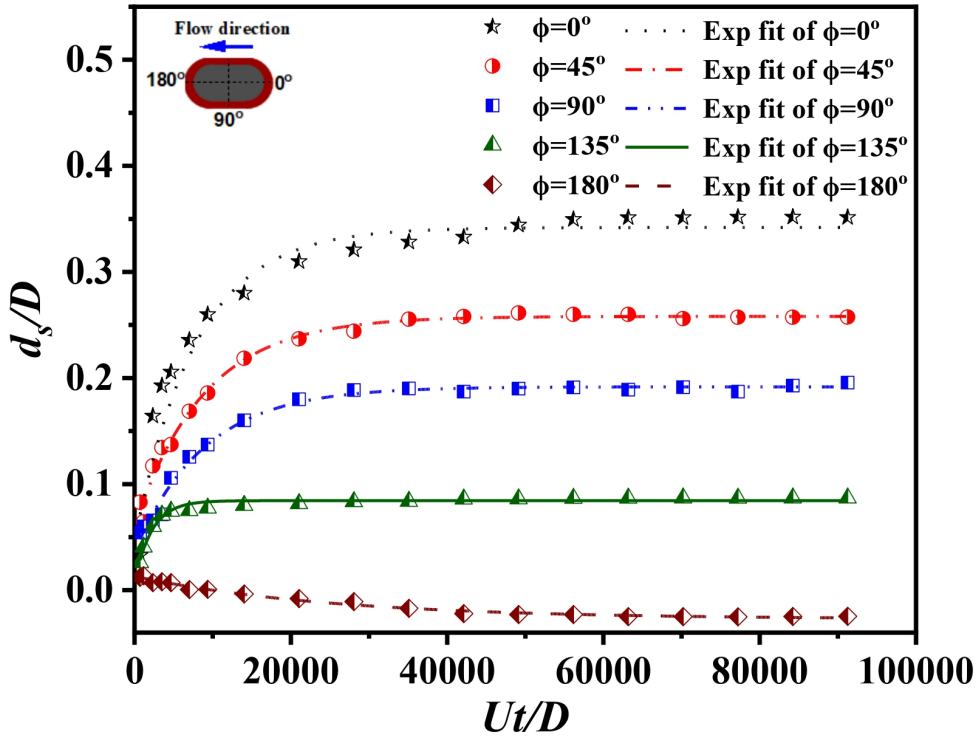


Fig. 5.48. Temporal variation of scour depth in non-dimensional form for different ϕ *W/D*= 1.5, and *L/D*=2.

The temporal variation of the scour depth is studied and presented in Fig. 5.48 for different positions around the collar. The figure indicates that the non-dimensional scour depth increases rapidly with nondimensional time for 0° and 45° cases initially. Later the increment rate is sloth and after around 3 hours, the scour rate almost remains unchanged and equilibrium is reached. However, there is a lower rate of scour for 90^0 and 135^0 positions

initially compared to the previous cases. Fig. 5.48 also indicates the deposition of sand for the cases of 180°. The rate of deposition is slow for the case of 180°. For all the cases, both for the scour and deposition, the experimental data are fitted to the exponential data fit and for all the cases, the R^2 value remains between 0.98 to 0.99.

5.3 Comparisons of scour depth for different angles of scour position

The temporal scour depth for a particular position around the collar, for different *W/D* ratios is studied and presented in this section. It is to be mentioned that the said study is carried out for different *L/D* ratios respectively. The scour depth for a particular position is further compared with the case of without the collar.

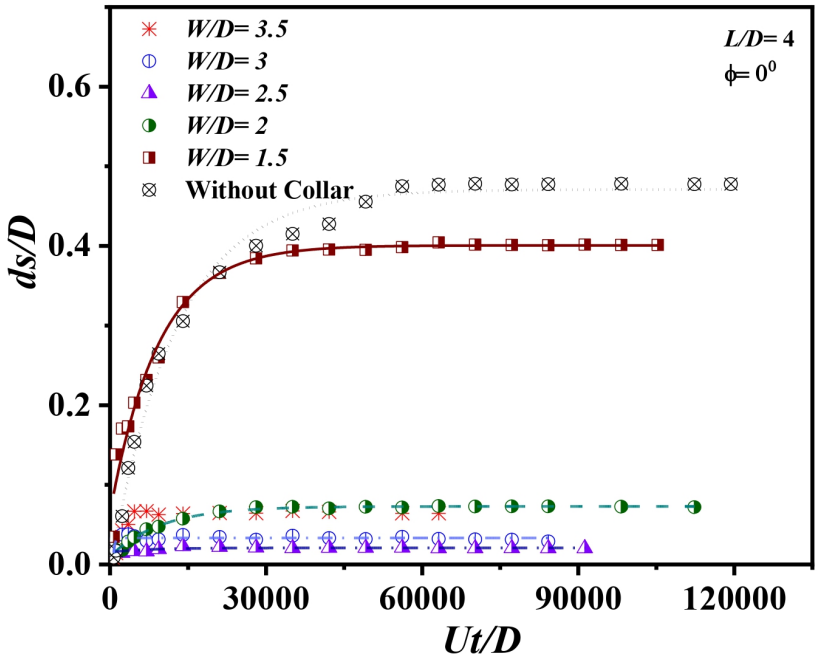


Fig. 5.49. Temporal variation of scour depth in non-dimensional form for different *W/D* ratios when *L/D*=4, and ϕ=0°.

Figure 5.49 represents the nondimensional temporal scour depth variation for 0° case and *L/D* ratio = 4. The figure indicates that the trend of variation of scour depth is almost equivalent for different *W/D* ratios. However, the slope and intensity of variation are different. With the increasing *W/D* ratio, the scour inception diminishes gradually. For a lower *W/D* ratio, i.e., *W/D*=1.5, the scour inception is almost equivalent to the case without the collar. There is an interesting fact that increasing the *W/D* ratio to just 0.5 i.e., when the *W/D* ratio is 2, the scour depth is considerably low compared to the previous case. Minimum scour depth is present for the case of *W/D*=2.5. There is higher scour depth for *W/D* ratio 3 and 3.5 compared to the 2.5 case. However, the change of scour depth for changing the *W/D* ratio

from 3 to 3.5, there is no such considerable change in depth. Hence during the design of the collar, the cost factor and depth cases both have to be co-compared from efficient and economic perspectives respectively.

Figure 5.50 represents the nondimensional temporal scour depth variation for the 45° case and *L/D* ratio = 4. The figure indicates that the trend of variation of scour depth is almost equivalent for different *W/D* ratios. However, the slope and intensity of variation are different. With the increasing *W/D* ratio, the scour inception diminishes gradually. For a lower *W/D* ratio, i.e., *W/D*=1.5, the scour inception is almost equivalent to the case without the collar. There is an interesting fact that increasing the *W/D* ratio to just 0.5 i.e., when the *W/D* ratio is 2, the scour depth is considerably high compared to the previous scour position. Minimum scour depth is present for the case of *W/D*=2.5. There is higher scour depth for *W/D* ratio 3 and 3.5 compared to the 2.5 case. However, for the change of scour depth for changing the *W/D* ratio from 3 to 3.5, there is no such considerable change in depth.

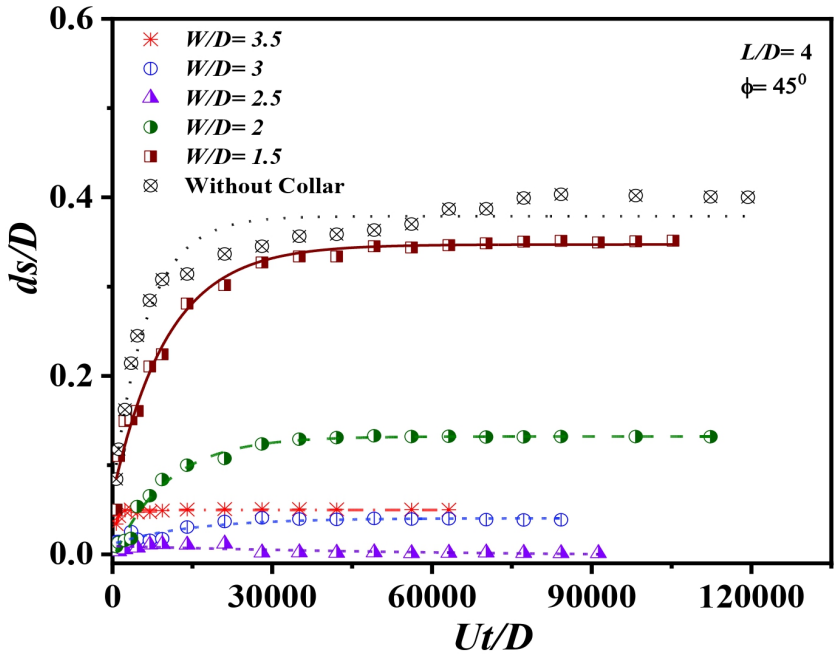


Fig. 5.50. Temporal variation of scour depth in non-dimensional form for different *W/D* ratios when *L/D*=4, and ϕ=45⁰.

Figure 5.51 represents the nondimensional temporal scour depth variation for 90° case and *L/D* ratio, 4. The figure indicates that the sand deposition is evident in the scenario without a collar. Importantly, the rate of deposition is slow under this condition. The figure also demonstrates the trend of variation of scour depth is almost equivalent for different *W/D* ratios. However, the slope and intensity of variation are different. With the increasing *W/D* ratio, the scour inception does not diminish gradually compared to the previous case. For a lower *W/D* ratio, i.e., *W/D*=1.5, the scour inception is high. There is an interesting fact that

when the *W/D* ratio is 3.5, the scour depth is considerably high compared to the previous scour position. Minimum scour depth is present for the case of *W/D*=2 and 2.5. There is a higher scour depth for *W/D* ratios of 3 and 3.5 compared to the 2 and 2.5 cases. However, the change of scour depth for changing the *W/D* ratio from 2 to 2.5, there is no such considerable change in depth.

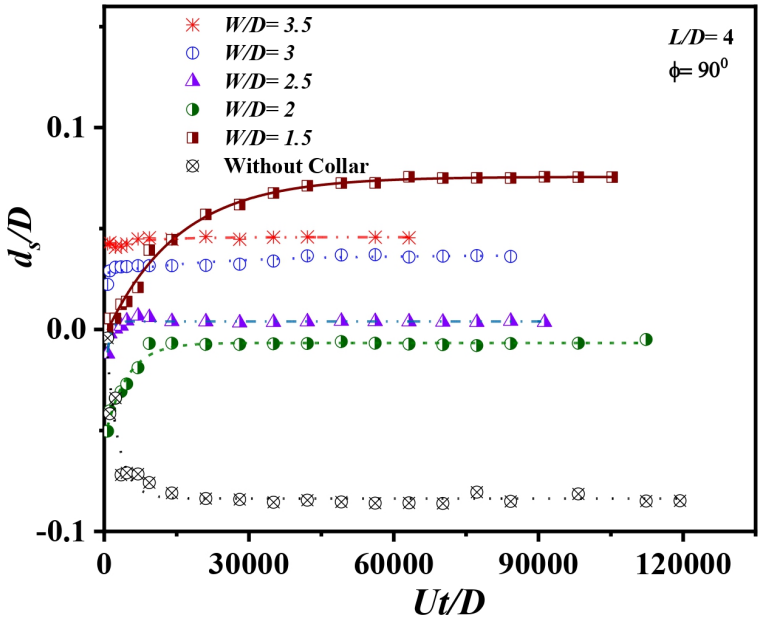


Fig. 5.51. Temporal variation of scour depth in non-dimensional form for different *W/D* ratios when *L/D*=4, and ϕ=90^0.

Figure 5.52 illustrates the temporal variation of nondimensional scour depth for 135^o cases and *L/D* ratio of 4. The figure indicates that the trend of variation of scour depth is almost equivalent for different *W/D* ratios. However, the slope and intensity of variation are different. As the *W/D* ratio increases, the scour does not diminish gradually in comparison to Figures 4.49 and 4.50. For a lower *W/D* ratio, i.e., *W/D*=1.5, the scour inception is almost equivalent to the case without the collar and the scour depth is lower compared to the other *W/D* ratios. Maximum scour depth is present for the case of *W/D*=2. However, the change of scour depth for changing the *W/D* ratio from 2.5 to 3, there is no such considerable change in depth. An intriguing observation is that when the *W/D* ratio increases to 0.5 and 3, specifically *W/D* ratios of 2 and 3.5, there is a higher scour depth compared to the previous case.

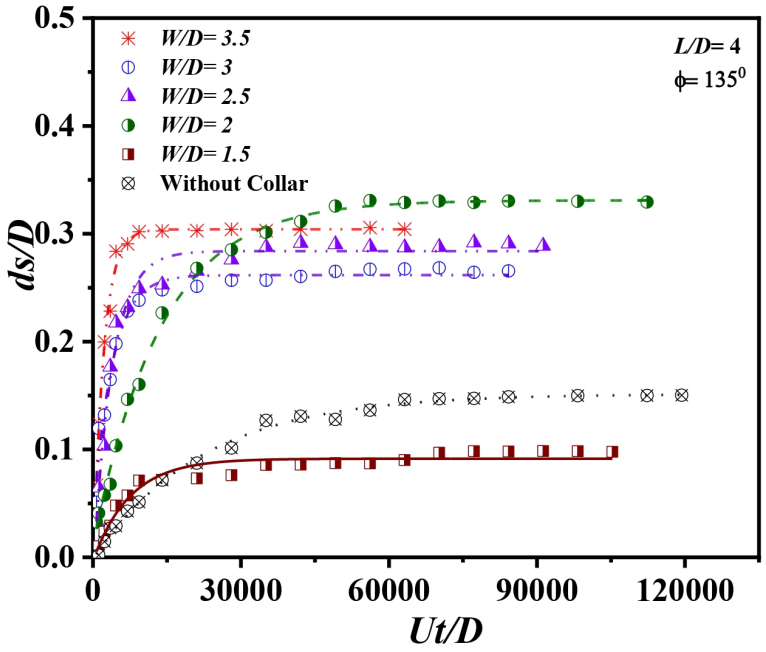


Fig. 5.52. Temporal variation of scour depth in non-dimensional form for different *W/D* ratios when *L/D*=4, and ϕ=135^0.

Figure 5.53 represents the temporal variation of nondimensional scour depth for 180^o case and *L/D* ratio, 4. The figure demonstrates the trend of variation of scour depth is almost equivalent for different *W/D* ratios. However, the slope and intensity of variation are different. For a lower *W/D* ratio, i.e., *W/D*=1.5, the scour inception is almost equivalent to the case without the collar and scour depth is minimized compared to the previous case. The maximum scour depth occurs for *W/D* ratios of 2 and 3.5, with higher scour depths observed for these ratios compared to the cases of 2.5 and 3. However, the transition from a *W/D* ratio of 2.5 to 3 shows no significant change in scour depth. This suggests that within this range, slight adjustments in the *W/D* ratio may not have a substantial impact on the scour depth.

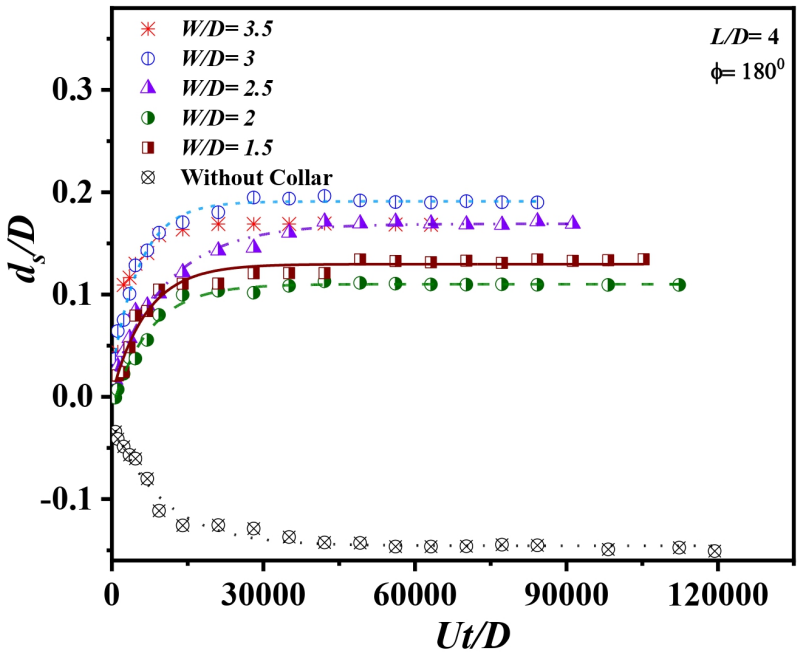


Fig. 5.53. Temporal variation of scour depth in non-dimensional form for different *W*/*D* ratios when *L*/*D*=4, and ϕ=180^0.

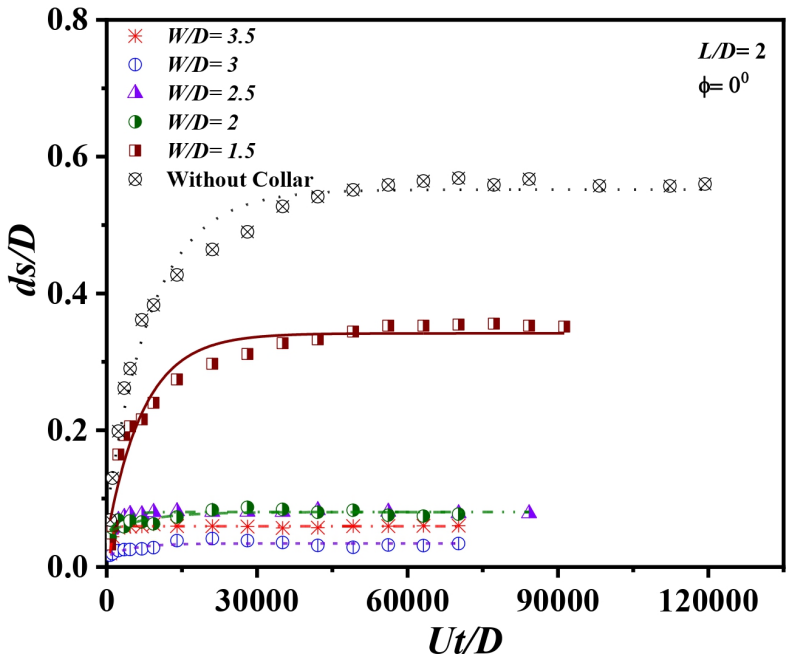


Fig. 5.54. Temporal variation of scour depth in non-dimensional form for different *W*/*D* ratios when *L*/*D*=2, and ϕ=0^0.

Figure 5.54 illustrates the temporal variation of nondimensional scour depth for the case of 0^o and *L*/*D* ratio of 2. The figure indicates that the trend of variation of scour depth is

almost equivalent for different *W/D* ratios. However, the slope and intensity of variation are different. With the increasing *W/D* ratio, the scour inception diminishes gradually. For a lower *W/D* ratio, i.e., *W/D*=1.5, the scour inception is almost equivalent to the case without the collar. There is an interesting fact that increasing the *W/D* ratio to just 0.5 i.e. when the *W/D* ratio is 2, the scour depth is considerably low compared to the previous case. Minimum scour depth is present for the case of *W/D*=3. There is a lower scour depth for *W/D* ratio 3 and 3.5 compared to the 2 and 2.5 cases. However, for the change of scour depth for changing the *W/D* ratio from 2 to 2.5, there is no such considerable change in depth. This suggests that small adjustments in the *W/D* ratio within this range may not result in substantial variations in scour depth.

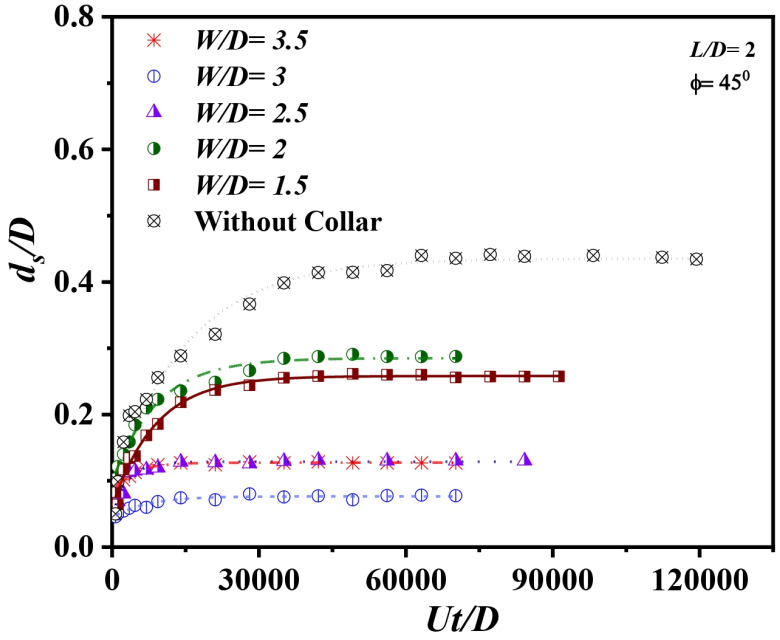


Fig. 5.55. Temporal variation of scour depth in non-dimensional form for different *W/D* ratios when *L/D*=2, and ϕ=45^0.

Figure 5.55 illustrates the temporal variation of nondimensional scour depth for the case of 45^o and *L/D* ratio of 2. The figure indicates that the trend of variation of scour depth is almost equivalent for different *W/D* ratios. However, the slope and intensity of variation are different. With the increasing *W/D* ratio, the scour inception diminishes gradually. For lower *W/D* ratios, specifically *W/D*=1.5 and 2, the onset of scour is nearly comparable to the scenario without a collar. However, the rate of scouring is diminished in comparison to when there is no collar present. There is an interesting fact that increasing the *W/D* ratio just 1.5 i.e., when the *W/D* ratio is 2.5, the scour depth is considerably low compared to the previous case. Minimum scour depth is present for the case of *W/D*=3. There is a lower scour depth for *W/D* ratio 3 and 3.5 compared to the 2 and 2.5 cases. However, the change of scour depth for changing the *W/D* ratio from 1.5 to 2, there is no such considerable change in depth. This

suggests that small adjustments in the *W/D* ratio within this range may not result in substantial variations in scour depth.

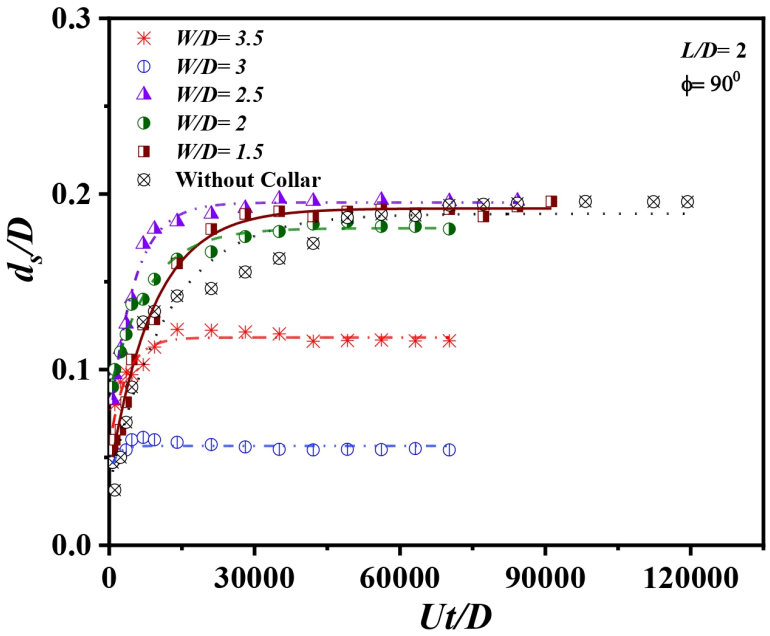


Fig. 5.56. Temporal variation of scour depth in non-dimensional form for different *W/D* ratios when *L/D*=2, and ϕ=90^0.

Figure 5.56 illustrates the temporal variation of nondimensional scour depth for the case of 90^o and *L/D* ratio of 2. The figure indicates that the trend of variation of scour depth is almost equivalent for different *W/D* ratios. However, the slope and intensity of variation are different. With the increasing *W/D* ratio, the scour inception diminishes gradually. For lower *W/D* ratios, specifically *W/D*=1.5, 2.0 and 2.5, the onset of scour is nearly comparable to the scenario without a collar. However, the rate of scouring is not reduced compared to the scenario where there is no collar, as seen in the previous case. An intriguing observation arises when the W/D ratio is increased to 2, specifically when the *W/D* ratio reaches 3. At this ratio, the scour depth notably decreases in comparison to the preceding scenario. The minimum scour depth is observed in the case where *W/D* equals 3. Notably, there is a diminished scour depth for a W/D ratio of 3 compared to the scenario where the ratio is 3.5.

Figure 5.57 illustrates the temporal variation of nondimensional scour depth for the case of 135^o and *L/D* ratio of 2. The figure indicates that the trend of variation of scour depth is almost equivalent for different *W/D* ratios. However, the slope and intensity of variation are different. As the *W/D* ratio increases, there is no gradual decrease in scour inception. The minimum scour depth is notably observed, especially when considering lower *W/D* ratios, particularly at values of *W/D*=1.5 and 2. The figure also indicates the scenario where there is no collar present to prevent it, sand deposition occurs naturally. The maximum scour depth is observed for a *W/D* ratio of 3. However, when altering the *W/D* ratio to 2.5 and 3.5, there is

negligible change in scour depth. This suggests that minor modifications in the *W/D* ratio within this range are unlikely to result in significant alterations in scour depth.

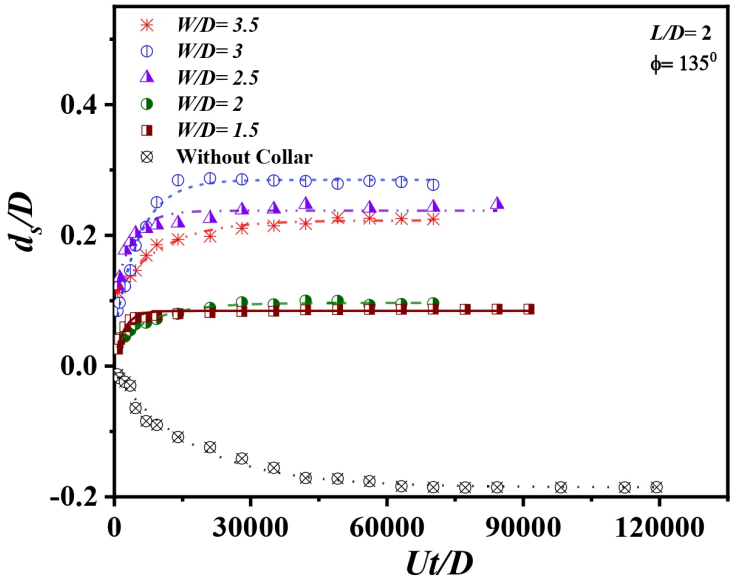


Fig. 5.57. Temporal variation of scour depth in non-dimensional form for different *W/D* ratios when *L/D*=2, and ϕ=135^0.

Figure 5.58 represents the temporal variation of nondimensional scour depth for the case of 180^o and *L/D* ratio of 2. The figure shows that scour depth changes similarly across different *W/D* ratios, but the slope and magnitude of the change vary. Particularly, as the *W/D* ratio increases, there's no gradual decrease in scour inception. This suggests that higher *W/D* ratios might not always result in a proportional decrease in scour depth. The minimum sand deposition is particularly noticeable, especially when considering lower *W/D* ratios, notably at values of *W/D*=1.5 and 2. The figure also indicates the scenario where there is no collar present to prevent it, maximum sand deposition occurs naturally. The maximum scour depth is observed for a *W/D* ratio of 3 and 3.5. The scour depth is notably reduced when considering the *W/D* ratio of 2.5 in comparison to the scenarios with *W/D* ratios of 3 and 3.5.

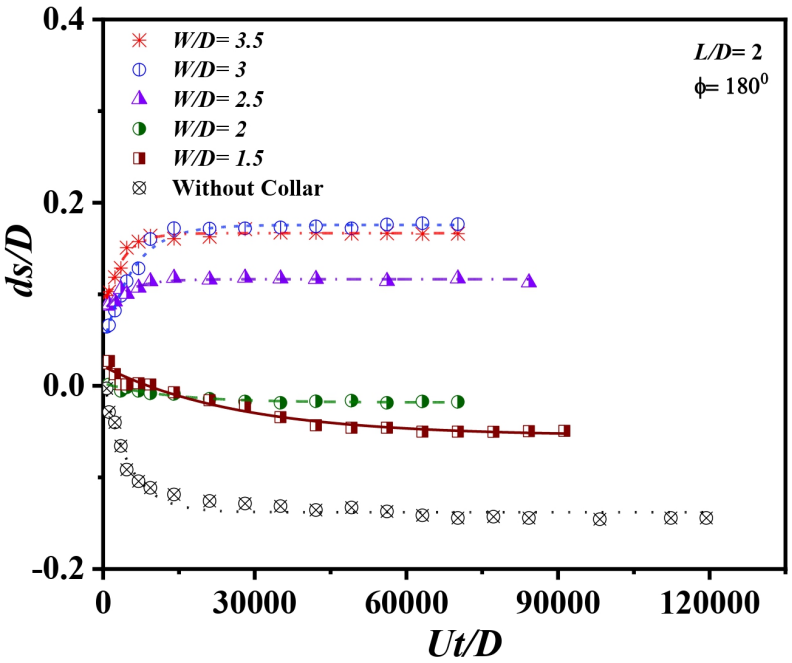


Fig. 5.58. Temporal variation of scour depth in non-dimensional form for different *W/D* ratios when *L/D*=2, and ϕ=180^0.

5.4 Comparison of scour depths varying with *W/D* for different *L/D* ratios

From the observation of the previous section 6.3 it is observed that increasing the *W/D* ratio there is a critical case of *W/D* after which instead of decreasing the scour depth, it increases further. Hence, identifying an optimal *W/D* ratio becomes imperative to reduce scour depth around the oblong pier. Consequently, this study seeks to investigate the minimum *W/D* ratio for both *L/D* ratios of 2 and 4, while accounting for different angles of scour position.

Figure 5.59 indicates the behavior of scour depth at 0° angle position, for both the *L/D* ratio cases. Remarkably, it unveils a consistent trend where the scour depth initially decreases and then increases the pattern of variation. This observation suggests the presence of critical *W/D* ratios that minimize scour depth for both *L/D* ratio cases. For *L/D* ratios of 2 and 4, these critical *W/D* ratios are determined to be 3 and 2.5 respectively.

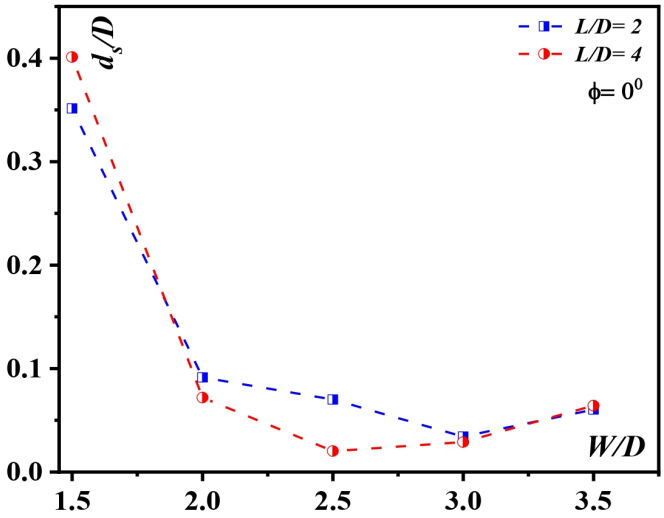


Fig. 5.59. Non-dimensional scour depth variation with *W/D* ratio for $\phi=0^0$.

Figure 5.60 indicates the behavior of scour depth at 45° angle position, for both the *L/D* ratio cases. Notably, it shows a consistent trend where the scour depth initially decreases then increasing pattern of variation, in contrast to the previous case. This observation suggests the presence of critical *W/D* ratios that minimize scour depth for both *L/D* ratio cases. For an *L/D* ratio of 4, the critical *W/D* ratios are found to be 2.5, whereas for an *L/D* ratio of 2, these critical *W/D* ratios are determined to be 3.

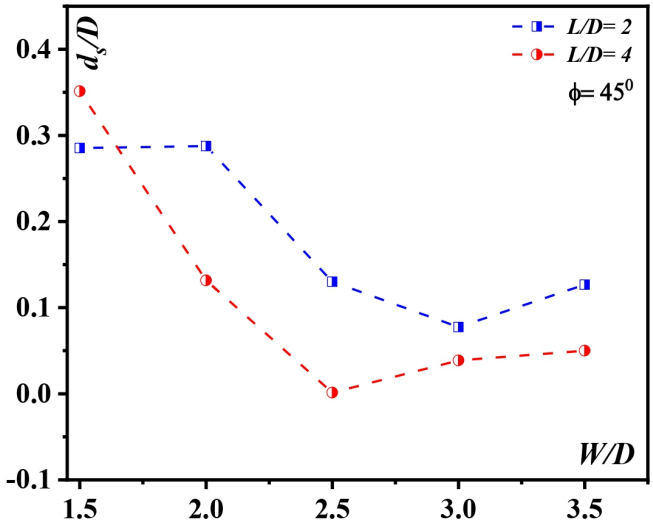


Fig. 5.60. Non-dimensional scour depth variation with *W/D* ratio for $\phi=45^0$.

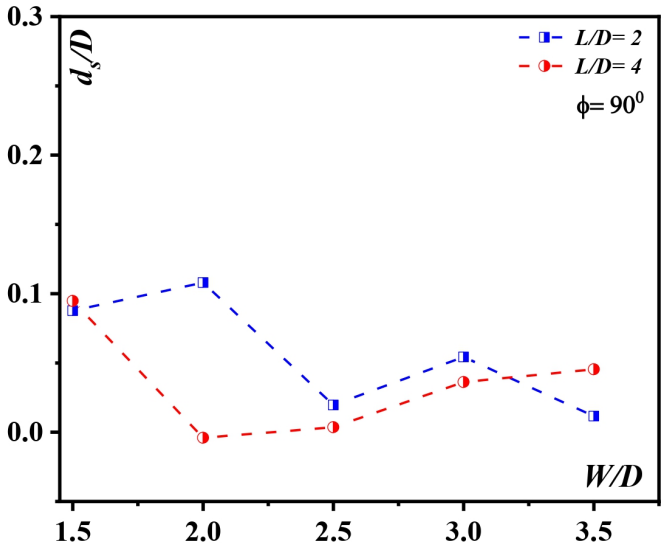


Fig. 5.61. Non-dimensional scour depth variation with *W/D* ratio for $\phi=90^0$.

Figure 5.61 indicates the behavior of scour depth at 90^0 angle position, for both the *L/D* ratio cases. Interestingly, it demonstrates a lack of consistent trend compared to the previous case, wherein the scour depth initially decreases and then increases the pattern of variation. For an *L/D* ratio of 4, the scour depth initially increases before decreasing, while for an *L/D* ratio of 2, the scour depth follows a pattern of initially increasing, then decreasing, and finally increasing again. This observation suggests the presence of critical *W/D* ratios that minimize scour depth for both *L/D* ratio cases. For an *L/D* ratio of 4, the critical *W/D* ratios are found to be 2, whereas for an *L/D* ratio of 2, these critical *W/D* ratios are determined to be 2.5.

Figure 5.62 indicates the behavior of scour depth at 135^0 angle position, for both the *L/D* ratio cases. Interestingly, it demonstrates a lack of consistent trend compared to the previous case, wherein the scour depth initially decreases and then increases the pattern of variation. For an *L/D* ratio of 4, the scour depth initially increases, then decreases, and finally increases while for an *L/D* ratio of 2, the scour depth follows a pattern of initially increasing before decreasing. This observation suggests the presence of critical *W/D* ratios that minimize scour depth for both *L/D* ratio cases. For both *L/D* ratios of 2 and 4, For *L/D* ratios of 2 and 4, these critical *W/D* ratios are determined to be 1.5.

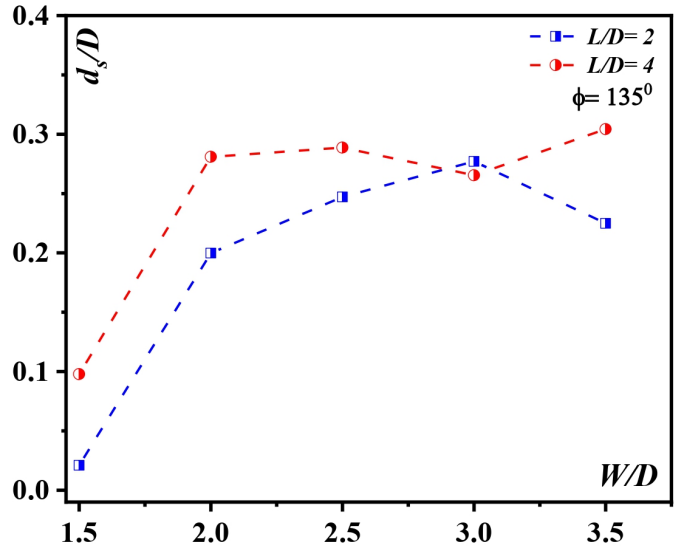


Fig. 5.62. Non-dimensional scour depth variation with *W/D* ratio for ϕ=135^0.

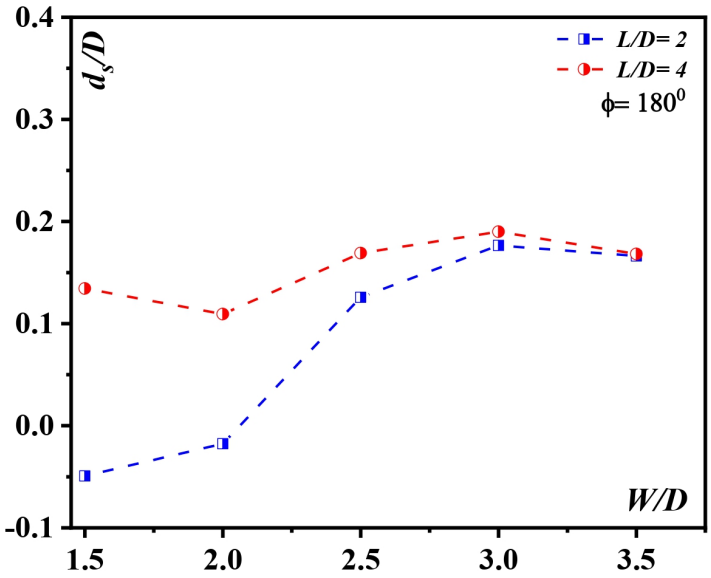


Fig. 5.63. Non-dimensional scour depth variation with *W/D* ratio for ϕ=180^0.

Figure 5.63 indicates the behavior of scour depth at 180^0 angle position, for both the *L/D* ratio cases. Interestingly, it demonstrates a lack of consistent trend compared to the previous case, wherein the scour depth initially decreases and then increases the pattern of variation. For an *L/D* ratio of 4, the scour depth initially decreases, then increases, and finally decreases again while for an *L/D* ratio of 2, the scour depth follows a pattern of initially increasing before decreasing. This observation suggests the presence of critical *W/D* ratios

that minimize scour depth for both *L/D* ratio cases. For *L/D* ratios of 2 and 4, these critical *W/D* ratios are determined to be 1.5 and 2 respectively.

5.5 Comparisons of scour depth with *L/D* ratio for different *W/D* ratios and different angles of scour position

From the observation of the previous section 6.4, it is evident that when maintaining the same *W/D* ratio for both *L/D* ratios 2 and 4, scour depth varies due to the *L/D* ratio. Additionally, when the collar is absent, a decrease in the *L/D* ratio leads to an increase in scour depth. Thus, it becomes crucial to establish an optimal *L/D* ratio to minimize scour depth around the pier. Therefore, this study aims to explore the minimum *L/D* ratio for different *W/D* ratios while considering various angles of scour position.

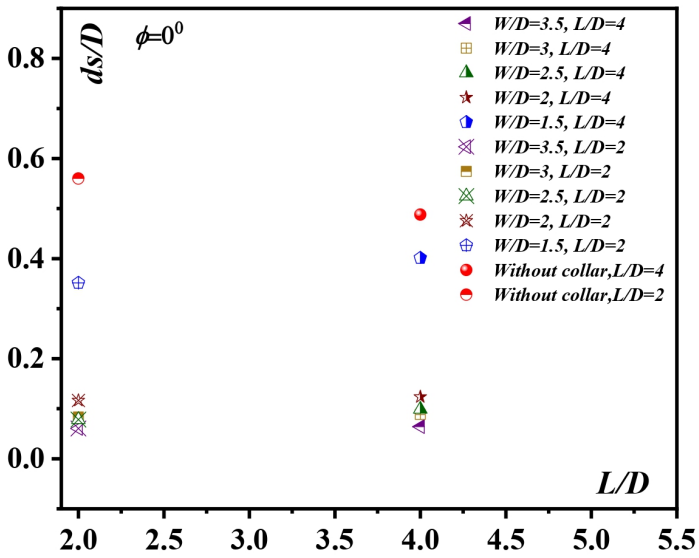


Fig. 5.64. Nondimensional scour depth variation with *L/D* ratio for $\phi=0^0$.

Figure 5.64 illustrates the scour depth behavior at a 0^0angle position for different *W/D* ratios across various *L/D* ratios. As the *L/D* ratio increases, scour depth decreases notably without a collar. However, at the minimum W/D ratio of 1.5, *L/D* ratio 4 exhibits higher scour depth compared to L/D ratio 2. Furthermore, within *W/D* ratios ranging from 2 to 3.5, there's minimal variation in scour depth for both *L/D* ratios. This observation suggests the presence of critical *L/D* ratios that minimize scour depth for different *W/D* ratios. For *W/D* ratios ranging from 1.5 to 3.5, these critical *L/D* ratios are noted for both *L/D* ratios of 2 and 4, particularly at higher *W/D* ratios, such as 3.5.

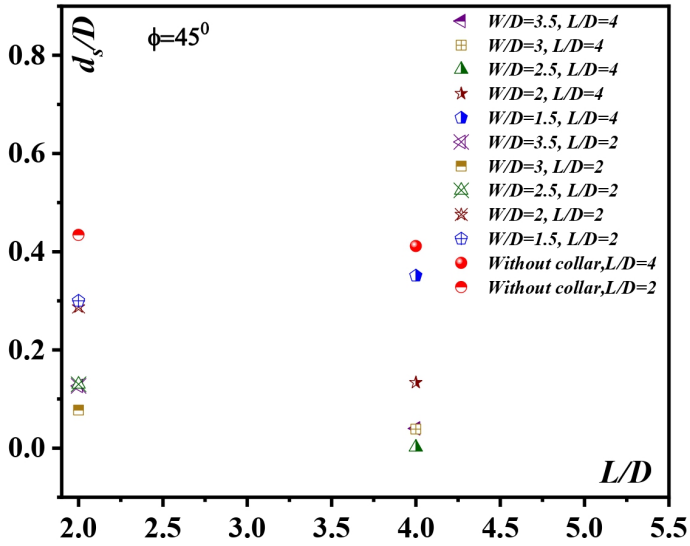


Fig. 5.65. Non-dimensional scour depth variation with *L/D* ratio for ϕ=45^0.

Figure 5.65 illustrates the scour depth behavior at a 45^0 angle position for different *W/D* ratios across various *L/D* ratios. As the *L/D* ratio increases, scour depth decreases notably without a collar. However, at the minimum *W/D* ratio of 1.5, *L/D* ratio 4 exhibits higher scour depth compared to *L/D* ratio 2. Furthermore, within W/D ratios ranging from 2.5 to 3.5, there's minimal variation in scour depth for both *L/D* ratios. This observation suggests the presence of critical *L/D* ratios that minimize scour depth for different *W/D* ratios. For *W/D* ratios ranging from 1.5 to 3.5, these critical *L/D* ratios are observed, especially at an L/D ratio of 4, with particular significance at a *W/D* ratio of 2.5.

Figure 5.66 illustrates the scour depth behavior at a 90^0 angle position for different *W/D* ratios across various *L/D* ratios. As the *L/D* ratio increases, scour depth decreases, especially in the absence of a collar. Deposition occurs when there's no collar at an *L/D* ratio of 4. However, at the minimum *W/D* ratio of 1.5, *L/D* ratio 4 exhibits higher scour depth compared to *L/D* ratio 2. Furthermore, within *W/D* ratios ranging from 2 to 3.5, there's minimal variation in scour depth for both *L/D* ratios. This observation suggests the presence of critical *L/D* ratios that minimize scour depth for different *W/D* ratios. For *W/D* ratios ranging from 1.5 to 3.5, these critical *L/D* ratios are observed, especially at an *L/D* ratio of 4, with particular significance at *W/D* ratio 2.

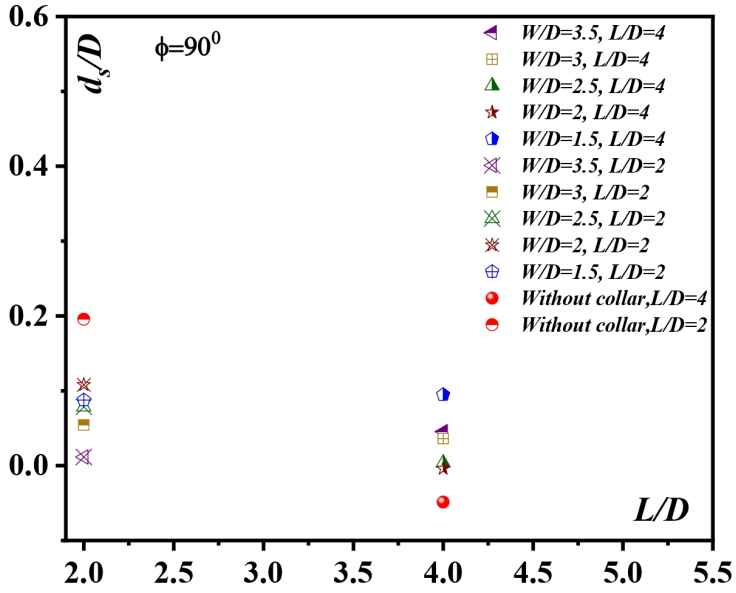


Fig. 5.66. Non-dimensional scour depth variation with *L/D* ratio for ϕ=90^0.

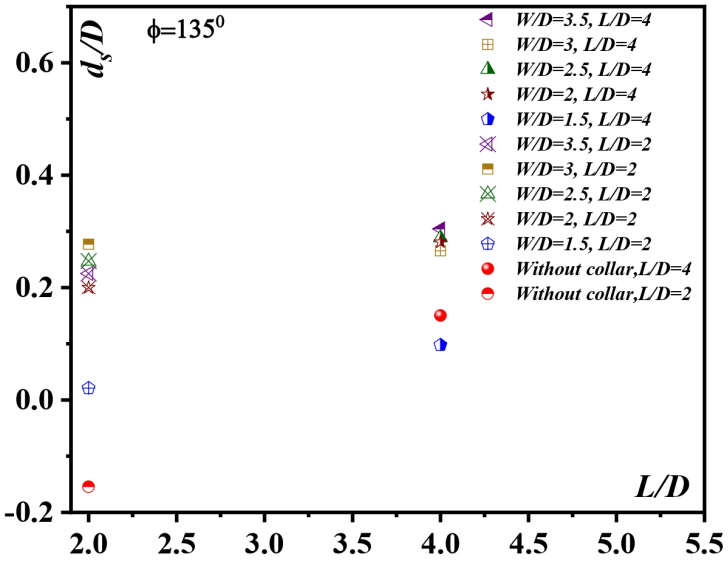


Fig. 5.67. Non-dimensional scour depth variation with *L/D* ratio for ϕ=135^0.

Figure 5.67 illustrates the scour depth behavior at a 135^0 angle position for different *W/D* ratios across various *L/D* ratios. In this scenario, as the *L/D* ratio increases, scour depth also increases, particularly when there's no collar, as opposed to the previous scenario. Deposition occurs when there's no collar at an *L/D* ratio of 2. However, at the minimum W/D ratio of 1.5, *L/D* ratio 4 exhibits higher scour depth compared to *L/D* ratio 2. Furthermore, within *W/D* ratios ranging from 2.5 to 3.5, there's minimal variation in scour depth for both

L/D ratios. This observation suggests the presence of critical *L/D* ratios that minimize scour depth for different *W/D* ratios. For *W/D* ratios ranging from 1.5 to 3.5, these critical *L/D* ratios are observed, especially at an *L/D* ratio of 2, with particular significance at a *W/D* ratio of 1.5.

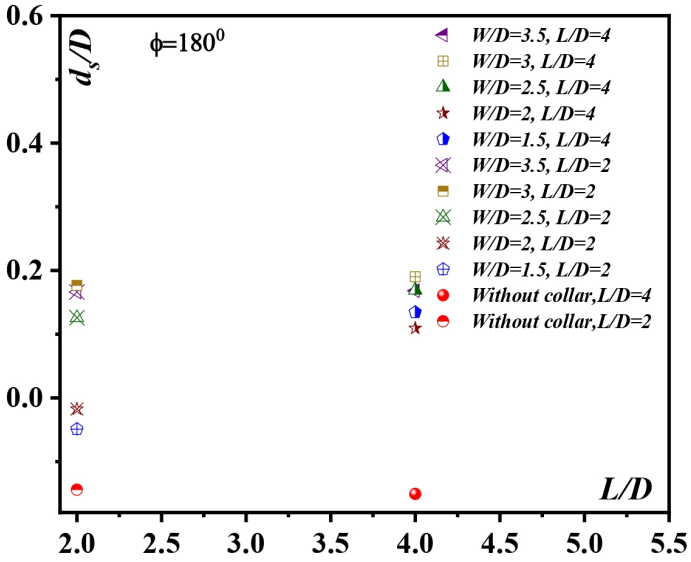


Fig. 5.68. Non-dimensional scour depth variation with *L/D* ratio for $\phi=180^0$.

Figure 5.68 illustrates the scour depth behavior at an 180^0 angle position for different *W/D* ratios across various *L/D* ratios. In this scenario, as the *L/D* ratio increases, scour depth also increases, particularly when there's no collar, as opposed to the previous scenario. Deposition occurs when there's no collar at an *L/D* ratio of 4. However, at the minimum *W/D* ratio of 1.5, *L/D* ratio 4 exhibits higher scour depth compared to *L/D* ratio 2 compared to the previous case. Furthermore, within *W/D* ratios ranging from 2.5 to 3.5, there's minimal variation in scour depth for both *L/D* ratios. This observation suggests the presence of critical *L/D* ratios that minimize scour depth for different *W/D* ratios. For *W/D* ratios ranging from 1.5 to 3.5, these critical *L/D* ratios are observed, especially at an *L/D* ratio of 4, with particular significance at *W/D* ratio 2.

5.6 Comparison of volume for different *W/D* and *L/D* ratios

In this section, we conduct a comparative analysis of deposition and scour volume across various *W/D* and *L/D* ratios with the help of surfer software. In Figure 5.69, it is evident that the scour volume peaks at W/D=2 for *L/D*=2, while the deposition volume reaches its maximum at *W/D*=2 for *L/D*=4.

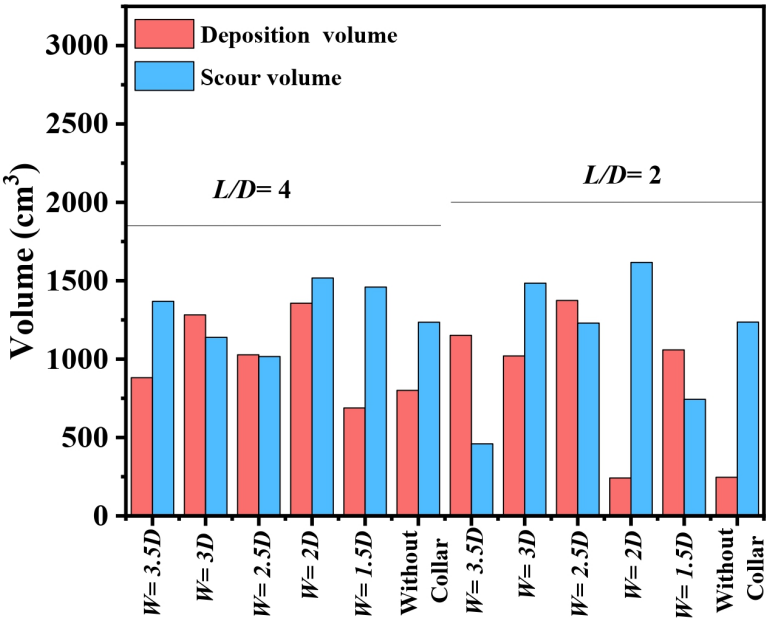


Fig. 5.69. Change of scour volume for different *L/D* and *W/D* ratios.

5.7 Comparison of planar area for different dimensions

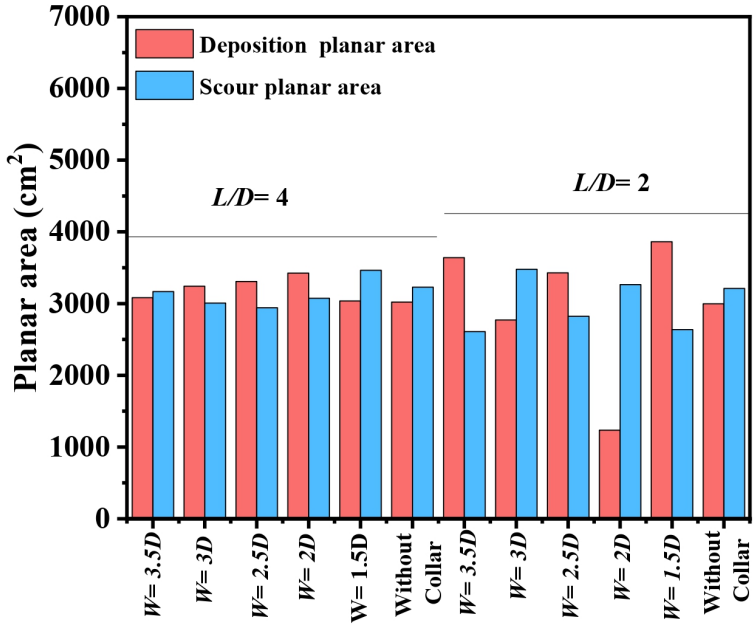


Fig. 5.70. Change of scour planar area for different *L/D* and *W/D* ratios.

In this section, we conduct a comparative analysis of deposition and scour planar area across various *W/D* and *L/D* ratios with the help of surfer software. In Figure 5.70, it is evident that

the scour planar area peaks at *W/D*=1.5 for *L/D*=4, while the deposition volume reaches its maximum at *W/D*=1.5 for *L/D*=2.

5.8 Comparison of surface area for different dimensions

In this section, we conduct a comparative analysis of deposition and scour surface area across various *W/D* and *L/D* ratios with the help of surfer software. In Figure 5.71, it is evident that the scour surface area peaks at *W/D*=1.5 for *L/D*= 4, while the deposition volume reaches its maximum at *W/D*=1.5 for *L/D*=2.

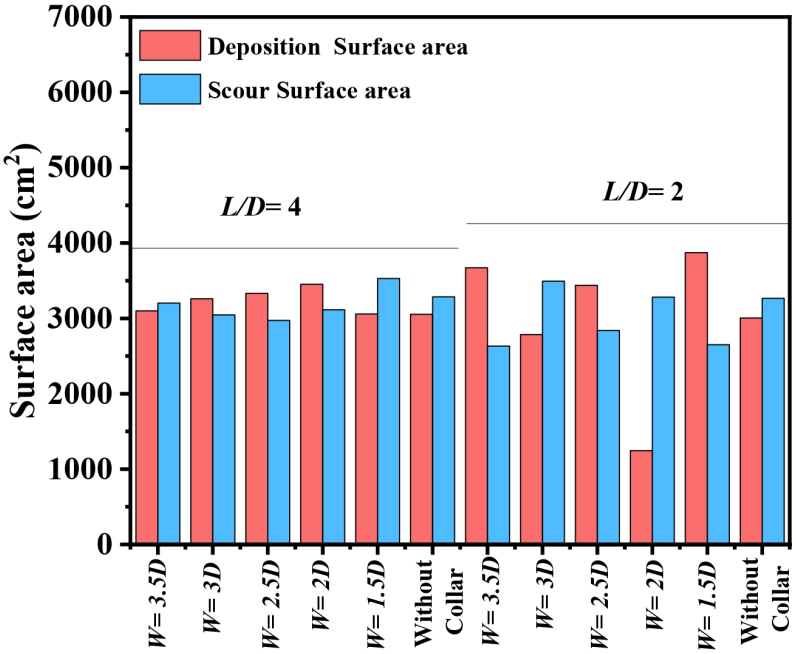


Fig. 5.71. Change of scour surface area for different *L/D* and *W/D* ratios.

5.9 Development of governing equation for temporal scour depth

With the help of observed data executed in the present analysis and other experimental data collected from open literature (Masjedi et al. (2010), Mashahir et al. (2008)) a governing equation for temporal scour prediction is developed with the help of Minitab Statistical Software. Initially, a sample equation is presented in Eq. (5.1). It is to be mentioned that the sample equation is taken in logarithmic variation with temporal data. The logarithmic variation is taken in compliance with the curve fitting of observed data as presented in Fig. 5.73. On the other hand, the non-dimensional scour depth is power variation to collar width to pier width, collar length to pier width, pier length to pier width, ratio of velocity to critical to pier width and collar position to pier width, as presented in Figs. 5.73, 5.74, 5.75, 5.76 and 5.77 respectively.

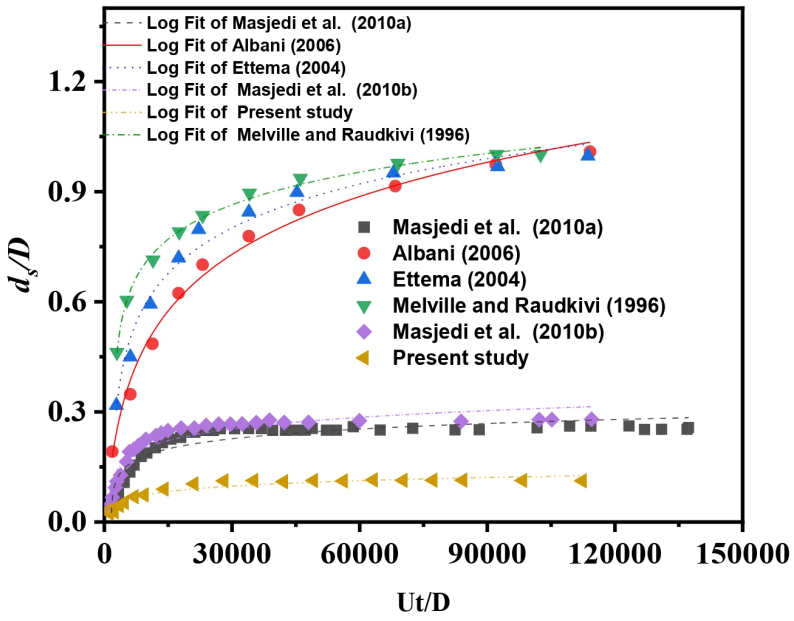


Fig. 5.72. Comparison of present experimental data with other data in open literature for temporal scour depth.

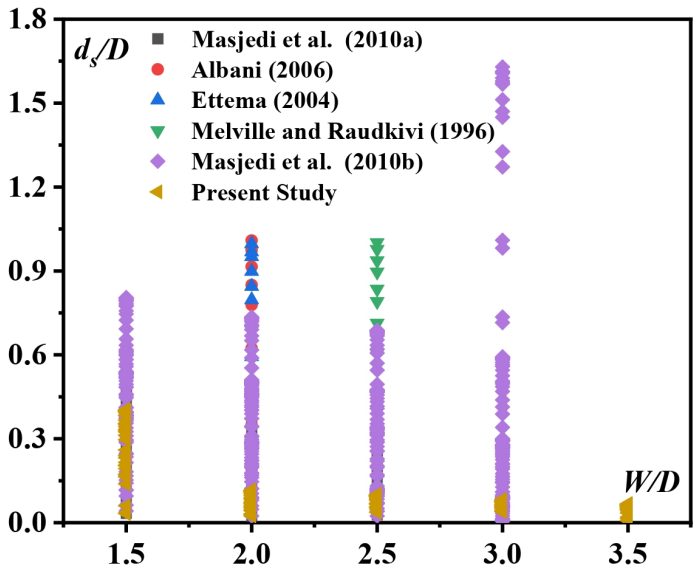


Fig. 5.73. Comparison of present experimental data with other data in open literature for Various *W/D* Ratio.

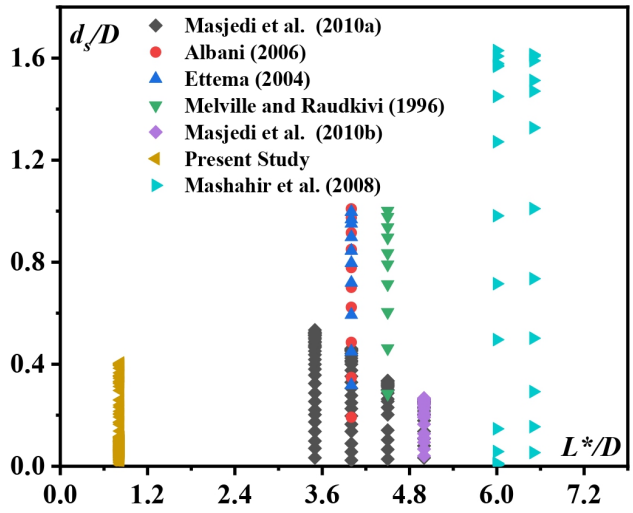


Fig. 5.74. Comparison of present experimental data with other data in open literature for Various L^*/D Ratio.

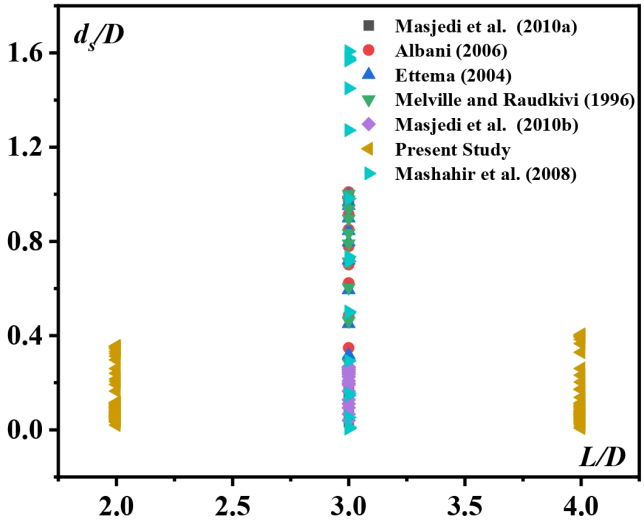


Fig. 5.75. Comparison of Observed and Predicted Values of Temporal Scour Depth for Various L/D Ratio.

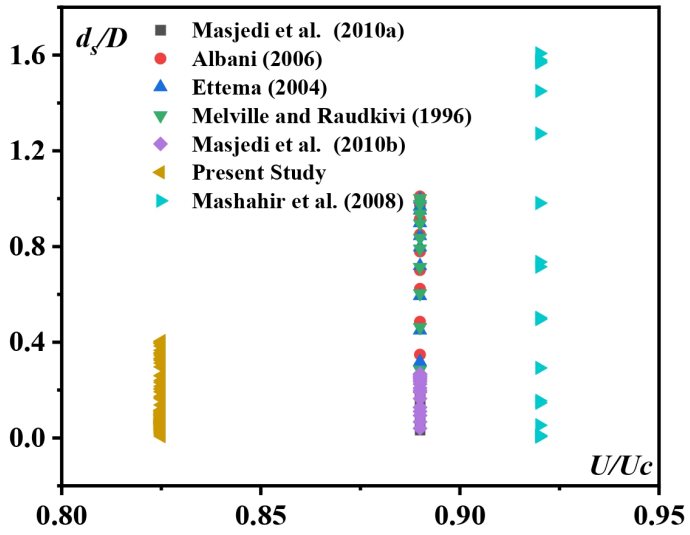


Fig. 5.76. Comparison of present experimental data with other data in open literature for Various U/U_c Ratio.

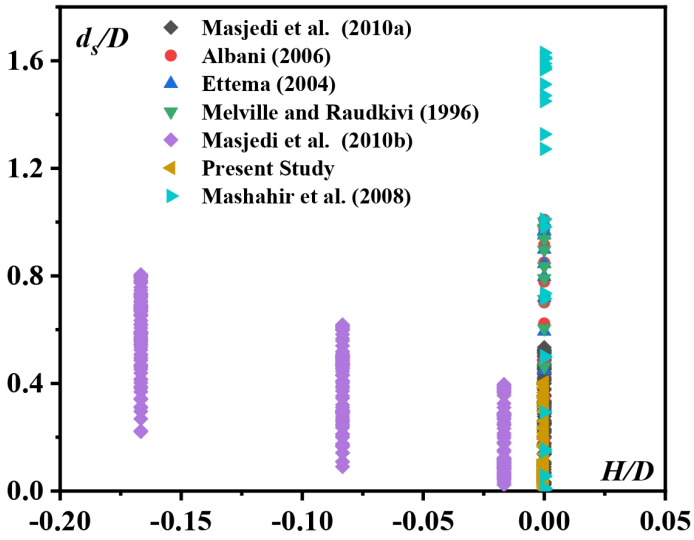


Fig. 5.77. Comparison of present experimental data with other data in open literature for Various H/D Ratio.

$$\frac{d_s}{D} = I\left(\frac{U}{U_C}\right)^J \times \left(\frac{W}{D}\right)^K \times \left(\frac{L}{D}\right)^M \times ln\left(\frac{Ut}{D}\right)^N \times \left(1-\frac{H}{D}\right)^O \times \left(\frac{L^*}{D}\right)^P \tag{5.1}$$

In Eq. (5.1), *I, J, K, M, N, O* and *P* are empirical constants and can be formed using observed data. These constants are identified by Minitab software with the help of the Gauss-Newton algorithm. The predicted data was found by Minitab Software and compared with the

present study by using the correlation method in Microsoft Excel Software. It is to be mentioned that an acceptable correlation value is set higher than 90%. It is further to be mentioned that from the available observed data, 80% data was used to develop the governing equation and the remaining 20% was used to test the equation. Finally, the following governing Eq. (5.2) of temporal scour prediction around an oblong pier with a collar is identified.

$$\frac{d_s}{D} = 4.5\times10^{-6}\left(\frac{U}{U_C}\right)^{54.26}\times\left(\frac{W}{D}\right)^{0.07}\times\left(\frac{L}{D}\right)^{13.04}\times ln\left(\frac{Ut}{D}\right)^{2.36}\times\left(1-\frac{H}{D}\right)^{3.8}\times\left(\frac{L^*}{D}\right)^{-1.63} \tag{5.2}$$

The temporal scour depth can be evaluated using Eq. (5.2). Figure 5.78 shows a comparison of experimental and predicted values of scour depth. The ±30% deviation intervals are added as dashed lines. It can be seen in Fig. (5.78) that 72% deviation occurs between the predicted and observed data in the range of -10% to +10%, -20% to +20% and -30% to +30% error. Hence, the calculated scour depth matches well with the observed data.

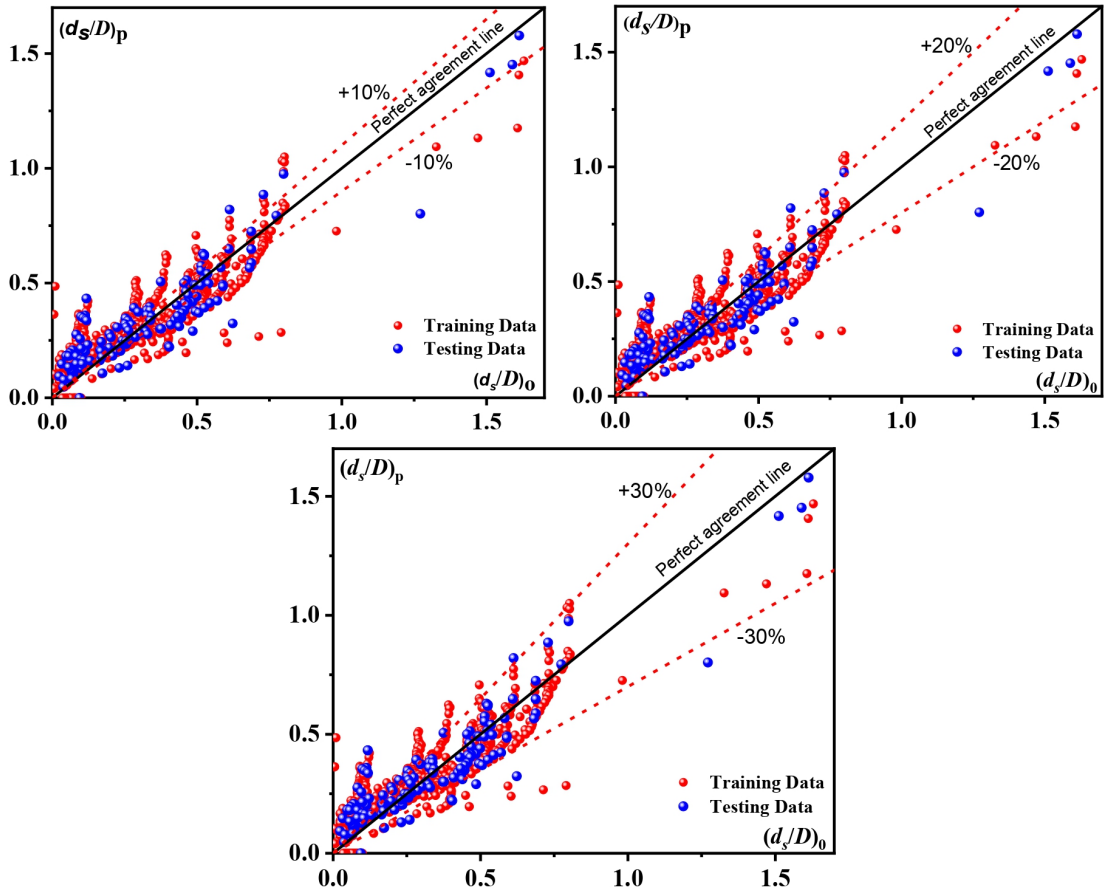


Fig. 5.78 Comparison between experimental and predicted values of temporal scour depth.

5.10 correlation coefficient (r)

In Correlation coefficients whose magnitude is between 0.7 and 0.9 indicate variables which can be considered highly correlated. Correlation coefficients whose magnitude is between 0.5 and 0.7 indicate variables which can be considered moderately correlated. The accuracy of the derive equation is identified the expression shown in Eq. (5.3)

$$\mathrm{r} = \frac{N\sum_{i=1}^{N}\left(\frac{d_s}{D}\right)_{oi} \times \left(\frac{d_s}{D}\right)_{pi} - \sum_{i=1}^{N}\left(\frac{d_s}{D}\right)_{oi} \sum_{i=1}^{N}\left(\frac{d_s}{D}\right)_{pi}}{N^2 \times \mathrm{SD}\left\{\left(\frac{d_s}{D}\right)_{o}\right\} \times \mathrm{SD}\left\{\left(\frac{d_s}{D}\right)_{p}\right\}} \tag{5.3}$$

5.11 Root Mean Squared Error (RMSE)

In the present work, Although, the values of RMSE may range between zero and infinity, however, an RMSE value between 0.2 and 0.5 shows how accurate the model is in predicting the actual value. n is the number of observations. The accuracy of the derive equation is identified the expression shown in Eq. (5.4)

$$\mathrm{RMSE} = \sqrt{\sum_{i=1}^{N} \frac{\left\{\left(\frac{d_s}{D}\right)_{oi} - \left(\frac{d_s}{D}\right)_{pi}\right\}^2}{N}} \tag{5.4}$$

5.12 Percent bias (PBIAS)

In terms of percent bias for accuracy, an ideal range is typically considered to be close to zero, indicating minimal bias or error in the model predictions. Percent bias values within ±5% or ±10% are usually deemed acceptable across various fields, although acceptance criteria may vary based on industry or specific analytical requirements. The accuracy of the derive equation is identified the expression shown in Eq. (5.5).

$$PBIAS = \frac{\sum_{i=1}^{N}\left\{\left(\frac{d_s}{D}\right)_{oi} - \left(\frac{d_s}{D}\right)_{pi}\right\}}{\sum_{i=1}^{N}\left(\frac{d_s}{D}\right)_{oi}} \tag{5.5}$$

5.13 Nash–Sutcliffe efficiency (NSE)

The Nash-Sutcliffe Efficiency (NSE) is a metric commonly used to assess the accuracy of hydrological models, particularly in streamflow simulations. An NSE value of 1 indicates a perfect match between observed and simulated data and greater than 0.5 is generally considered satisfactory for many applications. The accuracy of the derive equation is identified the expression shown in Eq. (5.6)

$$\mathrm{NSE} = 1 - \frac{\sum_{i=1}^{N}\left\{\left(\frac{d_s}{D}\right)_{oi} - \left(\frac{d_s}{D}\right)_{ci}\right\}^2}{\sum_{i=1}^{N}\left\{\left(\frac{d_s}{D}\right)_{oi} - \overline{\left(\frac{d_s}{D}\right)_{o}}\right\}^2} \tag{5.6}$$

Table 5.3. Accuracy analysis of the present study and the reference data.

Present study	**r**	**RMSE**	**PBIAS**	**NSE**	**P_{in} (10%)**	**P_{in} (20%)**	**P_{in} (30%)**
Present study	0.87	0.007	0.08	0.92	26.2%	48.3%	62.3%
Masjedi et al. (2010)	-0.02	0.01	-0.2	-0.008	7%	14%	20%

Figure 5.79 represents the predicted value of the proposed equation by Masjedi et al. with the observed data. The figure indicates that most of the data points are outside the 30% error range. Hence the comparison of two figures, Fig. 5.78 and Fig. 5.79 indicates the present proposed equation has higher accuracy of prediction with observed data. The error analysis of the data presented in Fig. 5.79 is shown in Table 5.3. It represents that r is 0.87, RMSE is 0.006, PBIAS is 0.07 and NSE is 0.91.

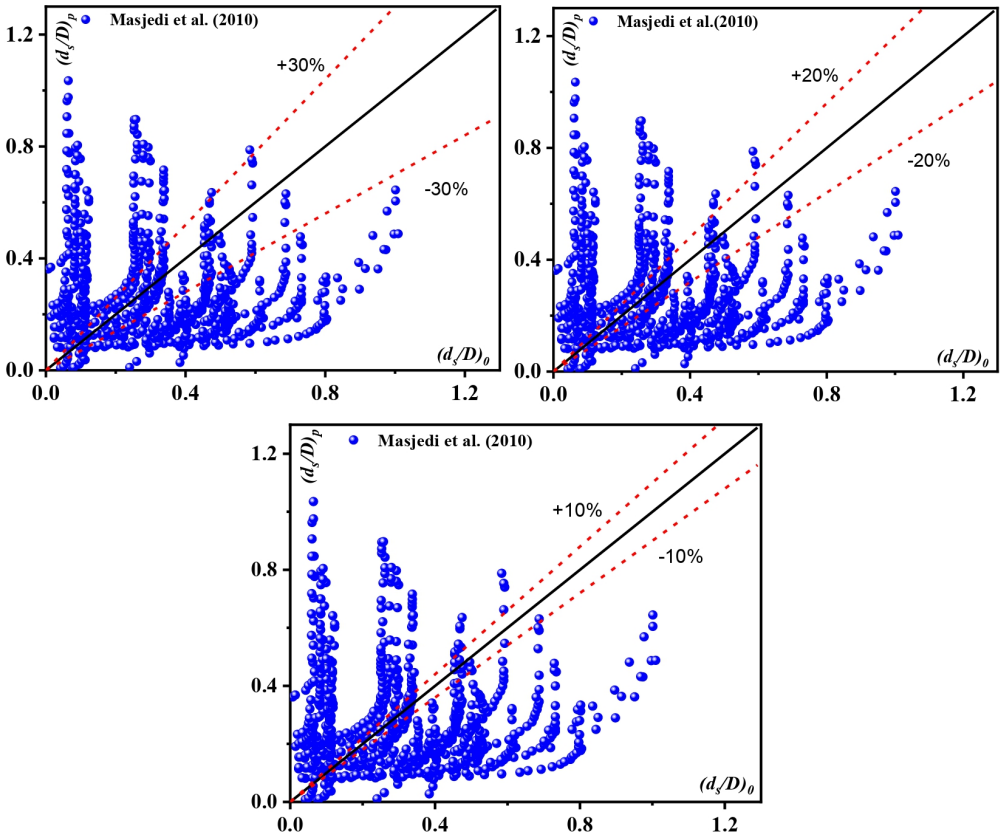


Fig. 5.79. Comparison between observed and predicted values of temporal scour depth, Masjedi et al. (2010).

Chapter 6

Conclusions

In the present work, an experimental analysis is carried out for an oblong pier with a collar. The study is carried out to investigate the parametric variation of scour depth with time. Also, the parametric variation of max scour depth is studied. To investigate the above-mentioned variation, different collar width to pier width and pier length to pier width are taken in the study. The study is carried out under clear water conditions. It is to be mentioned that, when the scour rate reaches below 1mm/hour, the equilibrium condition is considered. It is further to be mentioned that the scour depth of the pier without a collar is compared with the pier with different collar dimensions. The following important findings are noted from the present study.

6.1. Overall remarks

The major findings and contributions of the thesis are summarised below –

- For the case pier without a collar, the maximum scour near the position of angle 0^o. The maximum scour depth is 3.344 cm for *L/D* ratio 4 and 3.72 cm for *L/D* ratio 2.
- For the case pier with collar, collar width to pier ratio 3.5 the presence of maximum scour near the position of angle 135^o. The maximum scour depth is 2.13 cm for *L/D* ratio 4 and 1.57 cm for *L/D* ratio 2.
- For the case pier with collar, collar width to pier ratio 3 the presence of maximum scour near the position of angle 135^o. The maximum scour depth is 2.1 cm for *L/D* ratio 4 and 1.94 cm for *L/D* ratio 2.
- For the case pier with collar, collar width to pier ratio 2.5 the presence of maximum scour near the position of angle 135^o. The maximum scour depth is 2.19 cm for *L/D* ratio 4 and 1.73 cm for *L/D* ratio 2.
- For the case pier with collar, collar width to pier ratio 2 the presence of maximum scour near the position of angle 135^o for *L/D* ratio 4 and 45^o for *L/D* ratio 2. The maximum scour depth is 2.3 cm for *L/D* ratio 4 and 2.013 cm for *L/D* ratio 2.
- For the case pier with collar, collar width to pier ratio 1.5 the presence of maximum scour near the position of angle 0^o. The maximum scour depth is 2.8 cm for *L/D* ratio 4 and 2.46 cm for *L/D* ratio 2.

- For the case of scour depth at 0° angle position the presence of critical *W/D* ratios that minimize scour depth for both *L/D* ratio cases. For *L/D* ratios of 2 and 4, these critical *W/D* ratios are determined to be 3 and 2.5 respectively to minimize scour depth.
- For the case of scour depth at the 45° angle position for an *L/D* ratio of 4, the critical *W/D* ratios are found to be 2.5, whereas, for an *L/D* ratio of 2, these critical *W/D* ratios are determined to be 3 for minimize scour depth.
- For the case of scour depth at 90° angle position for an *L/D* ratio of 4, the critical *W/D* ratios are found to be 2, whereas, for an *L/D* ratio of 2, these critical *W/D* ratios are determined to be 2.5 for minimize scour depth.
- For the case of scour depth at 135° angle position for both *L/D* ratios of 2 and 4, For *L/D* ratios of 2 and 4, these critical *W/D* ratios are determined to be 1.5 for minimize scour depth for minimize scour depth.
- For the case of scour depth at 180° angle position, the presence of critical *W/D* ratios minimizes scour depth for both *L/D* ratio cases. For *L/D* ratios of 2 and 4, these critical *W/D* ratios are determined to be 1.5 and 2 respectively.
- The presence of critical *L/D* ratios that minimize scour depth for different *W/D* ratios. For *W/D* ratios ranging from 1.5 to 3.5, these critical *L/D* ratios are noted for both *L/D* ratios of 2 and 4.
- the scour volume peaks at *W/D*=2 for *L/D*=2, while the deposition volume reaches its maximum at *W/D*=2 for *L/D*=4.
- The scour planar area peaks at *W/D*=1.5 for *L/D*=4, while the deposition volume reaches its maximum at *W/D*=1.5 for *L/D*=2 and the scour surface area peaks at *W/D*=1.5 for *L/D*=4, while the deposition volume reaches its maximum at *W/D*=1.5 for L/D=2.

Finally, with the help of observation, a governing equation for temporal scour prediction is developed. The error analysis of predicted and observed data represents that CC is 0.87, RMSE is 0.006, PBIAS is 0.07 and NSE is 0.91. The developed non-dimensional equation may further be utilized to estimate the scour depth in a real scenario of a bridge pier.

6.2. Scope of future work

The scope of future endeavors is outlined below.

- The collar positions considered in this thesis work are taken at bed level. However, in future, the effect of changing the collar position above and below the bed on scour depth can be evaluated further.
- The present study is carried out under fixed flow velocity. However, the effect of changing the flow velocity on scour depth can be evaluated further.
- The present study is carried out under a fixed depth of water. However, the effect of changing the depth of water on scour depth can be evaluated further.
- The present study is carried out under a straight flow channel. However, the effect of the bend flow channel can be evaluated further.

References

Abed, B.S. and Majeed, H. Q. (2020). The Behavior of Scouring Around Multiple Bridge Piers Having Different Shapes. Proceedings of the IOP Conference Series on "Materials Science and Engineering", Vol. 745, Art. No. 012158. https://doi.org/10.1088/1757-899X/745/1/012158.

Amir, R., Zarrati, H., Gholami and M.B. Mashahir. (2004). Application of collar to control scouring around rectangular bridge piers. *Journal of Hydraulic Research*, Vol. 42, Issue 1, pp. 97-103, https://doi.org/10.1080/00221686.2004.9641188.

Beg, S. and Beg, M. (2017). Application of Collars Around Bevel-Nosed Rectangular Pier. *In Development of Water Resources in India*, pp. 387-395. https://doi.org/10.1007/978-3-319-55125-833.

Bento, A.M., Pego, J.P., Viseu, T. and Couto, L. (2022). Scour Development Around an Oblong Bridge Pier: A Numerical and Experimental Study. Water, Vol. 15, Issue 16, Art. No. 2867. https://doi.org/10.3390/w15162867.

Bhattacharya, A. K., Basack, S. and Bhattacharya, G. (2003). Reduction Of Local Scour Around Non-Cylindrical Bridge Piers at High Angles of Attack Using Collar. *ISH Journal of. Hydraulic Engineering*, Vol. 9, Issue 2, pp. 1-10. https://doi.org/10.1080/09715010.2003.10514729.

Breusers, H.N.C. and Raudkivi, A.J., (1991). Scouring, First Edition. IAHR hydraulic structures design manual, Rotterdam, The Netherlands.

Brice, J. C. and Blodgett, J. C. (1978). Countermeasures for hydraulic problems at bridges. Report No. FHWA-RD-78-162, Federal Highway Administration, USA.

Chang, F. M. (1973). A Statistical Summary of the Cause and Cost of Bridge Failures. Report No. FHWA-RD-75-87, Federal Highway Administration, U.S. Dept. of Transportation, Washington, D.C.

Chen, S. C., Tfwala, S., Wu TY., Chan, HC. and Chou, HT. (2018). A hooked collar for bridge piers protection: flow fields and scour. Vol. 10, no.9, pp. 1251-1262. https://doi.org/10.3390/w10091251.

Chiew, Y.M, (1992). Scour protection at bridge piers. *Journal of. Hydraulic Engineering*, *ASCE*, Vol. 118, Issue 9, pp. 1260-1269. https://doi.org/10.1061/(ASCE)0733-9429(1992)118:9(1260).

Das R., Khwairakpam P., Das S. and Mazumdar A. (2014*a*). Clear-water local scour around eccentric multiple piers to shift the line of sediment deposition. *Asian Journal of Water, Environment and Pollution*. Vol. 1, Issue 3, pp. 47-54.

Das S., Das R. and Mazumdar A. (2016). Comparison of local scour characteristics around two eccentric piers of different shapes. *Arabian Journal of Science and Engineering,* Vol. 41, Issue 4, Pp. 1199-1213. https://doi.org/10.1007/s13369-015-1817-4.

Das, R., Das, S., Jaman, H. and Mazumdar, A. (2019). Impact of upstream bridge pier on the scouring around adjacent downstream bridge pier. *Arabian Journal for Science and Engineering*, Vol. 44, pp. 4359-4372. https://doi.org/10.1007/s13369-018-3418-5.

Das, R., Das, S., Jaman, H. and Mazumdar, A. (2019). Impact of upstream bridge pier on the scouring around adjacent downstream bridge pier. *Arabian Journal for Science and Engineering*, Vol. 44, pp. 4359-4372. https://doi.org/10.1007/s13369-018-3418-5.

Das, S. and Mazumdar, A. (2018). Evaluation of hydrodynamic consequences for horseshoe vortex system developing around two eccentrically arranged identical piers of diverse shapes. *KSCE Journal of Civil Engineering*, Vol. 22, pp. 2300-2314. https://doi.org/10.1007/s12205-017-1842-9.

Das, S., Das, R. and Mazumdar, A. (2013). Circulation characteristics of horseshoe vortex in scour region around circular piers. *Water Science and Engineering*, Vol. 6, Issue 1, pp. 59-77. https://doi.org/10.3882/j.issn.1674-2370.2013.01.005.

Das, S., Das, R. and Mazumdar, A. (2013). Comparison of characteristics of horseshoe vortex at circular and square piers. *Research Journal of Applied Sciences, Engineering and Technology*, Vol. 5, Issue 17, pp. 4373-4387.

Das, S., Das, R. and Mazumdar, A. (2015). Velocity profile measurement technique for scour using ADV. Proceedings of the International Conference on "Testing and Measurement: Techniques and Applications" (TMTA), pp. 249-252, Jun. 2015.

Das, S., Das, R., Kuila, A. and Mazumdar, A. (2014*b*). Analysis of clear-water equilibrium scour around two eccentric circular piers to increase self-dredging. In Seminar on "Dredging: Equipment and Applications" EADA, Kolkata: India.

Das, S., Ghosh, R., Das, R. and Mazumdar, A. (2014). Clear water scour geometry around circular piers. *Ecology Environment and Conservation*, Vol. 20, Issue 2, pp. 479-492.

Das, S., Ghosh, R., Das, R. and Mazumdar, A. (2014). Clear water scour geometry around circular piers. *Ecology, Environment and Conservation*, Vol. 20, Issue 2, pp. 479-492.

Das, S., Ghosh, S., and Mazumdar, A. (2014*c*). Kinematics of horseshoe vortex in a scour hole around two eccentric triangular piers. *International Journal of Fluid Mechanics Research*, Vol. 41, Issue 4, pp. 296-317. https://doi.org/10.1615/InterJFluidMechRes.v41. i4.20.

Das, S., Jaman, H., Chatterjee, A., Das, R. and Mazumdar, A. (2017). Hydrodynamic behavior of Flow past three typically arranged circular piers on different horizontal planes. *International Journal of Fluid Mechanics Research*, Vol. 44, Issue 5, pp. 457-468. https://doi.org/10.1615/InterJFluidMechRes.2017019421.

Das, S., Midya, R., Das, R. and Mazumdar, A. (2013). A study of wake vortex in the scour region around a circular pier. *International Journal of Fluid Mechanics Research*, Vol. 40, Issue 1, pp. 42-59. https://doi.org/10.1615/InterJFluidMechRes.v40.i1.40.

Dehghan, D., Vaghefi, M. and Ghodsian, M. (2021). The effect of collar width ratio on the flow pattern around oblong pier in bend. *Water Supply*, Vol. 21, Issue 8, pp. 4130-4144. https://doi.org/10.2166/ws.2021.165.

Dehghan, D., Vaghefi, M. and Ghodsian, M. (2023). Effects of increasing the width of collar on reduction of scouring surrounding the rectangular piers in a 180-degree bend. *Applied Water Science,* Vol. 13, Issue 3, Art. No. 76. https://doi.org/10.1007/s13201-023-01884-8.

Dey, S. (1997). Local Scour at Piers: A Review of Developments of Research. *International Journal of Sediment Research*, Vol.1 2, Issue 2, pp. 527-540. http://dx.doi.org/10.1080/09715010.2020.1752830.

Dey, S. (1999). Time-variation of scour in the vicinity of circular piers. *Proceedings of the Institution of Civil Engineers-Water Maritime and Energy*, Vol. 136, Issue 2, pp. 67-75. https://doi.org/10.1680/iwtme.1999.31422.

Fael, C., Lança R. and Cardoso, A. (2016). Effect of pier shape and pier alignment on the equilibrium scour depth at single piers. *International Journal of Sediment Research,* Vol. 31, Issue 3, pp. 244-250. https://doi.org/10.1016/j.ijsrc.2016.04.001

Farooq, R. and Ghumman, A.R. (2019). Impact Assessment of Pier Shape and Modifications on Scouring around Bridge Pier. *Water*, Vol. 11, Issue 9, Art. No. 1761. https ://doi.org/10.3390/w11091761.

Farooq, R., Azimi A.H., Rehman, M.A.U. and Ahmed, A. (2023). Effects of hooked-collar on the local scour around a lenticular bridge pier. *International Journal of Sediment Research*, Vol. 38, Issue 1, pp. 1-11. https://doi.org/10.1016/j.ijsrc.2022.07.002.

Farooq, R., Ghumman, A. R., Tariq, M. A. U. R., Ahmed, A. and Jadoon, K. Z. (2020). Optimal octagonal hooked collar countermeasure to reduce scour around a single bridge pier. *Periodica Polytechnica Civil Engineering*, Vol. 64, Issue 4, pp. 1026-1037. https://doi.org/10.3311/PPci.15966.

Farooq, R., Ghumman, A.R. and Hashmi, H.N. (2017). Influence of pier modification techniques for reducing scour around bridge piers. *International Journal of Civil and Environmental Engineering*, Vol. 11, Issue 4, pp. 462-468. https://doi.org/10.5281/zenodo.1130133.

Farooq, R., Ghumman, A.R., Ahmed, A., Latif, A. and Masood, A. (2021). Performance Evaluation of Scour Protection around a Bridge Pier through Experimental Approach. *Tehnički vjesnik* 28.Vol. 28, Issue 6. pp. 1975-1982.

Garg, V., Setia, B. and Verma, D. V. S. (2008). Combination Of Scour Protection Devices Around Oblong Bridge Pier. *Ish Journal of Hydraulic Engineering*, Vol. 14, Issue 3, pp. 56-68. https://doi.org/10.1080/09715010.2008.10514922.

Ghaderi, A. and Abbasi, S. (2019). CFD simulation of local scouring around airfoil-shaped bridge piers with and without collar. Vol. 44, Issue 10, Art. No. 216. https ://doi.org/10.1007/s12046-019-1196-8.

Ghorbani, B. and Kells, J.A. (2008). Effect of submerged vanes on the scour occuring at a cylindrical Pier. *Journal of Hydraulic Research,* Vol. 46, Issue 5, pp. 610-619. https ://doi.org/10.3826/jhr.2008.3003.

Grimaldi, C., Gaudio, R., Calomino, F. and Cardoso, A. H. (2009). Countermeasures against local scouring at bridge piers: Slot and combined system of slot and bed sill. *Journal of Hydraulic Engineering*, Vol. 135, Issue 5, pp. 425-431. https://doi.org/10.1061/(ASCE)HY.1943-7900.0000035.

Hamill, L. (1999). Bridge hydraulics, First Edition. E. and F. N. Spon: London, UK.

Heidarpour, M., Afzalimehr, H., and Izadinia, E. (2010). Reduction of local scour around bridge pier groups using collars, *International Journal of Sediment Research*, Vol. 25, Issue 4, pp. 411-422. https://doi.org/10.1016/S1001-6279(11)60008-5.

Huber, F. (1991). Update: bridge scour, civil engineering. *Journal of Hydraulic Engineering*, Vol. 61, Issue 9, pp. 62-63.

Imamzadehei N., Heidarpour M., Imamzadehei N.M., Ghorbani B. and Haghiabi A. (2016). Control of the local scouring around the cylindrical bridge pier using armed soil by geotextile. *International Journal of Geosynthetics and Ground Engineering,* Vol. 2, Issue 1, pp. 1-8. https://doi.org/10.1007/s4089 1-016-0045-7.

Ismael, A., Gunal, M. and Hamid, H., (2014). Use of Downstream-Facing Airfoil-Shaped Bridge Piers to Reduce Local Scour. *International Journal of Civil Engineering and Technology*, Vol. 5, Issue 11, pp. 44-56.

Jahangirzadeh, A., Basser, H., Akib, S., Karami, H., Naji, S. and Shamshirband, S. (2014). Experimental and numerical investigation of the effect of different shapes of collars on the reduction of scour around a single bridge pier. PloS One, Vol. 9, Issue 2, e98592. https://doi.org/10.1371/journal.pone.0098592.

Keshavarz A., Vaghefi M. Ahmadi G. (2021). Investigation of flow pattern around rectangular and oblong piers with collar located in a 180° sharp bend. *Scientia Iranica,* Vol. 28 Issue 5, pp. 2479-2492. https://doi.org/10.24200/2021.55320.4169

Khosravinia, P., Malekpour, A., Hosseinzadehdalir, A. and Farsadizadeh, D. (2018). Effect of trapezoidal collars as a scour countermeasure around wing-wall abutments. *Water Science and Engineering*, Vol. 11, Issue 1, pp. 53-60. http://dx.doi.org/10.1016/j.wse.2018.03.001.

Kothyari, U.C., Raju, K.G.R. and Garde, R.J. (1992a). Live-bed scour around cylindrical bridge piers. *Journal of Hydraulic Research*, Vol. 30, Issue 5, pp. 701-715. https://doi.org/10.1080/00221689209498889.

Kothyari, U.C., Raju, K.G.R. and Garde, R.J. (1992b). Temporal variation of scour around circular bridge piers. *Journal of Hydraulic Engineering*, Vol. 118, Issue 8, pp. 1091-1106. https://doi.org/10.1061/(ASCE)0733-9429(1992)118:8(1091)

Kumar, V., Raju, K.G.R. and Vittal, N. (1999). Reduction of local scour around bridge piers using slots and collars. *Journal of Hydraulic Engineering*, Vol. 125, Issue 12, pp. 1302-1305. https://doi.org/10.2166/ws.2020.022.

Kumar, V., Ranga, K.G.R. and Vittal, N. (1999). Reduction Of Local Scour Around Bridge Piers Using Slots and Collars. *Journal of Hydraulic Engineering*, Vol. 125, Issue 12, pp. 1302-1305. https://doi.org/10.2166/ws.2020.022.

Kumcu, S. Y., Kokpinar, M. A. and Gogus, M. (2014). Scour protection around vertical-wall bridge abutments with collars. *KSCE Journal of Civil Engineering*, Vol. 18, Issue 6, pp. 1884-1895. http://dx.doi.org/10.1007/s12205-014-0245-4.

Lagasse, P. F., Schall, J. D., Johnson, F., Richardson, E. V., Richardson, J. E. and Chang, F. (1991). Stream stability at highway structures. Report No. FHWA-IP-90-014, Hydraulic Engineering Circular, U.S. Dept. of Transportation.

Lauchlan, C.S. and Melville, B.W. (2001). Riprap protection at bridge piers. *Journal of Hydraulic Eng*. Vol. 127, pp. 412–418. https ://doi.org/10.1061/0733-9429127:5(412).

Manouchehr, H., Hossein, A. and Elham, I. (2010). Reduction of local scour around bridge pier groups using collars. *International Journal of Sediment Research*, Vol. 25, Issue 4, pp. 411-422. https://doi.org/10.1016/S1001-6279(11)60008-5.

Mashahir, M. B., Zarrati, A. R. and Mokallaf, E. (2008). Effect of Collar Length on Time Development of Scouring Around Rectangular Bridge Piers. Fourth International Conference on "Scour and Erosion", Nov. 2008.

Mashahir, M.B. and Zarrati, A.R. (2002). Effect Of Collar on Time Development of Scouring around Rectangular Bridge Piers, Fifth International Conference on "Hydroscience and Engineering, Warsaw", Poland.

Mashahir, M.B., Zarrati, A. R. and Mokallaf, E. (2010). Application of Riprap and Collar to Prevent Scouring around Rectangular Bridge Piers. *Journal of Hydraulic Engineering*, Vol. 136, Issue 3, pp. 183-187. https://doi.org/10.1061/1943-7900.0000145.

Mashahir, M.B., Zarrati, A.R. and Rezayi, M. J. (2004). Time Development of Scouring around a Bridge Pier Protected by Collar. Second International Conference on "Scour and Erosion" (ICSE-2). Singapore: Nanyang Technological University, pp. 14-17, Nov. 2004.

Masjedi, A., Bejestan, M.S. and Esfandi, A. (2010). Reduction of local scour at a bridge pier fitted with a collar in a 180 degree flume bend (Case study: oblong pier). *Journal of Hydrodynamics,* Vol. 22, Issue 5, pp. 646-650. https://doi.org/10.1016/S1001-6058(10)60012-1.

Melville, B. W. and Hadfield, A. C. (1992). Use of Sacrificial Piles as Pier Scour Countermeasures, *Journal of Hydraulic Engineering*, Vol. 125, No. 11, pp. 1221-1224.

Melville, B. W. and Sutherland, A. J. (1988). Design method for local scour at bridge piers. American Society of Civil Engineering. *Journal of the Hydraulics Division,* Vol. 114, Issue 10, pp. 1210-1225.

Melville, B.W. and Coleman, S. E. (2000). Bridge Scour, *Water Resources publication*.

Moghanloo, M., Vaghefi, M. and Ghodsian, M. (2019). Experimental investigation on the effect of increasing the collar thickness on the flow pattern around the oblong pier in 180 sharp bend with balanced bed. *Journal Applied Fluid Mechanics.* Vol. 13, Issue 1, pp. 245-260. https://doi.org/10.29252/jafm.13.01.30164.

Moghanloo, M., Vaghefi, M. and Ghodsian, M. (2020). Experimental Study on the Effect of Thickness and Level of the Collar on the Scour Pattern in 180° Sharp Bend with Bridge Pier. *Iranian Journal of Science and Technology, Transactions of Civil Engineering,* Vol. 46, Issue 6, pp. 1-19. https://doi.org/10.1007/s40996-020-00511-9.

Nandi, B. and Das, S. (2023). Identify most promising temporal scour depth formula for circular piers proposed over last six decades, *Ocean Engineering*, Vol. 286, Issue 2, Art. No. 115639.

Nandi, B. and Das, S. (2023a). Equation for time-dependent local scour at pier-like structures with eccentric in-line arrangements. *Proceedings of the Institution of Civil Engineers-Water Management*, pp. 1-14. https://doi.org/10.1680/jwama.23.00006.

Nandi, B. and Das, S. (2023b). Identify most promising temporal scour depth formula for circular piers proposed over last six decades. Ocean Engineering. Vol. 286, Issue 2, Art. No. 115639. https://doi.org/10.1016/j.oceaneng.2023.115639.

Nandi, B., Patel, G. and Das, S. (2024a). Prediction of maximum scour depth at clear water conditions: Multivariate and robust comparative analysis between empirical equations and machine learning approaches using extensive reference metadata. *Journal of Environmental Management*, Vol. 354. https://doi.org/10.1016/j.jenvman.2024.120349.

Nandi, B., Sasmal, K. and Das, S. (2024b). Evolution of Four Formulae Derived Over Five Decades to Predict Temporal Scour at Circular Pier. In International Conference on "Science, Technology and Engineering", Singapore: Springer Nature Singapore, pp. 131-139.

Negm, A. M., Moustafa, G. M., Abdalla Y. M. and Fathy A.A. (2009). Optimal Shape of Collar to Minimize Local Scour Around Bridge Piers. Thirteenth International Water Technology Conference (IWTC 13), Hurghada: Egypt, pp. 12-15, Jan. 2009.

Raudkivi, A.J. (1986). Functional trends of scour at bridge piers. *Journal of Hydraulic Engineering*, Vol. 112, Issue 1, pp. 1-13. https://doi.org/10.1061/(ASCE)0733-9429(1986)112:1(1).

Raudkivi, A.J. (1998). "Loose Boundary Hydraulics", 4rd Edition, Pergamon Press.

Saadati, S. M. R. S., Heydari, M. M. and Saneie, M. (2017). Experimental investigation of ridged collar effect on scour process on the periphery of circular pier in clear water condition. *Fresenius Environmental Bulletin,* Vol. 25, pp. 4525-4536. http://dx.doi.org/10.3880/j.issn.1006-7647.2023.02.001.

Safaei, A., Solimani B.M., Aghamajidi, R. and Eftekhar, P. (2021). Experimental Study Effect of the Flexible Collar on Bridge Pier Scouring Depth. *Irrigation Sciences and Engineering*, Vol. 44, pp. 53-66. https://doi.org/10.22055/jise.2021.37936.1982.

Salamatian M., Zarrati A.R., Zokaei SA. and Karimaee M. (2013). Study on scouring around bridge piers protected by collar using low density sediment. *International Journal of Civil Engineering*, Vol. 11, Issue 3, pp. 199-205. http://ijce.iust.ac.ir/article-1-618-en.html.

Shirhole, A.M. and Holt, R.C. (1991). Planning for a comprehensive bridge safety program. Transportation Research. Record No. 1290, Transportation Research Board, National Research Council, Washington, D.C., USA.

Simons, D.B. and F. Sentürk. (1976). Sediment transport technology. *Water Resources Publications*, Fort Collins. Jansen. P.Ph. (ed.) (1979). Principles of River Engineering. The non-tidal alluvial river. Pitman, London.

Solati, S., Vaghefi, M. and Ahmadi, G. (2023). Scour pattern around a pier in a 180° sharp bend: influence of pier shape under unsteady currents*, Hydrological Sciences Journal,* Vol. 68, Issue. 12, pp. 1711-1723, https ://doi.org/ 10.1080/02626667.2023.2236089

Tipireddy, R.T. and Barkdoll, B.D. (2019). Scour reduction by air injection at a cylindrical bridge pier: experimental determination of optimal configuration. *Journal of Hydraulic Eng* Vol. 145, Issue 1. https://doi.org/10.1061/1943-7900.0001555

Tseng, M. H., Yen, C. L. and Song, C. C. (2000). Computation of three-dimensional flow around square and circular piers. *International journal for numerical methods in fluids*, Vol. 34, Issue. 3, pp. 207-227. https://doi.org/10.1002/1097-0363(20001015)34:3%3C207::AID-FLD31%3E3.0.CO;2-R.

Vaghefi, M., Ghodsian, M. and Salimi, S. (2016). Scour formation due to laterally inclined circular pier. *Arabian Journal for Science and Engineering,* Vol. 41, Issue 4, pp. 1311-1318. https://doi.org/10.1007/s1336 9-015-1920-6.

Van Rijn, L. C. (1984). Sediment transport, part I: bed load transport. *Journal of hydraulic engineering*, Vol. 110, Issue No. 10, pp. 1431-1456. https://doi.org/10.1061/(ASCE)0733-9429(1984)110:10(1431).

Vijayasree, B.A., Eldho T.I., Mazumder, B.S. and Viswanadham, B.V.S. (2018). Effectiveness of combinations of raft foundation with aprons as a protection measure against bridge pier scour. *Indian Academy of Sciences.* Vol. 43, pp. 1-13. https://doi.org/10.1007/s1204 6-018-0784-3.

Zarrati, A. R., Nazariha, M. and Mashahir, M. B. (2006). Reduction of Local Scour in the Vicinity of Bridge Pier Groups Using Collars and Riprap. *Journal of Hydraulic Engineering*, Vol. 132, Issue 2, pp. 154-162. https://doi.org/10.1061/0733-9429(2006)132:2(154).

Zarrati, A.R., Gholami, H. and Mashahir, M.B. (2004). Application of Collar to Control Scouring around Rectangular Bridge Piers. *Journal of Hydraulic Research* Vol. 42, Issue 1, pp. 97-103. http://dx.doi.org/10.1080/00221686.2004.9641188.

Zokaei, S A., Salamatian, M., Zarrati, A R. and Karimaee M. (2013). Study on scouring around bridge piers protected by collar using low density sediment *International Journal of Civil Engineering*, Vol. 11, Issue 3, pp. 199-205. http://ijce.iust.ac.ir/article-1-618-en.html.